NONSMOOTH IMPACT MECHANICS OF A FREE FALLING BODY

by

ALEXEY TITOVICH

A thesis submitted to the

Graduate School-New Brunswick

Rutgers, The State University of New Jersey

in partial fulfillment of the requirements

for the degree of

Master of Science

Graduate Program in Mechanical and Aerospace Engineering

written under the direction of

Dr. Haim Baruh

and approved by

_____

_____

_____

New Brunswick, New Jersey

January, 2011

Abstract of the Thesis

Nonsmooth Impact Mechanics of a Free Falling Body

by Alexey Titovich

Thesis Director: Dr. Haim Baruh

In this study, several models are developed for analyzing the oblique impact of a container dropped from a height above the impacting surface. The governing equations for impact of rigid bodies in the presence of friction are developed. A clear relationship for determining sliding behavior is presented. For both frictional regimes, the dependence of the energy loss on the initial parameters is analyzed. Several vibrational impact models are presented and analyzed. These models produce a transient description of the impact force and aid in the determination of the ratio of the cushion and cargo stiffness which produce the best impact outcome. The effect of aerodynamic drag prior to impact is also analyzed. The equations governing the aerodynamics form a set of coupled nonlinear differential equations. The numerical solution of these equations illustrates that there exists a point where the object's velocity reaches a favorable minimum, which is substantially below the terminal velocity. An approximate solution, obtained by decoupling the aerodynamic equations, is presented and validated. Both the rigid body impact mechanics and the aerodynamics are combined in a simulation code capable of analyzing subsequent impact. The simulated tumbling distances for a container, which was designed for the U.S. Army, are compared to experimental drop test data. The results validate the use of the rigid body model for this type of container.

Acknowledgements

This work would not have been possible without the guidance and assistance of the many people around me. I would like to begin by thanking my advisor, Professor Haim Baruh. Besides being extremely knowledgeable in his field, he is also a very genuine person and a pleasure to talk to. As anyone in the department knows, Dr. Baruh's door is always open for questions or simply advice, a fact that I might have overused throughout the years. He introduced me to this project and spent countless hours deliberating its course with me. He has always looked out for me and helped me in times of need, something that I am extremely grateful for.

Another person who has helped me tremendously over the years is Professor William J. Bottega. He inspired me to not take things for granted when it comes to mechanics. He taught me to investigate the origins of theories, because with these fundamental tools one has the power to explore new ways of formulating problems. Having taken five courses with Dr. Bottega has left a lasting mark on my view of mechanics.

I would also like to thank Professors Elsayed and Basily for giving me a sneak peak at the construction of the containers analyzed in this thesis. I thank my committee members Professors Bottega and Elsayed who actually read and revised this lengthy thesis. Furthermore, I would like to thank the faculty members at Rutgers University who made an impact, no pun intended, on my collegiate experience and reinforced my interests in science.

Great thanks go out to the Mechanical and Aerospace Engineering department at Rutgers University, which provided me with financial support through a teaching assistantship. I am also grateful for the opportunity to teach a summer course. These experiences have bolstered my desire to share knowledge and helped me develop the tools to do so effectively.

Several graduate students have helped me tackle the problems of graduate school over the years. First and foremost, I thank Vinesh Nishawala. Our discussions of the many aspects of mechanics, which more often than none led to debates, have resulted in a deeper understanding of the topics, and will undoubtedly resonate throughout our professional careers. Mark Seitel, whose ability to retain knowledge is inexplicable, has helped me in many ways, and quite often was a part of our discussions with Vinesh. I would also like to thank Tushar Saraf, John Doyle, Adam Nagy, Jonathan Torres, and Eugene Sosnov for their contributions to my graduate school experience.

Aside from my professional endeavors, this thesis would not have been possible without the support of my family and friends. My parents, Sergey and Natalia Titovich, have always guided me through life and rewarded me for my academic achievements, which is the reason I am where I am today. My older brother, Alexander Titovich, has always looked out for me, lending a helping hand whenever I required it. His wife, Oksana Titovich, helped me take my mind off of my studies by helping me conquer countless empires in the Age of Empires game. My uncle, Walter Titovich, is the reason I am in this country doing what I love. I want to thank my best friend, Eugene Spikalovas, for always being there for me. Also, the colorful personality of a dear friend, Lucas Osemlak, has kept my spirits up and laughing for years.

Dedication

To my parents Sergey and Natalia Titovich, my brother and his wife, Alexander and Oksana Titovich, and their newborn heir, Michael Titovich.

Table of Contents

List of Tables

List of Figures

List of Abbreviations

$[A]$ Coefficient matrix of the final velocity vector for the no sliding case

A Planform area

a_x Component of the acceleration in the *x* direction

a_y Component of the acceleration in the *y* direction

a_z Component of the acceleration in the *z* direction

$[B]$ Coefficient matrix of the initial velocity vector for the no sliding case

$[C]$ Coefficient matrix of the final velocity vector for the sliding case

$\{C\}$ Vector of constant for the two degree of freedom solution

C Contact point

C_D Coefficient of drag

C_j Integration constants for $j = 1,2$

c Damping coefficient

c_1 Damping coefficient for damper 1

c_2 Damping coefficient for damper 2

$[D]$ Coefficient matrix of the initial velocity vector for the sliding case

D_j Integration constants for $j = 1,2$

e_n Normal coefficient of restitution

e_x Horizontal coefficient of restitution

e_y Vertical coefficient of restitution

$\vec{F}$ Impact force

$\hat{\vec{F}}$ Impact impulse

$\hat{\vec{F}}_R$ Tangential impact impulse

F_D Drag force

$(F_D)_x$ Component of the drag force in the *x* direction

$(F_D)_y$ Component of the drag force in the *y* direction

$(F_D)_z$ Component of the drag force in the *z* direction

$\hat{F}_R$ Magnitude of the tangential impulse

$\hat{F}_x$ Component of the impact force in the *x* direction

$\hat{F}_y$ Component of the impact force in the *y* direction

$\hat{F}_z$ Component of the impact force in the *z* direction

$\hat{F}_x''$ Normalized component of the impact force in the *x* direction

$\hat{F}_y''$ Normalized component of the impact force in the *y* direction

$\hat{F}_z''$ Normalized component of the impact force in the *z* direction

$[G]$ Coefficient matrix of modal vectors

G Center of mass

g Gravitational acceleration

$\vec{H}_G$ Initial angular momentum

$\vec{H}_G'$ Final angular momentum

h Time step

$[I_G]$ Inertia matrix

$[I_G']$ Rotated inertia matrix

I_G Mass moment of inertia about G

I_{pq} Components of the inertia matrix for $p, q = x, y, z$

$\hat{i}$ Unit vector along the *x* direction

$\hat{j}$ Unit vector along the *y* direction

$[k]$ Stiffness matrix

$[\tilde{k}]$ Modal stiffness matrix

k Stiffness coefficient

$\hat{k}$ Unit vector along the *z* direction

$\hat{k}$ Stiffness ratio

$\breve{k}$ Change in the *x* velocity after a time step h in the Runge-Kutta solution

$\breve{k}_i$ Components of $\breve{k}$ for $i = 1,2,3,4$

k_1 Stiffness coefficient for spring 1

k_2 Stiffness coefficient for spring 2

K_{final} Final kinetic energy

$K_{initial}$ Initial kinetic energy

K_{loss} Kinetic energy loss

$\breve{l}$ Change in the *y* velocity after a time step h in the Runge-Kutta solution

$\breve{l}_i$ Components of $\breve{l}$ for $i = 1,2,3,4$

$\vec{M}_G$ Moment about *G*

$[m]$ Mass matrix

$[\tilde{m}]$ Modal mass matrix

m Mass

$\hat{m}$ Mass ratio

$\breve{m}$ Change in the *x* position after a time step h in the Runge-Kutta solution

$\breve{m}_i$ Components of $\breve{m}$ for $i = 1,2,3,4$

m_1 Mass 1

m_2 Mass 2

n Exponential power of the stiffness term in the nonlinear vibrational model

$\breve{n}$ Change in the y position after a time step h in the Runge-Kutta solution

$\breve{n}_i$ Components of $\breve{n}$ for $i = 1,2,3,4$

$[Q]$ Rotation matrix

$[Q_x]$ Rotation matrix about x-axis

$[Q_z]$ Rotation matrix about z-axis

$\vec{R}$ Position vector from point C to G

R Distance from the contact point to the center of mass

R_x Component of the position vector from points C to G in the x direction

R_y Component of the position vector from points C to G in the y direction

R_z Component of the position vector from points C to G in the z direction

$\overline{R}_x$ Horizontal component of the position vector from points C to G normalized by R

$\overline{R}_y$ Vertical component of the position vector from points C to G normalized by R

$[T]$ Transformation matrix to modal coordinates

t Time

$\tilde{t}$ Dimensionless time

t^* Time at the end of impact

$\vec{U}$ Wind velocity

U_x Component of the wind velocity in the x direction

$\tilde{U}_x$ Dimensionless component of the wind velocity in the x direction

U_y Component of the wind velocity in the y direction

$\tilde{U}_y$ Dimensionless component of the wind velocity in the y direction

U_z Component of the wind velocity in the z direction

$\tilde{U}_z$ Dimensionless component of the wind velocity in the z direction

$\vec{V}$ Initial velocity

$\vec{V}'$ Final velocity

$\vec{V}^C$ Initial velocity of the contact point

$\vec{V}'^C$ Final velocity of the contact point

$\vec{V}_{rel}$ Velocity of the air flowing past the body

$\{V\}$ Initial velocity vector

$\{V'\}$ Final velocity vector

V Magnitude of the velocity

V_{impact} Impact velocity

V_{term} Terminal velocity

V_x Initial velocity in the *x* direction

$V_x(t)$ Component of the velocity in the *x* direction

$\tilde{V}_x(t)$ Dimensionless component of the velocity in the *x* direction

V_y Initial velocity in the *y* direction

$V_y(t)$ Component of the velocity in the *y* direction

$\tilde{V}_y(t)$ Dimensionless component of the velocity in the *y* direction

V_z Initial velocity in the *z* direction

$V_z(t)$ Component of the velocity in the *z* direction

$\tilde{V}_z(t)$ Dimensionless component of the velocity in the *z* direction

V_x' Final velocity in the *x* direction

V_y' Final velocity in the *y* direction

V_z' Final velocity in the *z* direction

V_x'' Normalized final velocity in the *x* direction

V_y'' Normalized final velocity in the *y* direction

V_0 Initial velocity

V_x^0 Initial velocity in the *x* direction

V_y^0 Initial velocity in the *y* direction

V_z^0 Initial velocity in the *z* direction

x Cartesian coordinate

$x(t)$ Displacement variable in the *x* direction

$\tilde{x}(t)$ Dimensionless displacement variable in the *x* direction

x_0 Initial *x* position

$\{Y\}$ Modal vector

$Y^{(i)}$ Components of the modal vector for $i = 1,2$

y Cartesian coordinate

$y(t)$ Displacement variable in the *y* direction

$\tilde{y}(t)$ Dimensionless displacement variable in the *y* direction

$\{y_0\}$ Vector of initial positions and velocities

y_0 Initial *y* position

$y_1(t)$ Displacement variable of mass 1 in the *y* direction

$y_2(t)$ Displacement variable of mass 2 in the *y* direction

z Cartesian coordinate

$z(t)$ Displacement variable in the *z* direction

$\tilde{z}(t)$ Dimensionless displacement variable in the *z* direction

z_0 Initial *z* position

α Coefficient of the radius of gyration

β Angle between the line connecting points *C* to *G* and the *x* direction

γ	Angle between the line connecting points *C* to *G* and the vertical
δ	Angle between the line connecting points *C* to *G* and the *y* direction
Δt	Time increment
ς	Damping factor
ς_1	First modal damping factor
ς_2	Second modal damping factor
$\eta_1(t)$	Modal displacement variable 1
$\eta_2(t)$	Modal displacement variable 2
θ	Angle of approach with the horizontal
κ	Coefficient of the stiffness term in the nonlinear vibrational model
λ_z	Normalized initial angular velocity about the *z* axis
μ	Coefficient of friction
$\overline{\mu}$	Coefficient of friction which takes into account the direction of slip
μ_x	Coefficient of friction in the *x* direction
μ_z	Coefficient of friction in the *y* direction
$\overline{\mu}_x$	Coefficient of friction which takes into account the direction of slip in the *x* direction
$\overline{\mu}_z$	Coefficient of friction which takes into account the direction of slip in the *y* direction
ξ	Coefficient of the damping term in the nonlinear vibrational model
ρ_{air}	Density of air
ρ_x	Normalized initial velocity in the *x* direction
σ	Proportionality constant or Rayleigh damping
ϕ	Angle defining the slip direction in the slip plane
χ	Orientation angle with respect to the horizontal

χ_f Front orientation angle

χ_s Side orientation angle

ψ Angle defining the aspect ratio of the container

ψ_f Front face angle defining the aspect ratio of the container

ψ_s Side face angle defining the aspect ratio of the container

$\vec{\omega}$ Initial angular velocity

$\vec{\omega}'$ Final angular velocity

ω Natural frequency

ω_1 First modal natural frequency

ω_2 Second modal natural frequency

ω_x Initial angular velocity about the *x* axis

ω_y Initial angular velocity about the *y* axis

ω_z Initial angular velocity about the *y* axis

ω_x' Final angular velocity about the *x* axis

ω_y' Final angular velocity about the *y* axis

ω_z' Final angular velocity about the *z* axis

ω_z'' Normalized final angular velocity about the *z* axis

Chapter 1

Introduction

Physical impact of bodies can be found in almost every aspect of life. Impact occurs in something as simple as a finger striking a key on the keyboard to something as complex as multi car collisions and everything in the middle. All sports involving balls, such as basketball soccer and tennis as well as physical contact among players, are governed by laws of impact and mastering how impact takes place can lead one to victory. At the other side of the spectrum, scientists in biomedical disciplines study impact in order to prevent failure of bones under impulsive loading. It would be impossible to list all processes in which impact occurs, but one can look at it this way. In our everyday lives, things do not just move on their own, but are rather fixed as to prevent this. However, at some point these things had to be placed into that position, and since people, in general, are not very patient, impact almost certainly occurred.

The reason why impact is so important is that unlike static loads or other types of dynamic loads, the magnitude of impact forces is much larger. The forces exerted during impact can be characterized as having large amplitudes and a very short time duration. This is the reason why many devices fail under impact loading, and also what makes it such an important field of study. During impact the position of the body changes slightly, but the velocity changes dramatically. This formulates the typical impact problem: determine the velocities after impact having specified the initial velocities.

Due to the complexity of accurately modeling the behavior of a solid undergoing impact, numerous facets of mechanics have been employed to describe the impact phenomena. From the mechanics of solids, the field utilizes rigid body dynamics, vibrational analysis, elastic wave propagation, contact mechanics, and the theory of plasticity among others. Also computational tools such as the finite element method are often used. Besides solid mechanics, fluid mechanics is also used to describe the flow of material for high energy impacts. Similarly, thermodynamics is used to analyze the heat dissipation during impact. The sound wave propagation due to the percussion of impact is modeled using acoustics. And, of course, aerodynamics plays a crucial role in determining the pre-impact velocities. In this thesis we will restrict our analysis to certain aspects of solid mechanics.

Rigid body impact is thought to have been introduced by Galileo, according to W. Goldsmith [13]. The first rigorous impact study was published in the late seventeenth century. Newton later used these developments in his manuscripts. As a result, the rigid body impact model that we still use today came into existence. In this model, energy dissipated through impact is modeled by a parameter called the coefficient of restitution. The original definition of the coefficient of restitution is attributed to Newton, and defines the ratio of initial to final vertical velocity of the contact point. Over the years, other definitions have been proposed by Poisson, and more recently by W.J. Stronge [37-40]. Also, a large collection of coefficients of restitution, some of which are empirical, has been compiled by B. Brogliato [8]. However, the analysis of impact is not complete without the study of friction. The tribology of rigid body impact has also been thoroughly studied over the years [6, 7, 9, 11, 13, 16, 20, 25, 29, 40, 41, 44]. Friction is typically

modeled using the Amonton - Coulomb Law of dry friction. A useful graphical method of analyzing the behavior of the friction force during impact was introduced by E.J. Routh [35]. This method is typically used in analyzing the friction force for rigid body impacts, where the transient description of this force cannot be ascertained directly [6, 13, 23, 27, 37, 41]. Impact analysis has been extended to multi–body systems as well, partially due to the advancements in robotics [3, 12, 23, 27, 37]. The rigid body impact model depends on the knowledge of certain coefficients. Due to this, numerous experiments have been devised to study the behavior of the coefficient of restitution [10, 33, 36] and the coefficient of friction [9, 28, 29] during impact. Along with friction, resistance to rolling has also been investigated [43].

Another way of modeling impact is enabled by vibrational models. These consist of differential equations, which are often nonlinear due to the nonlinear nature of the impact force. The solution of such differential equations produces the transient description of the impact force, something the rigid body model is not capable of. Numerous articles have been published on this topic [15, 18, 21, 24, 32, 34, 39, 42].

The developments in the theory of elasticity allowed the study of multi-dimensional wave propagation due to impact in elastic solids. A rather complete study of longitudinal and transverse waves in rods was presented by St. Venant and Boussinesq. Modern texts by J.A. Zucas [45] and W. Goldsmith [13] provide an extensive review of this type of impact analysis. The next improvement in the analysis of impact mechanics was the due to the advancement of contact mechanics. The theory of the mechanics of contact is compiled by K.L. Johnson [19]. In his text Johnson derives Hertz’s solution for the contact of two elastic spheres. This way of modeling the contact stiffness allowed

K.H. Hunt and F.R.E. Crossley to develop a nonlinear vibrational impact model, which, due to its structure, can be easily applied to experiment [15]. The study of plasticity came next and allowed the analysis of plastic effects during impact. Karman with Duwez, as well as others, formulated complete theories on the topic.

In more recent times, the improvements in the speed of computers increased the interest in computational methods to solve impact problems. This area is dominated by the finite element method. It presents an approximate solution to the deformation of solid objects during impact. The power of this method is in its ability to approximately solve the most complex problems in solid mechanics, analytical solutions to which do not exist. Numerous texts and articles have been published on this topic and are readily available. Several commercial finite element packages have been developed for impact analysis, but all have certain limitations.

The problem which this thesis attempts to solve is the impact of a cargo container with the ground. The container analyzed in this thesis was developed for the U.S. Army Logistics Innovation Agency to provide aerial resupply in hard to reach areas. Lack of runways and security issues associated with hostile forces or bandits in such areas requires that supplies be dropped from the aircraft. Instead of using parachutes, which are susceptible to large drift distances and are notoriously unreliable, the containers are to be dropped from a height of 50 to 100 feet, allowing them to free fall to the ground. The cargo is placed in the middle of the container which is comprised of an array of cushions. As the impact takes place the cushion absorbs some of the impact energy and the container continues to tumble across the impact surface. As was pointed out before, it is next to impossible to describe such an impact exactly because of the, hard to predict,

nonlinear behavior of the impact force. There also many uncertainties associated with the orientation of the container at impact, buckling of cushion layers, as well as the cushion-cargo interaction. This is why this type of impact is perfect for the rigid body analysis.

This thesis begins with an analysis of the frictional oblique impact of a rigid body with a rigid plane. In Chapter 2 we formulate the rigid body impact model for both two and three dimensional motion. We then analyze the frictional regime of the impact (sliding or not sliding) and compare the energy loss for each case. We also show that the rigid body impact model can be formulated in several ways and relate them. The chapter is concluded with a comprehensive example. Chapter 3 presents linear vibrational impact models and their application for investigating the cushion-cargo interaction. This chapter also analyzes a popular nonlinear vibrational model, namely its dependence on certain parameters. Chapter 4 presents a study of the aerodynamics of free fall. The equations governing the object's trajectory are derived and a numerical solution is presented. We show that there exists a favorable minimum resultant velocity of the center of gravity. An approximate solution to the nonlinear governing equations is also presented and validated. Lastly, Chapter 5 compiles the aerodynamics of free fall together with the rigid body impact analysis in order to analyze subsequent impacts. Simulations of the subsequent impacts of a container are presented. The simulated tumbling distances are then compared to experimental data.

Chapter 2

Rigid Body Impact Mechanics

Faced with an impact problem, one often begins the analysis with the rigid body model of impact. The rigid body assumption is primarily made to obtain a simple model. However, one should not underestimate its utility. We will show here that a great deal of useful information can be ascertained from this model. The simplicity comes from lumping all of the pertinent impact parameters into a few so called *coefficients*. There is no question about the suitability of defining these coefficients for a given set of initial conditions. One's main concern is whether single-valued coefficients can be used for a range of initial conditions. In the literature, numerous experiments have been devised to study the applicability of the model and will be discussed later in this chapter. As the name suggests, we are assuming that the impacting bodies do not deform through impact and that the impact itself is instantaneous. It thus becomes impossible to determine the motion of the bodies during impact and our solutions consist of post impact velocities and angular velocities. But, no matter how constricting the limitations of this model might seem, one can still apply it to a plethora of useful problems.

2.1 Nonsmooth Oblique Planar Impact

In this subsection we will concentrate on developing the tools to analyze nonsmooth oblique impact. By nonsmooth impact we mean that frictional effects can no longer be neglected. A good example of such an impact occurs in almost every sport which utilizes a ball. The planar impact assumption restricts the initial angular velocity to

only have a component about an axis parallel to a tangent of the impact surface and perpendicular to the plane defined by the components of the initial velocity.

Let us begin the analysis by introducing an arbitrary body in a Cartesian coordinate system oriented such that the horizontal or x-axis coincides with the tangent to the surface at the point of impact.

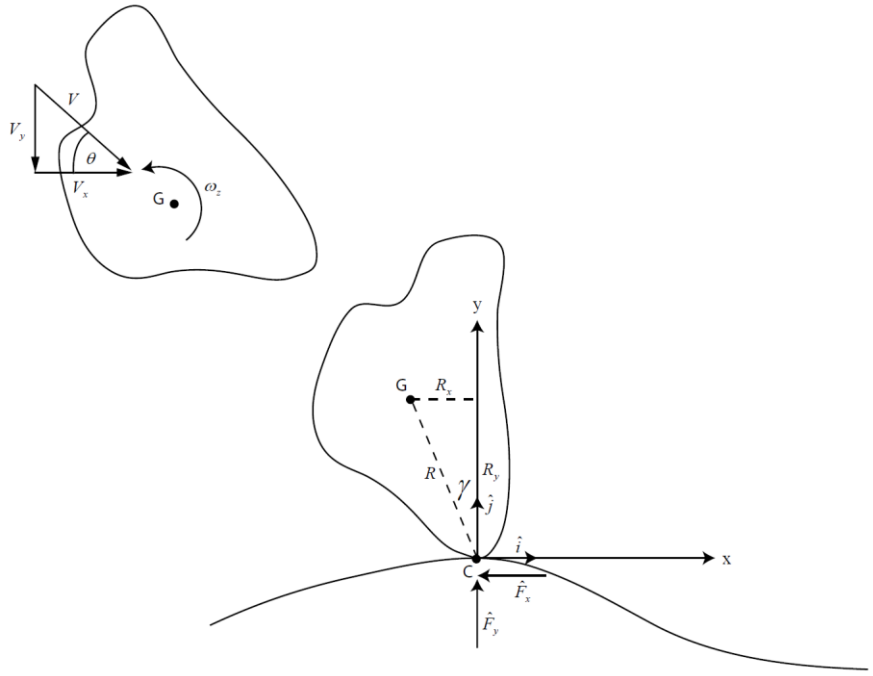

Figure 2.1*: Orientation of the impacting body.*

Since the impact is two dimensional there will be only two forces between the object and the impacting surface. Figure 2.1 shows the vertical impact force as well as the horizontal friction force acting at the contact point *C*. We will neglect the gravitational force on the body because it is non-impulsive and in most instances its magnitude is miniscule compared to the large impact force. Note that the direction of the tangential force indicates that the object is traveling in the positive x direction, since friction always opposes motion. The previous statement becomes less clear when the object has an initial rotation. The position vector of the contact point with respect to the center of mass is

defined by an angle γ from the positive y-axis. This angle will be taken positive counterclockwise. We can therefore express this position vector as follows.

$$\vec{R} = R_x \hat{i} + R_y \hat{j} \tag{2.1a}$$

$$R_x = R\sin(\gamma) \tag{2.1b}$$

$$R_y = -R\cos(\gamma) \tag{2.1c}$$

We will now formulate the kinematics of this impact problem. Let us define the initial velocity of the center of mass, point *G* in Fig. 2.1, and angular velocity as

$$\vec{V} = V_x \hat{i} + V_y \hat{j} \tag{2.2}$$

$$\vec{\omega} = \omega_z \hat{k} \tag{2.3}$$

Therefore the contact point velocity $\vec{V}^C$ at the beginning of impact will be

$$\vec{V}^C = \vec{V} + \vec{\omega} \times \vec{R} = \left(V_x \hat{i} + V_y \hat{j}\right) + \omega_z \left(R_x \hat{j} - R_y \hat{i}\right) \tag{2.4}$$

Similarly the post-impact or final velocity, angular velocity and contact point velocity will be denoted by a prime in the superscript and are

$$\vec{V}' = V_x' \hat{i} + V_y' \hat{j} \tag{2.5}$$

$$\vec{\omega}' = \omega_z' \hat{k} \tag{2.6}$$

$$\vec{V}'^C = \left(V_x' \hat{i} + V_y' \hat{j}\right) + \omega_z' \left(R_x \hat{j} - R_y \hat{i}\right) \tag{2.7}$$

Writing the conservation of linear momentum for this problem we obtain

$$mV_x - \hat{F}_x = mV_x' \tag{2.8}$$

$$mV_y + \hat{F}_y = mV_y' \tag{2.9}$$

where $\hat{F}_x$ and $\hat{F}_y$ are the impulses in the x and y directions, respectively, and m is the

impacting body's mass. Consider the conservation of angular momentum about the center of mass *G*, which is expressed by the following equations

$$I_G\vec{\omega} + \vec{R}\times\vec{\hat{F}} = I_G\vec{\omega}' \tag{2.10a}$$

$$I_G\omega_z + \hat{F}_x R_y + \hat{F}_y R_x = I_G\omega_z' \tag{2.10b}$$

where I_G is the moment of inertia about the center of mass, *G*.

$$I_G = \alpha m R^2 \tag{2.11}$$

The coefficient α in equation (2.11) depends on the geometry of the impacting body.

One can greatly improve the understanding and parameterization of the governing equations of rigid body impact by nondimensionalizing. The question in this situation is what would be a good quantity to nondimentionalize the velocity. One of the answers, the one used in this thesis, will be to nondimensionalize all velocity quantities with respect to the vertical component of the initial velocity. This allows the use of these equations for vertical impacts, even when the horizontal component of the initial velocity vanishes. Let us define the following dimensionless pre-impact quantities.

$$\rho_x \equiv \frac{V_x}{V_y} \qquad \lambda_z \equiv \frac{\omega_z R}{V_y} \tag{2.12a,b}$$

Similarly, we will nondimensionalize the post-impact quantities and denote them with a double prime in the superscript.

$$V_x'' \equiv \frac{V_x'}{V_y} \qquad V_y'' \equiv \frac{V_y'}{V_y} \qquad \omega_z'' \equiv \frac{\omega_z' R}{V_y} \tag{2.13a,b,c}$$

The dimensionless representations of the impact impulses are

$$\hat{F}_x'' \equiv \frac{\hat{F}_x}{mV_y} \qquad \hat{F}_y'' \equiv \frac{\hat{F}_y}{mV_y} \tag{2.14a,b}$$

Lastly, let us also define the following dimensionless components of the position vector between the points *C* and *G*.

$$\overline{R}_x \equiv \frac{R_x}{R} = \sin(\gamma) \qquad \overline{R}_y \equiv \frac{R_y}{R} = -\cos(\gamma) \tag{2.15a,b}$$

Dividing equation (2.8) and (2.9) by mV_y we obtain the dimensionless representations.

$$\rho_x - \hat{F}_x'' = V_x'' \tag{2.16a}$$

$$1 + \hat{F}_y'' = V_y'' \tag{2.16b}$$

Dividing equation (2.10b) by mRV_y we get

$$\alpha\lambda_z + \hat{F}_x''\overline{R}_y + \hat{F}_y''\overline{R}_x = \alpha\omega_z'' \tag{2.16c}$$

We have obtained the governing equations for the rigid body impact. The three equations (2.16a,b,c) do not form a closed system because there are five unknowns: $V_x'', V_y'', \omega_z'', \hat{F}_x'', \hat{F}_y''$. The two equations that we still need will be derived in the following subsections.

2.2 Coefficient of Restitution

One of the hardest feats to accomplish in any impact analysis is to accurately represent the impact force. The simplest way is to model the gross effects of the impact force rather than try to obtain its transient representation. This is where we introduce the coefficient of restitution as the ratio of final to initial vertical velocity of the contact point. This definition is attributed to Newton [13] and can be stated mathematically as

$$e_n = -\frac{\vec{V}'^C \cdot \hat{j}}{\vec{V}^C \cdot \hat{j}} \tag{2.17}$$

where e_n is the coefficient of restitution, and the subscript $(\ )_n$ denotes the direction normal to the impacting surface, in this case the $\hat{j}$ direction. The negative sign in equation (2.17) guarantees a positive value for the coefficient of restitution in the case when velocity reversal occurs. This coefficient can take on values in the range $0 \le e_n \le 1$; a value of 1 denotes a completely elastic impact and a value of 0 denotes a completely plastic impact. Also note that if the object penetrates the impacting surface, the coefficient can take on negative values $-1 \le e_n < 0$ [6]. In this thesis we will concentrate on the positive spectrum of the coefficient of restitution.

The coefficient of restitution depends on the mechanical properties of both the impacting body and the impacting surface, which in general can vary with temperature [33]. It can also vary with the initial velocity [13] as well as the orientation of the impacting body if it is not axis-symmetric. When faced with an impact problem one should decide whether a constant valued coefficient can be used to determine the post-impact behavior.

Let us now obtain a nondimensional expression for the coefficient of restitution. Substituting (2.4) and (2.7) into (2.17), we obtain

$$e_n = -\frac{\left[\left(V_x'\hat{i} + V_y'\hat{j}\right) + \omega_z'\left(R_x\hat{j} - R_y\hat{i}\right)\right]\cdot\hat{j}}{\left[\left(V_x\hat{i} + V_y\hat{j}\right) + \omega_z\left(R_x\hat{j} - R_y\hat{i}\right)\right]\cdot\hat{j}} = -\frac{V_y' + \omega_z' R_x}{V_y + \omega_z R_x} \tag{2.18}$$

Equation (2.18) can be nondimensionalized by dividing all quantities by the initial vertical velocity V_y.

$$e_n = -\frac{V_y'' + \dfrac{\omega_z' R}{V_y}\left(\dfrac{R_x}{R}\right)}{1 + \dfrac{\omega_z R}{V_y}\left(\dfrac{R_x}{R}\right)}$$

Using the definitions (2.11), (2.12), and (2.14) we arrive at the nondimensional form of the coefficient of restitution.

$$e_n = -\frac{V_y'' + \omega_z'' \overline{R}_x}{1 + \lambda_z \overline{R}_x} \tag{2.19}$$

Equation (2.19) is the fourth equation in the system, discussed in the previous subsection, required to solve a rigid body impact problem. One more relation remains to be determined before one can solve the impact problem. This expression will come from analyzing the friction forces developed during impact.

2.3 Tribology of Impact

Friction is an important part of rigid body impact. It governs the transfer of linear momentum to angular momentum and hence all post-impact quantities. Friction effects will be defined by the Coulomb Law [1] of friction as absolute value of the ratio of horizontal to vertical impulse components. This relationship is depicted below

$$\mu = \left| \frac{\hat{F}_x}{\hat{F}_y} \right| \tag{2.20}$$

where μ is called the coefficient of friction. The above expression governs the relationship between the impulses if sliding occurs; it will also be shown to be the condition required for sliding to initiate. We can nondimensionalize the right hand side of definition (2.20) with respect to mV_y obtaining equation (2.21).

$$\mu = \left| \frac{\hat{F}_x''}{\hat{F}_y''} \right| \tag{2.21}$$

Once again, our solution will assume a constant value of the coefficient of friction. The coefficient of friction is a function of the mechanical properties of both contacting surfaces. It has also been shown that for some objects [9] it can depend on the sliding velocity, the relative speed between the contact point and the impact surface. But, in the general case, it has been argued that the coefficient of friction is independent of the sliding velocity unless it is very small, in which case thermal processes must be considered [29]. Furthermore the friction force can even reverse its direction during impact [28, 35]. But, as was stated previously in the rigid body analysis of impact we are only concerned with the gross effects of friction.

In this thesis we will consider the two extremes of frictional effects during impact. One possibility will be that the impacting body rolls or pivots during impact, which corresponds to the case when the impulse ratio is less than the critical value governed by equation (2.20) and hence the object does not slide. The major difference between rolling and pivoting during impact is that for rolling the magnitude of the position vector, R, between points *C* to *G*, seen in Fig. 2.1, can change during impact, while for pivoting it is assumed to remain constant. In this thesis we will assume that R remains constant throughout the impact. In the case when no sliding occurs, the remaining mathematical condition will come from the equations for rolling [1], namely

$$\vec{V}'^{CP} \cdot \hat{i} = 0 \qquad (2.22)$$

Equation (2.22) requires that the horizontal component of the contact point velocity vanishes if no sliding occurs during impact. Substituting equation (2.7) into (2.22) yields

$$\left(\left(V_x'\hat{i} + V_y'\hat{j}\right) + \omega_z'\left(R_x\hat{j} - R_y\hat{i}\right)\right)\cdot\hat{i} = 0$$

$$V_x' - \omega_z' R_y = 0 \qquad (2.23)$$

Nondimensionalizing equation (2.23) with respect to V_y and using definitions (2.13) and (2.15) we get the following expression.

$$V_x'' - \omega_z'' \overline{R}_y = 0 \qquad (2.24)$$

The second possibility occurs when the impulse of the frictional force cannot prevent sliding. This corresponds to an impulse ratio which exceeds the coefficient of friction μ. In this rigid body analysis we will not consider the cases of the object initially sticking and then sliding or vice versa. We will concentrate on the scenario that if the impacting body slides at the instant of impact it will continue to slide until the end of impact. Therefore, according to Coulomb Law of friction, if sliding occurs then the ratio of the impulsive forces will be governed by equation (2.20) or the dimensionless form (2.21).

Now that we have closed the system of equations for rigid body impact with (2.24) for no-sliding and (2.21) for sliding, we need to determine when to use which. This required condition can be stated mathematically as

$$\mu < \left| \frac{\hat{F}_x''}{\hat{F}_y''} \right| \qquad (2.25)$$

that is, if the absolute value of the ratio of the impulses exceeds the value of the coefficient of friction then sliding will occur. One question arises is whether to use the static or kinetic coefficient of friction. It has been shown through experiment [6] that, due to the short duration of impact, the kinetic coefficient of friction should be used in this analysis.

2.4 Post-Impact Quantities

The rigid body model of impact is good for approximating the velocities and rotation immediately after impact. In the next two subsections we will discuss the solution to the planar impact problem for two distinct regimes of impact. The two possible impact scenarios are: sliding or no sliding during impact. Also, the condition that determines the regime of impact will be derived.

2.4.1 No Sliding Case

In this subsection we will solve the impact problem for the case when no sliding occurs during impact. The five dimensionless governing equations have been derived in the previous subsections and are (2.16a,b,c), (2.19), and (2.24). Putting them in matrix form can be computationally useful, but we will also solve them directly. Doing this gives

$$\begin{bmatrix} 1 & 0 & 0 & 1 & 0 \\ 0 & 1 & 0 & 0 & -1 \\ 0 & 0 & \alpha & -\overline{R}_y & -\overline{R}_x \\ 0 & 1 & \overline{R}_x & 0 & 0 \\ 1 & 0 & -\overline{R}_y & 0 & 0 \end{bmatrix} \begin{bmatrix} V_x'' \\ V_y'' \\ \omega_z'' \\ \hat{F}_x'' \\ \hat{F}_y'' \end{bmatrix} = \begin{bmatrix} \rho_x \\ 1 \\ \alpha\lambda_z \\ -e_n\left(1+\lambda_z \overline{R}_x\right) \\ 0 \end{bmatrix} \tag{2.26}$$

We will begin by solving equations (2.16a) and (2.16b) for $\hat{F}_x''$ and $\hat{F}_y''$, respectively. Substituting these expressions into equation (2.16c), we eliminate the impulsive forces and are left with

$$\alpha\lambda_z + \left(\rho_x - V_x''\right)\overline{R}_y + \left(V_y'' - 1\right)\overline{R}_x = \alpha\omega_z'' \tag{2.27}$$

Solving (2.19) for V_y'' and (2.24) for V_x''

$$V_y'' = -\omega_z''\overline{R}_x - e_n\left(1+\lambda_z\overline{R}_x\right) \tag{2.28a}$$

$$V_x'' = \omega_z''\overline{R}_y \tag{2.28b}$$

Substituting (2.28a,b) into (2.27)

$$\alpha\lambda_z + \left(\rho_x - \omega_z''\overline{R}_y\right)\overline{R}_y + \left(-\omega_z''\overline{R}_x - e_n\left(1+\lambda_z\overline{R}_x\right)-1\right)\overline{R}_x = \alpha\omega_z''$$

Combining terms

$$\lambda_z\left(\alpha - e_n\overline{R}_x{}^2\right) + \left(\rho_x\overline{R}_y - \left(e_n+1\right)\overline{R}_x\right) - \omega_z''\left(\overline{R}_y{}^2 + \overline{R}_x{}^2\right) = \alpha\omega_z''$$

Solving for ω_z''

$$\omega_z'' = \frac{\left(\rho_x\overline{R}_y - \left(e_n+1\right)\overline{R}_x\right) + \lambda_z\left(\alpha - e_n\overline{R}_x{}^2\right)}{\alpha + \left(\overline{R}_y{}^2 + \overline{R}_x{}^2\right)}$$

Recall the definitions (2.15a) and (2.15b) and substitute them into the above

$$\omega_z'' = \left(\frac{1}{\alpha+1}\right)\left[-\rho_x\cos(\gamma) - \left(e_n+1\right)\sin(\gamma) + \lambda_z\left(\alpha - e_n\sin^2(\gamma)\right)\right] \qquad (2.29)$$

Equation (2.29) gives the dimensionless expression for the final angular velocity in an impact where no sliding occurs. Substituting equation (2.29) into equation (2.28b) and using equation (2.15b) we obtain

$$V_x'' = \left(\frac{1}{\alpha+1}\right)\left[\rho_x\cos^2(\gamma) + \left(e_n+1\right)\cos(\gamma)\sin(\gamma) - \lambda_z\left(\alpha - e_n\sin^2(\gamma)\right)\cos(\gamma)\right] \quad (2.30)$$

Equation (2.30) is the expression for the final horizontal component of velocity for the no sliding case. Similarly substituting (2.29) into (2.28a) gives

$$V_y'' = \left(\frac{1}{\alpha+1}\right)\left[\rho_x\cos(\gamma)\sin(\gamma) + \left(e_n+1\right)\sin^2(\gamma) - \lambda_z\left(\alpha - e_n\sin^2(\gamma)\right)\sin(\gamma)\right] - e_n\left(1+\lambda_z\sin(\gamma)\right)$$

Simplifying further

$$V_y'' = \left(\frac{1}{\alpha+1}\right)\left[\rho_x\cos(\gamma)\sin(\gamma) + \left(e_n+1\right)\sin^2(\gamma) - \lambda_z\left(\alpha - e_n\sin^2(\gamma) + e_n\left(\alpha+1\right)\right)\sin(\gamma)\right] - e_n$$

$$V_y'' = \left(\frac{1}{\alpha+1}\right)\left[\rho_x\cos(\gamma)\sin(\gamma) + \left(e_n+1\right)\sin^2(\gamma) - \lambda_z\left(\alpha\left(e_n+1\right) + e_n\left(1-\sin^2(\gamma)\right)\right)\sin(\gamma)\right] - e_n$$

Recalling the trigonometric identity $\cos^2(\gamma)+\sin^2(\gamma)=1$ we arrive at

$$V_y'' = \left(\frac{1}{\alpha+1}\right)\left[\rho_x \cos(\gamma)\sin(\gamma)+(e_n+1)\sin^2(\gamma)-\lambda_z\left(\alpha(e_n+1)+e_n\cos^2(\gamma)\right)\sin(\gamma)\right]-e_n \tag{2.31}$$

Equation (2.31) is the expression for the final vertical velocity. We have therefore solved the rigid body impact problem for the case of no sliding during impact. We can also put the final solution in matrix form as

$$\begin{bmatrix} V_x'' \\ V_y'' \\ \omega_z'' \end{bmatrix} = \left(\frac{1}{\alpha+1}\right)\left\langle \begin{bmatrix} \cos^2(\gamma) & -\left(\alpha-e_n\sin^2(\gamma)\right)\cos(\gamma) \\ \cos(\gamma)\sin(\gamma) & -\left(\alpha(e_n+1)+e_n\cos^2(\gamma)\right)\sin(\gamma) \\ -\cos(\gamma) & \left(\alpha-e_n\sin^2(\gamma)\right) \end{bmatrix}\begin{bmatrix} \rho_x \\ \lambda_z \end{bmatrix} + \begin{bmatrix} (e_n+1)\cos(\gamma)\sin(\gamma) \\ \sin^2(\gamma)-e_n\left(\alpha+\cos^2(\gamma)\right) \\ -(e_n+1)\sin(\gamma) \end{bmatrix}\right\rangle \tag{2.32}$$

2.4.2 Sliding Case

We will now solve the problem of rigid body impact for the case when sliding occurs during impact. As for the no sliding case, the system of equations consists of (2.16a,b,c) and (2.19), but the last required equation will now be (2.21). Let us re-express equation (2.21) as follows. We can further simplify the expression by noting that the vertical component of the impact force will always act in the positive direction.

$$\left|\hat{F}_x''\right| = \mu\left|\hat{F}_y''\right| \tag{2.33}$$

On the other hand, the direction of the horizontal component of the impact force will depend solely on the direction of the horizontal component of the initial contact point velocity.

$$\left(\hat{F}_x''\right)\mathrm{sgn}\left(-\vec{V}^C\cdot\hat{i}\right) = \mu\left(\hat{F}_y''\right) \tag{2.34}$$

Substituting (2.4) into above we obtain the following expression

$$\left(\hat{F}_x''\right)\text{sgn}\left(-V_x+\omega_z R_y\right)=\mu\left(\hat{F}_y''\right)$$

which we will now nondimensionalize with respect to V_y. But, one must keep in mind that, in the specified coordinate system, in order for the object to strike the impacting surface it must initially have a negative vertical component of velocity; therefore the quantity inside the $\text{sgn}(\ )$ term must be negated to preserve its purpose.

$$\left(\hat{F}_x''\right)\text{sgn}\left(\rho_x-\lambda_z\overline{R}_y\right)=\mu\left(\hat{F}_y''\right) \tag{2.35}$$

In order to simplify the calculation let us restate equation (2.35) as follows

$$\left(\hat{F}_x''\right)=\overline{\mu}\left(\hat{F}_y''\right) \tag{2.36}$$

where $\overline{\mu}=\mu\,\text{sgn}\left(\rho_x-\lambda_z\overline{R}_y\right)$.

This full system of equations can once again be expressed in matrix form for computational convenience. Hence,

$$\begin{bmatrix}1&0&0&1&0\\0&1&0&0&-1\\0&0&\alpha&-\overline{R}_y&-\overline{R}_x\\0&1&\overline{R}_x&0&0\\0&0&0&1&-\overline{\mu}\end{bmatrix}\begin{bmatrix}V_x''\\V_y''\\\omega_z''\\\hat{F}_x''\\\hat{F}_y''\end{bmatrix}=\begin{bmatrix}\rho_x\\1\\\alpha\lambda_z\\-e_n\left(1+\lambda_z\overline{R}_x\right)\\0\end{bmatrix} \tag{2.37}$$

But we will also work out the analytical expressions for the post-impact velocities and angular velocity. As in the previous section, we can solve equation (2.16a) for $\hat{F}_x''$ and equation (2.16b) for $\hat{F}_y''$ and substitute into (2.16c) to obtain (2.27). Thus,

$$\alpha\lambda_z+\left(\rho_x-V_x''\right)\overline{R}_y+\left(V_y''-1\right)\overline{R}_x=\alpha\omega_z'' \tag{2.27}$$

$$\hat{F}_x''=\rho_x-V_x'' \tag{2.38a}$$

$$\hat{F}_y''=V_y''-1 \tag{2.38b}$$

Substituting equation (2.38a,b) into (2.36)

$$\left(\rho_x - V_x''\right) = \bar{\mu}\left(V_y'' - 1\right) \tag{2.39}$$

Solving equation (2.39) for V_x'' gives

$$V_x'' = \rho_x - \bar{\mu}\left(V_y'' - 1\right) \tag{2.40}$$

Solving equation (2.19) for ω_z'' yields

$$\omega_z'' = \frac{1}{\bar{R}_x}\left(-e_n\left(1+\lambda_z \bar{R}_x\right) - V_y''\right) \tag{2.41}$$

Substituting equations (2.40) and (2.41) into equation (2.27) results in

$$\alpha\lambda_z + \left(\rho_x - \left(\rho_x - \bar{\mu}\left(V_y'' - 1\right)\right)\right)\bar{R}_y + \left(V_y'' - 1\right)\bar{R}_x = \alpha\left(\frac{1}{\bar{R}_x}\left(-e_n\left(1+\lambda_z \bar{R}_x\right) - V_y''\right)\right)$$

Multiplying through by $\bar{R}_x$ and simplifying gives

$$\alpha\lambda_z \bar{R}_x + \bar{\mu}\left(V_y'' - 1\right)\bar{R}_y \bar{R}_x + \left(V_y'' - 1\right)\bar{R}_x^{\,2} = -\alpha e_n\left(1+\lambda_z \bar{R}_x\right) - \alpha V_y''$$

Combining terms yields

$$\lambda_z \alpha\left(e_n + 1\right)\bar{R}_x + \alpha e_n - \left(\bar{\mu}\bar{R}_y \bar{R}_x + \bar{R}_x^{\,2}\right) = -V_y''\left(\alpha + \bar{\mu}\bar{R}_y \bar{R}_x + \bar{R}_x^{\,2}\right)$$

Solving for V_y'' we have that

$$V_y'' = \frac{\left(\bar{\mu}\bar{R}_y \bar{R}_x + \bar{R}_x^{\,2} - \alpha e_n\right) - \lambda_z \alpha\left(e_n + 1\right)\bar{R}_x}{\alpha + \bar{\mu}\bar{R}_y \bar{R}_x + \bar{R}_x^{\,2}} \tag{2.42}$$

Equation (2.42) is the final vertical velocity for the impact during which sliding takes place. Upon substituting the above into equation (2.40) we obtain the horizontal component of the post-impact velocity,

$$V_x'' = \rho_x - \bar{\mu}\left(\frac{\left(\bar{\mu}\bar{R}_y \bar{R}_x + \bar{R}_x^{\,2}\right) - \alpha e_n - \lambda_z \alpha\left(e_n + 1\right)\bar{R}_x}{\alpha + \bar{\mu}\bar{R}_y \bar{R}_x + \bar{R}_x^{\,2}} - 1\right)$$

Simplifying this expression,

$$V_x'' = \rho_x + \bar{\mu}\left(\frac{\alpha(e_n+1) + \lambda_z \alpha(e_n+1)\bar{R}_x}{\alpha + \bar{\mu}\bar{R}_y \bar{R}_x + \bar{R}_x^{\,2}} \right) \tag{2.43}$$

Combining terms we arrive at the following,

$$V_x'' = \frac{\rho_x\left(\alpha + \bar{\mu}\bar{R}_y \bar{R}_x + \bar{R}_x^{\,2}\right) + \bar{\mu}\alpha(e_n+1) + \lambda_z \bar{\mu}\alpha(e_n+1)\bar{R}_x}{\alpha + \bar{\mu}\bar{R}_y \bar{R}_x + \bar{R}_x^{\,2}} \tag{2.44}$$

In order to simplify the calculation of the final angular velocity let us consider the following quantities which will utilize equations (2.42) and (2.43):

$$\hat{F}_x'' = \left(\rho_x - V_x''\right) = \bar{\mu}\left(\frac{-\alpha(e_n+1) - \lambda_z \alpha(e_n+1)\bar{R}_x}{\alpha + \bar{\mu}\bar{R}_y \bar{R}_x + \bar{R}_x^{\,2}} \right) \tag{2.45}$$

$$\hat{F}_y'' = \left(V_y'' - 1\right) = \left(\frac{-\alpha(e_n+1) - \lambda_z \alpha(e_n+1)\bar{R}_x}{\alpha + \bar{\mu}\bar{R}_y \bar{R}_x + \bar{R}_x^{\,2}} \right) \tag{2.46}$$

Substituting equations (2.45) and (2.46) into equation (2.27) gives

$$\alpha\lambda_z + \bar{\mu}\left(\frac{-\alpha(e_n+1) - \lambda_z \alpha(e_n+1)\bar{R}_x}{\alpha + \bar{\mu}\bar{R}_y \bar{R}_x + \bar{R}_x^{\,2}} \right)\bar{R}_y + \left(\frac{-\alpha(e_n+1) - \lambda_z \alpha(e_n+1)\bar{R}_x}{\alpha + \bar{\mu}\bar{R}_y \bar{R}_x + \bar{R}_x^{\,2}} \right)\bar{R}_x = \alpha\omega_z''$$

$$\omega_z'' = \lambda_z - \frac{\left(\bar{\mu}\bar{R}_y + \bar{R}_x\right)\left((e_n+1) + \lambda_z(e_n+1)\bar{R}_x\right)}{\alpha + \bar{\mu}\bar{R}_y \bar{R}_x + \bar{R}_x^{\,2}} \tag{2.47}$$

Combining terms we obtain

$$\omega_z'' = \frac{-(e_n+1)\left(\bar{\mu}\bar{R}_y + \bar{R}_x\right) + \lambda_z\left(-(e_n+1)\left(\bar{\mu}\bar{R}_y + \bar{R}_x\right)\bar{R}_x + \alpha + \bar{\mu}\bar{R}_y \bar{R}_x + \bar{R}_x^{\,2}\right)}{\alpha + \bar{\mu}\bar{R}_y \bar{R}_x + \bar{R}_x^{\,2}}$$

$$\omega_z'' = \frac{-(e_n+1)\left(\bar{\mu}\bar{R}_y + \bar{R}_x\right) + \lambda_z\left(-e_n\left(\bar{\mu}\bar{R}_y + \bar{R}_x\right)\bar{R}_x + \alpha\right)}{\alpha + \bar{\mu}\bar{R}_y \bar{R}_x + \bar{R}_x^{\,2}} \tag{2.48}$$

Equation (2.48) is the expression for the post-impact angular velocity for the case when sliding occurs during impact. Using definitions (2.15a,b) we can obtain the expression for the final quantities in terms of the orientation angle γ. Hence,

$$V_y'' = \frac{\left(-\bar{\mu}\cos(\gamma)\sin(\gamma)+\sin^2(\gamma)-\alpha e_n\right)-\lambda_z\alpha(e_n+1)\sin(\gamma)}{\left(\alpha-\bar{\mu}\cos(\gamma)\sin(\gamma)+\sin^2(\gamma)\right)} \tag{2.49}$$

$$V_x'' = \frac{\rho_x\left(\alpha-\bar{\mu}\cos(\gamma)\sin(\gamma)+\sin^2(\gamma)\right)+\bar{\mu}\alpha(e_n+1)+\lambda_z\bar{\mu}\alpha(e_n+1)\sin(\gamma)}{\left(\alpha-\bar{\mu}\cos(\gamma)\sin(\gamma)+\sin^2(\gamma)\right)} \tag{2.50}$$

$$\omega_z'' = \frac{-(e_n+1)\left(-\bar{\mu}\cos(\gamma)+\sin(\gamma)\right)+\lambda_z\left(-e_n\left(-\bar{\mu}\cos(\gamma)+\sin(\gamma)\right)\sin(\gamma)+\alpha\right)}{\left(\alpha-\bar{\mu}\cos(\gamma)\sin(\gamma)+\sin^2(\gamma)\right)} \tag{2.51}$$

Expression (2.52) shows the solution in matrix form.

$$\begin{bmatrix} V_x'' \\ V_y'' \\ \omega_z'' \end{bmatrix} = \begin{bmatrix} 1 & \left[\dfrac{\bar{\mu}\alpha(e_n+1)\sin(\gamma)}{\left(\alpha-\bar{\mu}\cos(\gamma)\sin(\gamma)+\sin^2(\gamma)\right)}\right] \\ 0 & \left[\dfrac{-\alpha(e_n+1)\sin(\gamma)}{\left(\alpha-\bar{\mu}\cos(\gamma)\sin(\gamma)+\sin^2(\gamma)\right)}\right] \\ 0 & \left[\dfrac{-e_n\left(-\bar{\mu}\cos(\gamma)+\sin(\gamma)\right)\sin(\gamma)+\alpha}{\left(\alpha-\bar{\mu}\cos(\gamma)\sin(\gamma)+\sin^2(\gamma)\right)}\right] \end{bmatrix} \begin{bmatrix} \rho_x \\ \lambda_z \end{bmatrix} + \begin{bmatrix} \left[\dfrac{\bar{\mu}\alpha(e_n+1)}{\left(\alpha-\bar{\mu}\cos(\gamma)\sin(\gamma)+\sin^2(\gamma)\right)}\right] \\ \left[\dfrac{\left(-\alpha e_n-\bar{\mu}\cos(\gamma)\sin(\gamma)+\sin^2(\gamma)\right)}{\left(\alpha-\bar{\mu}\cos(\gamma)\sin(\gamma)+\sin^2(\gamma)\right)}\right] \\ \left[\dfrac{-(e_n+1)\left(-\bar{\mu}\cos(\gamma)+\sin(\gamma)\right)}{\left(\alpha-\bar{\mu}\cos(\gamma)\sin(\gamma)+\sin^2(\gamma)\right)}\right] \end{bmatrix} \tag{2.52}$$

Now that we have solved both problems of sliding and no sliding during impact, we need to determine when to use which set of equations. The sliding condition is given by equation (2.25) and is based on the idea that sliding will commence if the force ratio exceeds the value of the coefficient of friction. We will use this idea to obtain a general expression for the sliding condition in terms of the initial impact parameters. Nondimensionalizing equation (2.25) we get

$$\frac{\left(\rho_x - V_x''\right)}{\left(V_y''-1\right)} > \bar{\mu} \tag{2.53}$$

Substituting equations (2.30) and (2.31) into above

$$\frac{\left(\rho_x - \left(\frac{1}{\alpha+1}\right)\left[\rho_x \cos^2(\gamma) + (e_n+1)\cos(\gamma)\sin(\gamma) - \lambda_z\left(\alpha - e_n \sin^2(\gamma)\right)\cos(\gamma)\right]\right)}{\left(\left(\frac{1}{\alpha+1}\right)\left[\rho_x \cos(\gamma)\sin(\gamma) + (e_n+1)\sin^2(\gamma) - \lambda_z\left(\alpha(e_n+1) + e_n\cos^2(\gamma)\right)\sin(\gamma)\right] - e_n - 1\right)} > \bar{\mu}$$

Combining terms and simplifying,

$$\frac{\rho_x\left(\alpha + 1 - \cos^2(\gamma)\right) - (e_n+1)\cos(\gamma)\sin(\gamma) + \lambda_z\left(\alpha - e_n\sin^2(\gamma)\right)\cos(\gamma)}{\rho_x\cos(\gamma)\sin(\gamma) + (e_n+1)\left(\sin^2(\gamma) - \alpha - 1\right) - \lambda_z\left(\alpha(e_n+1) + e_n\cos^2(\gamma)\right)\sin(\gamma)} > \bar{\mu}$$

Further simplifying

$$\frac{\rho_x\left(\alpha + \sin^2(\gamma)\right) - (e_n+1)\cos(\gamma)\sin(\gamma) + \lambda_z\left(\alpha - e_n\sin^2(\gamma)\right)\cos(\gamma)}{\rho_x\cos(\gamma)\sin(\gamma) - (e_n+1)\left(\alpha + \cos^2(\gamma)\right) - \lambda_z\left(\alpha(e_n+1) + e_n\cos^2(\gamma)\right)\sin(\gamma)} > \bar{\mu} \tag{2.54}$$

Substituting the expression for $\bar{\mu}$ into (2.54) and simplifying we get the final sliding condition.

$$\mu < \frac{\operatorname{sgn}\left(\rho_x + \lambda_z\cos(\gamma)\right)\left(\rho_x\left(\alpha + \sin^2(\gamma)\right) - (e_n+1)\cos(\gamma)\sin(\gamma) + \lambda_z\left(\alpha - e_n\sin^2(\gamma)\right)\cos(\gamma)\right)}{\left(\rho_x\cos(\gamma)\sin(\gamma) - (e_n+1)\left(\alpha + \cos^2(\gamma)\right) - \lambda_z\left(\alpha(e_n+1) + e_n\cos^2(\gamma)\right)\sin(\gamma)\right)} \tag{2.55}$$

2.5 Comparison of the (e_n, μ) and (e_y, e_x) Models

Another way of posing the impact problem is to define vertical and horizontal coefficients of restitution e_y and e_x, rather than define the coefficient of restitution e_n and the coefficient of friction μ. The vertical coefficient of restitution e_y will be defined the same way as e_n, via equation (2.19). The horizontal coefficient of restitution will be

defined as the negative ratio of final to initial horizontal components of the contact point velocity and is given by the following.

$$e_x = -\frac{\vec{V}'^{CP} \cdot \hat{i}}{\vec{V}^{CP} \cdot \hat{i}} \tag{2.56}$$

Substituting equations (2.4) and (2.7) into above we obtain the following:

$$e_x = -\frac{V_x' - \omega_z' R_y}{V_x - \omega_z R_y} \tag{2.57}$$

Nondimensionalizing (2.57) by dividing with V_y gives

$$e_x = -\frac{V_x'' - \omega_z'' \overline{R}_y}{\rho_x - \lambda_z \overline{R}_y} \tag{2.58}$$

Defining e_y using (2.19) gives

$$e_y = -\frac{V_y'' + \omega_z'' \overline{R}_x}{1 + \lambda_z \overline{R}_x} \tag{2.59}$$

Once again we now have five equations, (2.16a,b,c), (2.58), and (2.59), and five unknowns, $V_x'', V_y'', \omega_z'', \hat{F}_x'', \hat{F}_y''$. We will now solve this system for the post-impact quantities using the (e_y, e_x) model. Solving equations (2.16a) and (2.16b) for the impulses and substituting into equation (2.16c) we get equation (2.27). Now, solving equation (2.58) for V_x'' and equation (2.59) for V_y'' and substituting them into eq. (2.27)

$$V_x'' = -e_x\left(\rho_x - \lambda_z \overline{R}_y\right) + \omega_z'' \overline{R}_y \tag{2.60}$$

$$V_y'' = -e_y\left(1 + \lambda_z \overline{R}_x\right) - \omega_z'' \overline{R}_x \tag{2.61}$$

$$\alpha\lambda_z + \left(\rho_x + e_x\left(\rho_x - \lambda_z \overline{R}_y\right) - \omega_z'' \overline{R}_y\right)\overline{R}_y + \left(-e_y\left(1 + \lambda_z \overline{R}_x\right) - \omega_z'' \overline{R}_x - 1\right)\overline{R}_x = \alpha\omega_z'' \tag{2.62}$$

Combining terms in equation (2.62) yields

$$\rho_x(e_x+1)\overline{R}_y-(e_y+1)\overline{R}_x+\lambda_z\left(\alpha-e_x\overline{R}_y{}^2-e_y\overline{R}_x{}^2\right)=\left(\alpha+\overline{R}_y{}^2+\overline{R}_x{}^2\right)\omega_z''$$

Recalling that $\overline{R}_y{}^2+\overline{R}_x{}^2=1$ and solving for ω_z'' we get the final angular velocity,

$$\omega_z''=\left(\frac{1}{\alpha+1}\right)\left[\rho_x(e_x+1)\overline{R}_y-(e_y+1)\overline{R}_x+\lambda_z\left(\alpha-e_x\overline{R}_y{}^2-e_y\overline{R}_x{}^2\right)\right] \qquad (2.63)$$

Substituting equation (2.63) into (2.60) gives

$$V_x''=-e_x\left(\rho_x-\lambda_z\overline{R}_y\right)+\left(\frac{1}{\alpha+1}\right)\left[\rho_x(e_x+1)\overline{R}_y-(e_y+1)\overline{R}_x+\lambda_z\left(\alpha-e_x\overline{R}_y{}^2-e_y\overline{R}_x{}^2\right)\right]\overline{R}_y$$

Simplifying the above, we have

$$V_x''=\left(\frac{1}{\alpha+1}\right)\left[-e_x\left(\rho_x-\lambda_z\overline{R}_y\right)(\alpha+1)+\rho_x(e_x+1)\overline{R}_y{}^2-(e_y+1)\overline{R}_x\,\overline{R}_y+\lambda_z\left(\alpha-e_x\overline{R}_y{}^2-e_y\overline{R}_x{}^2\right)\overline{R}_y\right]$$

Combining terms

$$V_x''=\left(\frac{1}{\alpha+1}\right)\left[\rho_x\left((e_x+1)\overline{R}_y{}^2-e_x(\alpha+1)\right)-(e_y+1)\overline{R}_x\,\overline{R}_y+\lambda_z\left(\alpha-e_x\overline{R}_y{}^2-e_y\overline{R}_x{}^2+e_x(\alpha+1)\right)\overline{R}_y\right]$$

$$V_x''=\left(\frac{1}{\alpha+1}\right)\left[\rho_x\left(\overline{R}_y{}^2-e_x\left(\alpha+\overline{R}_x{}^2\right)\right)-(e_y+1)\overline{R}_x\,\overline{R}_y+\lambda_z\left(\alpha-e_y\overline{R}_x{}^2+e_x\left(\alpha+\overline{R}_x{}^2\right)\right)\overline{R}_y\right]$$

(2.64)

Equation (2.64) is the expression for the final horizontal velocity using this impact model.

We will obtain the final vertical velocity by substituting (2.63) into (2.61). This gives

$$V_y''=-e_y\left(1+\lambda_z\overline{R}_x\right)-\left(\frac{1}{\alpha+1}\right)\left[\rho_x(e_x+1)\overline{R}_y-(e_y+1)\overline{R}_x+\lambda_z\left(\alpha-e_x\overline{R}_y{}^2-e_y\overline{R}_x{}^2\right)\right]\overline{R}_x$$

Simplifying the above gives,

$$V_y''=\left(\frac{1}{\alpha+1}\right)\left[-e_y\left(\lambda_z\overline{R}_x\right)(\alpha+1)-\rho_x(e_x+1)\overline{R}_x\overline{R}_y+(e_y+1)\overline{R}_x{}^2-\lambda_z\left(\alpha-e_x\overline{R}_y{}^2-e_y\overline{R}_x{}^2\right)\overline{R}_x\right]-e_y$$

After combining terms we have

$$V_y'' = \left(\frac{1}{\alpha+1}\right)\left[-\rho_x(e_x+1)\overline{R}_x\overline{R}_y + (e_y+1)\overline{R}_x^{\,2} - \lambda_z\left(\alpha - e_x\overline{R}_y^{\,2} - e_y\overline{R}_x^{\,2} + e_y(\alpha+1)\right)\overline{R}_x\right] - e_y$$

Finally we obtain the expression for the final vertical velocity.

$$V_y'' = \left(\frac{1}{\alpha+1}\right)\left[-\rho_x(e_x+1)\overline{R}_x\overline{R}_y + (e_y+1)\overline{R}_x^{\,2} - \lambda_z\left(\alpha - e_x\overline{R}_y^{\,2} + e_y\left(\alpha + \overline{R}_y^{\,2}\right)\right)\overline{R}_x\right] - e_y \tag{2.65}$$

Comparing this (e_y, e_x) model to the (e_n, μ) model, we see that the no sliding case corresponds to $e_x = 0$. This statement guaranties that the final horizontal velocity of the contact region will be zero. Substituting $e_x = 0$ into equations (2.63), (2.64), and (2.65), results in the following system of the equations.

$$\omega_z'' = \left(\frac{1}{\alpha+1}\right)\left[\rho_x\overline{R}_y - (e_y+1)\overline{R}_x + \lambda_z\left(\alpha - e_y\overline{R}_x^{\,2}\right)\right] \tag{2.66a}$$

$$V_x'' = \left(\frac{1}{\alpha+1}\right)\left[\rho_x\overline{R}_y^{\,2} - (e_y+1)\overline{R}_x\,\overline{R}_y + \lambda_z\left(\alpha - e_y\overline{R}_x^{\,2}\right)\overline{R}_y\right] \tag{2.66b}$$

$$V_y'' = \left(\frac{1}{\alpha+1}\right)\left[-\rho_x\overline{R}_x\overline{R}_y + (e_y+1)\overline{R}_x - \lambda_z\left(\alpha + e_y\left(\alpha + \overline{R}_y^{\,2}\right)\right)\overline{R}_x\right] - e_y \tag{2.66c}$$

For easier comparison, let us use equations (2.15a,b) to simplify equations (2.66)

$$\omega_z'' = \left(\frac{1}{\alpha+1}\right)\left[-\rho_x\cos(\gamma) - (e_y+1)\sin(\gamma) + \lambda_z\left(\alpha - e_y\sin^2(\gamma)\right)\right] \tag{2.67a}$$

$$V_x'' = \left(\frac{1}{\alpha+1}\right)\left[\rho_x\cos^2(\gamma) + (e_y+1)\cos(\gamma)\sin(\gamma) - \lambda_z\left(\alpha - e_y\sin^2(\gamma)\right)\cos(\gamma)\right] \tag{2.67b}$$

$$V_y'' = \left(\frac{1}{\alpha+1}\right)\left[\rho_x\cos(\gamma)\sin(\gamma) + (e_y+1)\sin(\gamma) - \lambda_z\left(\alpha + e_y\left(\alpha + \cos^2(\gamma)\right)\right)\sin(\gamma)\right] - e_y$$

(2.67c)

Comparing equations (2.67a,b,c) to equation (2.29), (2.30), and (2.31) we see that they are identical. We can also obtain the general expressions for the final velocities of the (e_y, e_x) model in terms of the orientation angle γ. Substituting equations (2.15a,b) into equations (2.63), (2.64), and (2.65) results in the following.

$$\omega_z'' = \left(\frac{1}{\alpha+1}\right)\begin{bmatrix} -\rho_x(e_x+1)\cos(\gamma) - (e_y+1)\sin(\gamma) \\ +\lambda_z(\alpha - e_x\cos^2(\gamma) - e_y\sin^2(\gamma)) \end{bmatrix} \tag{2.68a}$$

$$V_x'' = \left(\frac{1}{\alpha+1}\right)\begin{bmatrix} \rho_x(\cos^2(\gamma) - e_x(\alpha+\sin^2(\gamma))) + (e_y+1)\cos(\gamma)\sin(\gamma) \\ -\lambda_z(\alpha - e_y\sin^2(\gamma) + e_x(\alpha+\sin^2(\gamma)))\cos(\gamma) \end{bmatrix} \tag{2.68b}$$

$$V_y'' = \left(\frac{1}{\alpha+1}\right)\begin{bmatrix} \rho_x(e_x+1)\cos(\gamma)\sin(\gamma) + (e_y+1)\sin^2(\gamma) \\ -\lambda_z(\alpha - e_x\cos^2(\gamma) + e_y(\alpha+\cos^2(\gamma)))\sin(\gamma) \end{bmatrix} - e_y \tag{2.68c}$$

Putting equations (2.68a,b,c) in matrix form gives

$$\begin{bmatrix} V_x'' \\ V_y'' \\ \omega_z'' \end{bmatrix} = \begin{bmatrix} \left[\frac{(\cos^2(\gamma) - e_x(\alpha+\sin^2(\gamma)))}{(\alpha+1)}\right] & \left[\frac{-(\alpha - e_y\sin^2(\gamma) + e_x(\alpha+\sin^2(\gamma)))\cos(\gamma)}{(\alpha+1)}\right] \\ \left[\frac{(e_x+1)\cos(\gamma)\sin(\gamma)}{(\alpha+1)}\right] & \left[\frac{-(\alpha - e_x\cos^2(\gamma) + e_y(\alpha+\cos^2(\gamma)))\sin(\gamma)}{(\alpha+1)}\right] \\ \left[\frac{-(e_x+1)\cos(\gamma)}{(\alpha+1)}\right] & \left[\frac{(\alpha - e_x\cos^2(\gamma) - e_y\sin^2(\gamma))}{(\alpha+1)}\right] \end{bmatrix} \begin{bmatrix} \rho_x \\ \lambda_z \end{bmatrix} + \begin{bmatrix} \left[\frac{(e_y+1)\cos(\gamma)\sin(\gamma)}{(\alpha+1)}\right] \\ \left[\frac{(e_y+1)\sin^2(\gamma) - e_y(\alpha+1)}{(\alpha+1)}\right] \\ \left[\frac{-(e_y+1)\sin(\gamma)}{(\alpha+1)}\right] \end{bmatrix} \tag{2.69}$$

Now we need to compare the coefficient of friction, $\bar{\mu}$, to the horizontal coefficient of restitution, e_x. Let us begin by substituting equations (2.60) and (2.61) into equation (2.39) to obtain

$$(\rho_x + e_x(\rho_x - \lambda_z\bar{R}_y) - \omega_z''\bar{R}_y) = \bar{\mu}(-e_y(1+\lambda_z\bar{R}_x) - \omega_z''\bar{R}_x - 1) \tag{2.70}$$

Solving equation (2.70) for $\bar{\mu}$ and simplifying gives

$$\bar{\mu} = \frac{\left(-\rho_x(e_x+1)+\lambda_z e_x \bar{R}_y + \omega_z'' \bar{R}_y\right)}{\left((e_y+1)+\lambda_z e_y \bar{R}_x + \omega_z'' \bar{R}_x\right)} \tag{2.71}$$

Substituting the expression for the final angular velocity equation (2.63) into equation (2.71) results in

$$\bar{\mu} = \frac{\left(-\rho_x(e_x+1)+\lambda_z e_x \bar{R}_y + \left(\frac{1}{\alpha+1}\right)\left[\rho_x(e_x+1)\bar{R}_y - (e_y+1)\bar{R}_x + \lambda_z\left(\alpha - e_x\bar{R}_y^{\,2} - e_y\bar{R}_x^{\,2}\right)\right]\bar{R}_y\right)}{\left((e_y+1)+\lambda_z e_y \bar{R}_x + \left(\frac{1}{\alpha+1}\right)\left[\rho_x(e_x+1)\bar{R}_y - (e_y+1)\bar{R}_x + \lambda_z\left(\alpha - e_x\bar{R}_y^{\,2} - e_y\bar{R}_x^{\,2}\right)\right]\bar{R}_x\right)} \tag{2.72}$$

Simplifying equation (2.72) gives

$$\bar{\mu} = \frac{\left(-\rho_x(\alpha+1)(e_x+1)+\lambda_z(\alpha+1)e_x\bar{R}_y + \rho_x(e_x+1)\bar{R}_y^{\,2} - (e_y+1)\bar{R}_x\bar{R}_y + \lambda_z\left(\alpha - e_x\bar{R}_y^{\,2} - e_y\bar{R}_x^{\,2}\right)\bar{R}_y\right)}{\left((\alpha+1)(e_y+1)+\lambda_z(\alpha+1)e_y\bar{R}_x + \rho_x(e_x+1)\bar{R}_x\bar{R}_y - (e_y+1)\bar{R}_x^{\,2} + \lambda_z\left(\alpha - e_x\bar{R}_y^{\,2} - e_y\bar{R}_x^{\,2}\right)\bar{R}_x\right)}$$

Combining terms

$$\bar{\mu} = \frac{\left(\rho_x(e_x+1)\left(-\alpha-1+\bar{R}_y^{\,2}\right) - (e_y+1)\bar{R}_x\bar{R}_y + \lambda_z\left(\alpha(e_x+1)+e_x\left(1-\bar{R}_y^{\,2}\right) - e_y\bar{R}_x^{\,2}\right)\bar{R}_y\right)}{\left(\rho_x(e_x+1)\bar{R}_x\bar{R}_y + (e_y+1)\left(\alpha+1-\bar{R}_x^{\,2}\right) + \lambda_z\left(\alpha(e_y+1) - e_x\bar{R}_y^{\,2} + e_y\left(1-\bar{R}_x^{\,2}\right)\right)\bar{R}_x\right)}$$

Further simplifying

$$\bar{\mu} = \frac{\left(-\rho_x(e_x+1)\left(\alpha+\bar{R}_x^{\,2}\right) - (e_y+1)\bar{R}_x\bar{R}_y - \lambda_z\left(-\alpha(e_x+1)+(e_y-e_x)\bar{R}_x^{\,2}\right)\bar{R}_y\right)}{\left(\rho_x(e_x+1)\bar{R}_x\bar{R}_y + (e_y+1)\left(\alpha+\bar{R}_y^{\,2}\right) + \lambda_z\left(\alpha(e_y+1)+(e_y-e_x)\bar{R}_y^{\,2}\right)\bar{R}_x\right)}$$

Upon substituting equations (2.15a,b) into the above, we obtain the expression in terms of the orientation angle γ. Hence,

$$\bar{\mu} = \frac{\left(-\rho_x(e_x+1)\left(\alpha+\sin^2(\gamma)\right) + (e_y+1)\cos(\gamma)\sin(\gamma) + \lambda_z\left(-\alpha(e_x+1)+(e_y-e_x)\sin^2(\gamma)\right)\cos(\gamma)\right)}{\left(-\rho_x(e_x+1)\cos(\gamma)\sin(\gamma) + (e_y+1)\left(\alpha+\cos^2(\gamma)\right) + \lambda_z\left(\alpha(e_y+1)+(e_y-e_x)\cos^2(\gamma)\right)\sin(\gamma)\right)} \tag{2.73}$$

Equation (2.73) is the final link between the two impact models we are considering. Note that if e_x is equal to zero, $\bar{\mu}$ is not necessarily equal to zero. For that case, equation

(2.73) gives the force ratio as a function of the orientation angle, γ, if all other parameters are held constant.

2.6 Energy Loss

A very important indicator of the survivability and/or damage of the object is the energy which it absorbs. The emphasis of this subsection is to develop a relationship for the energy loss during impact for both the sliding and no sliding cases. These expressions can then be used to determine the initial parameters which will yield the smallest energy loss. Typically, a smaller energy loss during impact corresponds to the object absorbing less energy, which is favorable.

The initial and final kinetic energies of the object can be expressed as follows

$$K_{initial} = \tfrac{1}{2} m\left(V_x^{\,2} + V_y^{\,2}\right) + \tfrac{1}{2} I_G \omega_z^{\,2} \tag{2.74a}$$

$$K_{final} = \tfrac{1}{2} m\left(V_x'^{2} + V_y'^{2}\right) + \tfrac{1}{2} I_G \omega_z'^{\,2} \tag{2.74b}$$

The difference in potential energy immediately before and after impact will be assumed to be negligible. The energy lost during impact can be stated mathematically as

$$K_{loss} = K_{initial} - K_{final} \tag{2.75}$$

Let us nondimensionalize equation (2.75) with respect to the initial kinetic energy. Hence,

$$\frac{K_{loss}}{K_{initial}} = 1 - \frac{\tfrac{1}{2} m\left(V_x'^{2} + V_y'^{2}\right) + \tfrac{1}{2} I_G \omega_z'^{\,2}}{\tfrac{1}{2} m\left(V_x^{\,2} + V_y^{\,2}\right) + \tfrac{1}{2} I_G \omega_z^{\,2}}$$

Recall that $I_G = \alpha m R^2$. Then,

$$\frac{K_{loss}}{K_{initial}} = 1 - \frac{\left(V_x'^{2} + V_y'^{2}\right) + \alpha\left(\omega_z'^{\,2} R^2\right)}{\left(V_x^{\,2} + V_y^{\,2}\right) + \alpha\left(\omega_z^{\,2} R^2\right)} \tag{2.76}$$

Multiplying equation (2.76) by $\frac{1/V_y^{\,2}}{1/V_y^{\,2}}$

$$\frac{K_{loss}}{K_{initial}} = 1 - \frac{V_x''^2 + V_y''^2 + \alpha\omega_z''^2}{\rho_x^{\,2} + 1 + \alpha\lambda_z^{\,2}} \tag{2.77}$$

Equation (2.77) gives the ratio of the energy lost during impact. All that remains is to substitute equations (2.29), (2.30), (2.31) for the no sliding case, or equations (2.49), (2.50), (2.51) for the sliding case into equation (2.77). We will not do this here in the complete form because the analytical expressions get rather cumbersome and the analysis is thereby hindered. In the next section we will obtain the energy loss expressions for two simplified cases: axis-symmetric objects and initially irrotational objects.

2.7 Simplifications

Now that we have finished the general solution to the planar impact problem we can see that the derived expressions are not easily analyzed by visual inspection. In order to gain insight about the behavior of the derived solution we will investigate a few special cases. The first simplification will be based on the assumption that the body is axisymmetric about the axis of rotation, such as a disk or a sphere. This will greatly simplify the derived expression for the final impact quantities and allow us to obtain a manageable expression for the kinetic energy loss during impact. The second simplification that will be used to abridge the solution is the assumption that the impacting body has no initial angular velocity. These two limiting cases of planar impact can be used to quickly obtain approximate solutions to more complex problems.

2.7.1 Axisymmetric Body

We know that for an axisymmetric body the impact force will have a line of action going through the center of mass, and hence that the orientation angle, γ, is zero. We will use this to simplify the no sliding and sliding equations, derive the energy loss for each case and lastly determine the simplified connection between the (e_n, μ) and (e_y, e_x) models. Let us begin by substituting $\gamma = 0$ into the no sliding equations for the final quantities defined in equations (2.29), (2.30), and (2.31). Doing this gives

$$\omega_z'' = \left(\frac{1}{\alpha+1}\right)\left[-\rho_x + \lambda_z\alpha\right] \tag{2.78a}$$

$$V_x'' = \left(\frac{1}{\alpha+1}\right)\left[\rho_x - \lambda_z\alpha\right] \tag{2.78b}$$

$$V_y'' = -e_n \tag{2.78c}$$

Substituting equations (2.78) into the energy loss expression given by equation (2.77), we arrive at

$$\frac{K_{loss}}{K_{initial}} = 1 - \frac{\left(\left(\frac{1}{\alpha+1}\right)\left[\rho_x - \lambda_z\alpha\right]\right)^2 + \left(-e_n\right)^2 + \alpha\left(\left(\frac{1}{\alpha+1}\right)\left[-\rho_x + \lambda_z\alpha\right]\right)^2}{{\rho_x}^2 + 1 + \alpha{\lambda_z}^2}$$

Simplifying gives

$$\frac{K_{loss}}{K_{initial}} = \frac{{\rho_x}^2 + 1 + \alpha{\lambda_z}^2 - \left(\frac{1}{\alpha+1}\right)\left(\rho_x - \lambda_z\alpha\right)^2 - \left(e_n\right)^2}{{\rho_x}^2 + 1 + \alpha{\lambda_z}^2}$$

Simplifying further we have that

$$\frac{K_{loss}}{K_{initial}} = \frac{\left(1 - {e_n}^2\right) + \left(\frac{\alpha}{\alpha+1}\right)\left(\rho_x + \lambda_z\right)^2}{{\rho_x}^2 + 1 + \alpha{\lambda_z}^2} \tag{2.79}$$

Looking at the RHS of equation (2.79) we see that the first term in the numerator is the energy lost in the vertical direction. The second term depends on $(\rho_x + \lambda_z)$, which is the horizontal component of the initial contact point velocity, and is therefore the energy lost in the horizontal direction.

Let us now determine the energy loss if the axisymmetric object slides during impact. After substituting $\gamma = 0$ into equations (2.49), (2.50), and (2.51), we get the following set of final velocities and angular velocity,

$$V_y'' = -e_n \tag{2.80a}$$

$$V_x'' = \rho_x + \bar{\mu}(e_n + 1) \tag{2.80b}$$

$$\omega_z'' = \frac{\bar{\mu}(e_n + 1) + \lambda_z \alpha}{\alpha} \tag{2.80c}$$

Substituting equation (2.80) into (2.77) we find the energy lost during a planar impact when sliding occurs.

$$\frac{K_{loss}}{K_{initial}} = 1 - \frac{\left(\rho_x + \bar{\mu}(e_n + 1)\right)^2 + (-e_n)^2 + \alpha\left(\frac{\bar{\mu}(e_n + 1) + \lambda_z \alpha}{\alpha}\right)^2}{\rho_x{}^2 + 1 + \alpha\lambda_z{}^2}$$

Simplifying

$$\frac{K_{loss}}{K_{initial}} = \frac{\rho_x{}^2 + 1 + \alpha\lambda_z{}^2 - \left(\rho_x + \bar{\mu}(e_n + 1)\right)^2 - (-e_n)^2 - \frac{1}{\alpha}\left(\bar{\mu}(e_n + 1) + \lambda_z \alpha\right)^2}{\rho_x{}^2 + 1 + \alpha\lambda_z{}^2}$$

Simplifying further

$$\frac{K_{loss}}{K_{initial}} = \frac{\left(1 - e_n{}^2\right) - 2(\rho_x + \lambda_z)\bar{\mu}(e_n + 1) - \frac{(\alpha + 1)}{\alpha}\bar{\mu}^2(e_n + 1)^2}{\rho_x{}^2 + 1 + \alpha\lambda_z{}^2} \tag{2.81}$$

We can also substitute the expression for $\bar{\mu}$ into equation (2.81) in order to obtain the energy loss in terms of the actual coefficient of friction μ. Recall the definition of $\bar{\mu}$, $\bar{\mu} = \mu \operatorname{sgn}(\rho_x + \lambda_z)$, where $(\rho_x + \lambda_z)$ is once again the contact point velocity for an axisymmetric object. Note that $\bar{\mu}^2 = \mu^2$, therefore equation (2.81) becomes

$$\frac{K_{loss}}{K_{initial}} = \frac{\left(1 - e_n^{\,2}\right) - 2(\rho_x + \lambda_z)\mu(e_n + 1)\operatorname{sgn}(\rho_x + \lambda_z) - \dfrac{(\alpha + 1)}{\alpha}\mu^2(e_n + 1)^2}{\rho_x^{\,2} + 1 + \alpha\lambda_z^{\,2}} \quad (2.82)$$

The first term in the numerator of equation (2.82) is once again the energy lost in the vertical direction. The second term is the energy lost in the horizontal direction because of its dependence on the contact point velocity. The last term can be viewed as coupling the energy loss in the horizontal and vertical directions.

In order to know when to use the no sliding equations and when to use the sliding equations we need to once again consider the critical value of the force ratio. Substituting $\gamma = 0$ into the sliding condition given by equation (2.55) we have the sliding condition for the impact of an axisymmetric body.

$$\mu < -\operatorname{sgn}(\rho_x + \lambda_z)\left(\frac{\alpha}{\alpha + 1}\right)\frac{(\rho_x + \lambda_z)}{(e_n + 1)} \quad (2.83)$$

We can also apply this energy loss derivation to the (e_y, e_x) impact model. Substituting $\gamma = 0$ into equation (2.73) we obtain the relationship between the two models.

$$\bar{\mu} = -\frac{(e_x + 1)}{(e_y + 1)}\left(\frac{\alpha}{\alpha + 1}\right)(\rho_x + \lambda_z) \quad (2.84)$$

Equation (2.84) allows us to formulate the solution given by equation (2.81) in terms of e_x, rather than μ.

We shall now graphically ascertain the behavior of the energy loss functions as we vary the initial parameters. The independent variable will be the initial rotation, λ_z, and we will vary the angle of approach θ, the coefficient of the radius of gyration α, the coefficient of restitution e_n, and lastly the coefficient of friction μ. In order to differentiate when to use equation (2.79) and when to use equation (2.82), we will utilize the sliding condition given by equation (2.83). Table 2.1 shows the variation of the impact parameters for the following figures.

Table 2.1*: Impact parameters for Fig. 2.2 through Fig. 2.5.*

Figure	θ	α	e_n	μ
2.2	30 – 90 deg	3/4	0.7	0.7
2.3	45 deg	1/4 - 1	0.7	0.7
2.4	45 deg	3/4	0.3 - 0.9	0.7
2.5	45 deg	3/4	0.7	0.5 - 0.9

Note that in the following figures the solid red curves indicate the no sliding regime, while the dashed blue curves indicate the sliding regime. From Fig. 2.2, we see that the angle of approach, θ, affects the energy loss only for positive values of λ_z. Also increasing the coefficient of the radius of gyration, α, decreases the energy loss as is seen in Fig. 2.3. The range of the no sliding regime is also decreased with increasing α. Fig. 2.4 demonstrates an interesting phenomenon that the energy loss can increase with increasing coefficient of restitution. Moreover, it shows that with an increasing coefficient of restitution, the energy loss increases in the sliding regime and decreases in the no sliding regime. From equation (2.79) we see that the coefficient of friction does not affect the energy loss in the no sliding regime. This is depicted in Fig. 2.5, along with the increase in the energy loss with increasing coefficient of friction in the sliding regime.

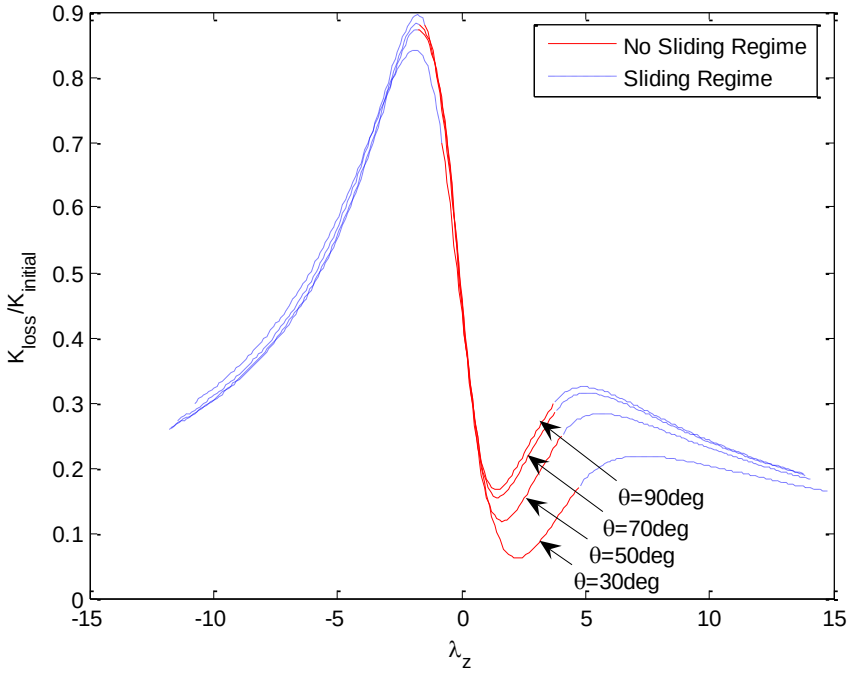

***Figure 2.2**: Influence of the angle of approach on the energy loss; axisymmetric body.*

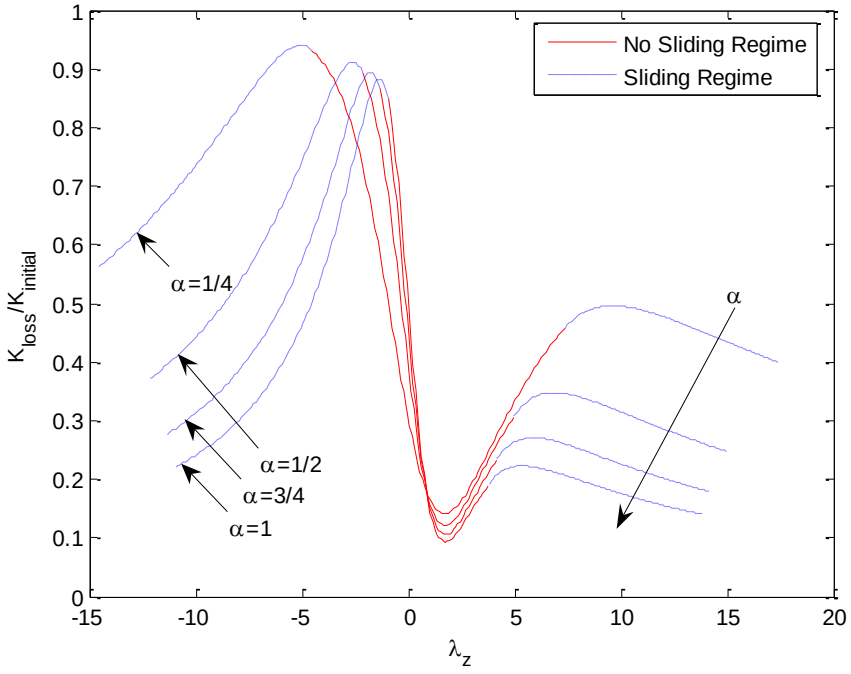

***Figure 2.3**: Influence of inertia on the energy loss; axisymmetric body.*

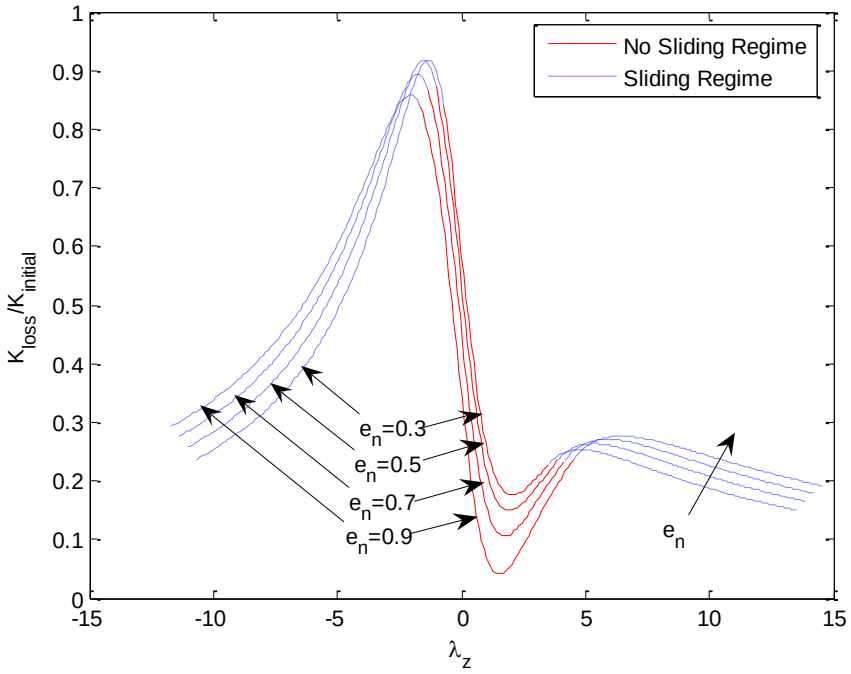

***Figure 2.4**: Influence of the coefficient of restitution on the energy loss; axisymmetric body.*

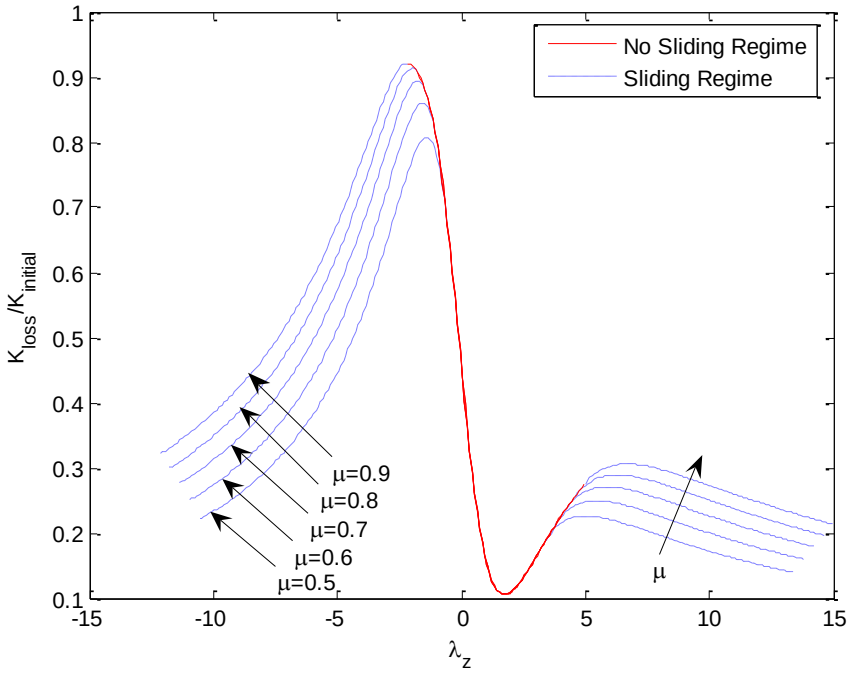

***Figure 2.5**: Influence of the coefficient of friction on the energy loss; axisymmetric body.*

2.7.2 Initially Irrotational

Another simplification that can be made to the general impact equations is when the object has no angular velocity before impact. Substituting $\lambda_z = 0$ into equations (2.29), (2.30), and (2.31) we obtain

$$\omega_z'' = \left(\frac{1}{\alpha+1}\right)\left[-\rho_x \cos(\gamma) - (e_n+1)\sin(\gamma)\right] \tag{2.85a}$$

$$V_x'' = \left(\frac{1}{\alpha+1}\right)\left[\rho_x \cos^2(\gamma) + (e_n+1)\cos(\gamma)\sin(\gamma)\right] \tag{2.85b}$$

$$V_y'' = \left(\frac{1}{\alpha+1}\right)\left[\rho_x \cos(\gamma)\sin(\gamma) + (e_n+1)\sin^2(\gamma)\right] - e_n \tag{2.85c}$$

Substituting equations (2.85) into the nondimensional energy loss expression (2.77)

$$\frac{K_{loss}}{K_{initial}} = 1 - \frac{\left(\frac{1}{\alpha+1}\right)^2 \left(\begin{array}{l} \left[\rho_x \cos^2(\gamma) + (e_n+1)\cos(\gamma)\sin(\gamma)\right]^2 \\ + \left[\rho_x \cos(\gamma)\sin(\gamma) + (e_n+1)\sin^2(\gamma) - (\alpha+1)e_n\right]^2 \\ + \alpha\left[-\rho_x \cos(\gamma) - (e_n+1)\sin(\gamma)\right]^2 \end{array} \right)}{{\rho_x}^2 + 1}$$

Multiplying out the quadratic terms and simplifying we arrive at

$$\frac{K_{loss}}{K_{initial}} = \frac{{\rho_x}^2\left(\alpha + \sin^2(\gamma)\right) - 2\rho_x \cos(\gamma)\sin(\gamma) + \left(1 - {e_n}^2\right)\left(\alpha + \cos^2(\gamma)\right)}{(\alpha+1)\left({\rho_x}^2 + 1\right)} \tag{2.86}$$

Equation (2.86) is the kinetic energy loss for the no sliding case of an initially irrotational body. Similarly let us substitute $\lambda_z = 0$ into equations (2.49), (2.50), and (2.51) in order to derive the energy loss for the sliding case.

$$V_y'' = \frac{\left(-\bar{\mu}\cos(\gamma)\sin(\gamma) + \sin^2(\gamma) - \alpha e_n\right)}{\left(\alpha - \bar{\mu}\cos(\gamma)\sin(\gamma) + \sin^2(\gamma)\right)} \tag{2.87a}$$

$$V_x'' = \frac{\rho_x\left(\alpha - \bar{\mu}\cos(\gamma)\sin(\gamma) + \sin^2(\gamma)\right) + \bar{\mu}\alpha(e_n+1)}{\left(\alpha - \bar{\mu}\cos(\gamma)\sin(\gamma) + \sin^2(\gamma)\right)} \tag{2.87b}$$

$$\omega_z'' = \frac{-(e_n+1)\left(-\bar{\mu}\cos(\gamma)+\sin(\gamma)\right)}{\left(\alpha-\bar{\mu}\cos(\gamma)\sin(\gamma)+\sin^2(\gamma)\right)} \tag{2.87c}$$

Substituting the final quantities (2.87) into the energy loss expression (2.77) yields

$$\frac{K_{loss}}{K_{initial}} = 1 - \frac{\left(\frac{1}{\left(\alpha-\bar{\mu}\cos(\gamma)\sin(\gamma)+\sin^2(\gamma)\right)^2}\right)\left(\begin{array}{l}\left(\rho_x\left(\alpha-\bar{\mu}\cos(\gamma)\sin(\gamma)+\sin^2(\gamma)\right)+\bar{\mu}\alpha(e_n+1)\right)^2 \\ +\left(-\bar{\mu}\cos(\gamma)\sin(\gamma)+\sin^2(\gamma)-\alpha e_n\right)^2 \\ +\alpha\left(-(e_n+1)\left(-\bar{\mu}\cos(\gamma)+\sin(\gamma)\right)\right)^2\end{array}\right)}{\rho_x{}^2+1}$$

Simplifying gives

$$\frac{K_{loss}}{K_{initial}} = \frac{\alpha(e_n+1)\left[\begin{array}{l}\bar{\mu}^2\left(2\rho_x\cos(\gamma)\sin(\gamma)-(e_n+1)\left(\alpha+\cos^2(\gamma)\right)\right)+ \\ 2\bar{\mu}\left(e_n\cos(\gamma)\sin(\gamma)-\rho_x\left(\alpha+\sin^2(\gamma)\right)\right)+(1-e_n)\left(\alpha+\sin^2(\gamma)\right)\end{array}\right]}{\left(\rho_x{}^2+1\right)\left(\alpha-\bar{\mu}\cos(\gamma)\sin(\gamma)+\sin^2(\gamma)\right)^2}$$

We can now use the definition of $\bar{\mu}=\mu\,\mathrm{sgn}\left(\rho_x+\lambda_z\cos(\gamma)\right)$ to simplify the above expression. Also note that $\bar{\mu}^2=\mu^2$ and since $\lambda_z=0$, we get $\bar{\mu}=\mu\,\mathrm{sgn}(\rho_x)$.

$$\frac{K_{loss}}{K_{initial}} = \frac{\alpha(e_n+1)\left[\begin{array}{l}\mu^2\left(2\rho_x\cos(\gamma)\sin(\gamma)-(e_n+1)\left(\alpha+\cos^2(\gamma)\right)\right)+ \\ 2\mu\,\mathrm{sgn}(\rho_x)\left(e_n\cos(\gamma)\sin(\gamma)-\rho_x\left(\alpha+\sin^2(\gamma)\right)\right)+(1-e_n)\left(\alpha+\sin^2(\gamma)\right)\end{array}\right]}{\left(\rho_x{}^2+1\right)\left(\alpha-\mu\,\mathrm{sgn}(\rho_x)\cos(\gamma)\sin(\gamma)+\sin^2(\gamma)\right)^2} \tag{2.88}$$

The sliding condition from equation (2.55) becomes the following, for an initially irrotational object.

$$\mu < \frac{\mathrm{sgn}(\rho_x)\left[\rho_x\left(\alpha+\sin^2(\gamma)\right)-(e_n+1)\cos(\gamma)\sin(\gamma)\right]}{\left[\rho_x\cos(\gamma)\sin(\gamma)-(e_n+1)\left(\alpha+\cos^2(\gamma)\right)\right]} \tag{2.89}$$

Lastly, if one prefers the (e_y, e_x) formulation of the impact problem, they can use the following conversion which was obtained by simplifying equation (2.73).

$$\bar{\mu} = \frac{\left(-\rho_x\left(e_x+1\right)\left(\alpha+\sin^2(\gamma)\right)+\left(e_y+1\right)\cos(\gamma)\sin(\gamma)\right)}{\left(-\rho_x\left(e_x+1\right)\cos(\gamma)\sin(\gamma)+\left(e_y+1\right)\left(\alpha+\cos^2(\gamma)\right)\right)} \tag{2.90}$$

Now that we have derived the energy loss expressions for an initially irrotational body, we can see how it varies with the orientation angle γ. This will be done graphically, where the variation of the impact parameters for the following figures is given in Table 2.2.

***Table 2.2**: Impact parameters for Fig. 2.6 through Fig. 2.9.*

Figure	θ	α	e_n	μ
2.6	30 – 90 deg	3/4	0.7	0.7
2.7	45 deg	1/4 - 1	0.7	0.7
2.8	45 deg	3/4	0.3 - 0.9	0.7
2.9	45 deg	3/4	0.7	0.5 - 0.9

The change in the energy loss due to a change in the angle of approach θ is given in Fig. 2.6 for an initially irrotational body. We see that increasing the angle of approach causes the energy loss to decrease in the no sliding regime for negative values of the orientation angle, while the behavior becomes more complex in the sliding regime. Unlike Fig. 2.3, Fig. 2.7 shows that increasing the coefficient of the radius of gyration causes the object to lose more energy. The predictable result that increasing the coefficient of restitution will cause a drop in the energy loss is shown in Fig. 2.8. Lastly, Fig. 2.9 shows the dependence of the energy loss on the coefficient of friction. We can see that more energy is lost with an increasing coefficient of friction if sliding occurs during impact.

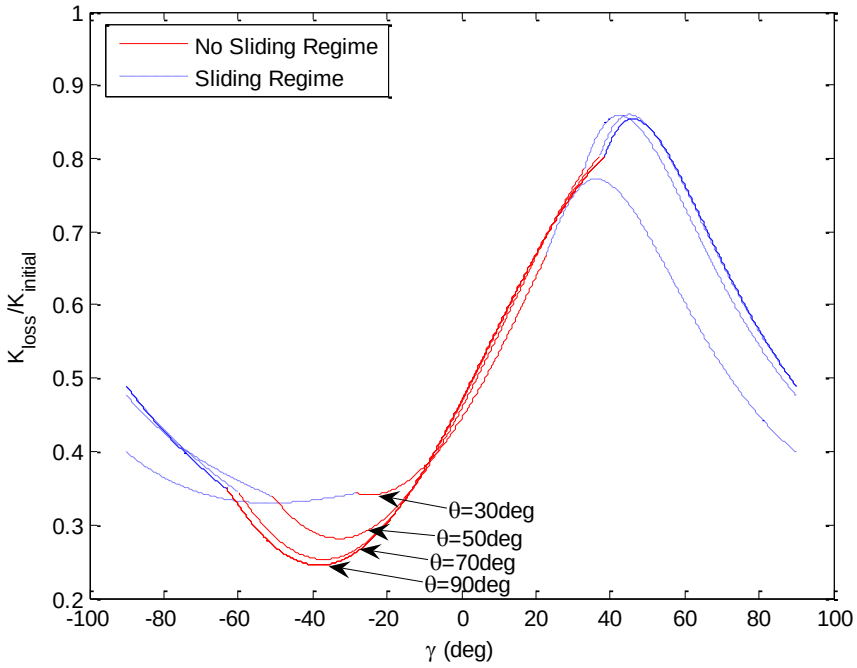

***Figure 2.6**: Influence of the angle of approach on the energy loss; irrotational impact.*

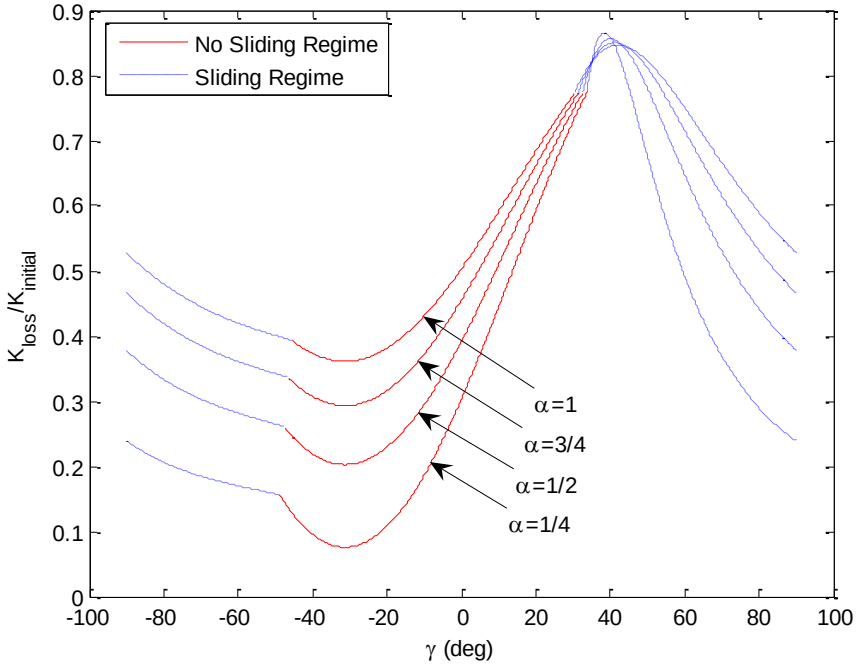

***Figure 2.7**: Influence of the inertia on the energy loss; irrotational impact.*

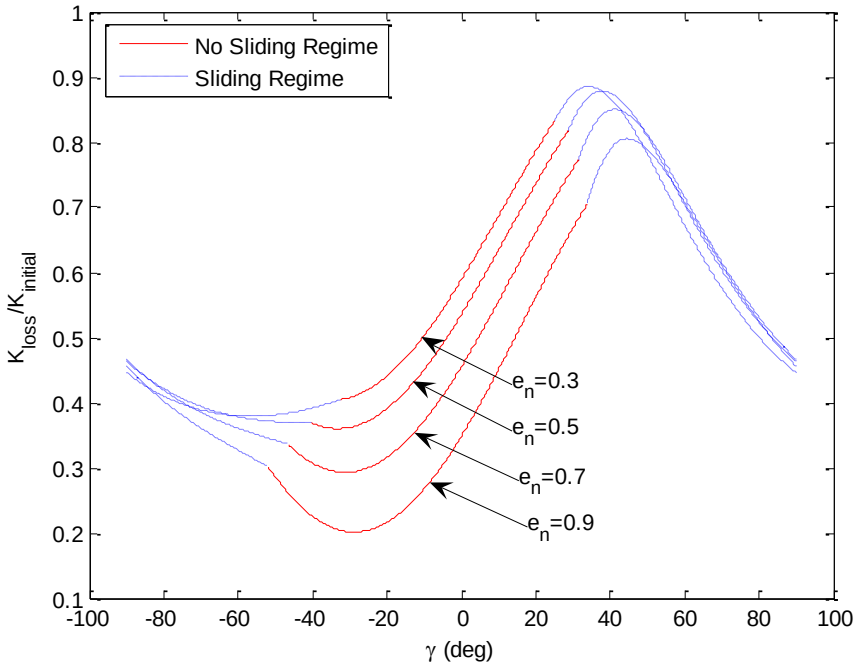

***Figure 2.8**: Influence of the coefficient of restitution on the energy loss; irrotational impact.*

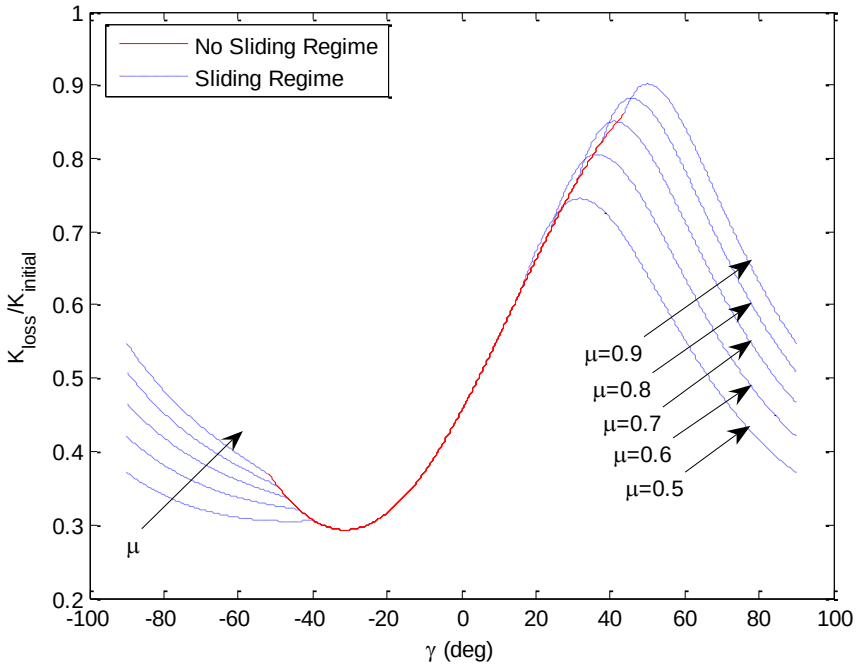

***Figure 2.9**: Influence of the coefficient of friction on the energy loss; irrotational impact.*

2.8 Nonsmooth Three Dimensional Impact

Thus far, we have presented a complete analysis and solution of a planar rigid body impact, and considered a few special cases. In this section, we extend the formulation to three dimensional impact. The primary difference is that now we will be dealing with three components of impulsive force, three components of velocity, and three components of angular velocity. This brings the total number of unknowns to nine, therefore we will require at least that many governing equations in order to close the system.

For consistency, let us define a coordinate system which is identical to that which was used for the planar analysis. The (x,z) plane is the plane of impact. The position vector between the center of mass and the contact point will now be a three dimensional vector, whose orientation will be defined by the angles from the coordinate axes. These direction angles from the x-axis, y-axis, and z-axis are β, γ, and δ, respectively.

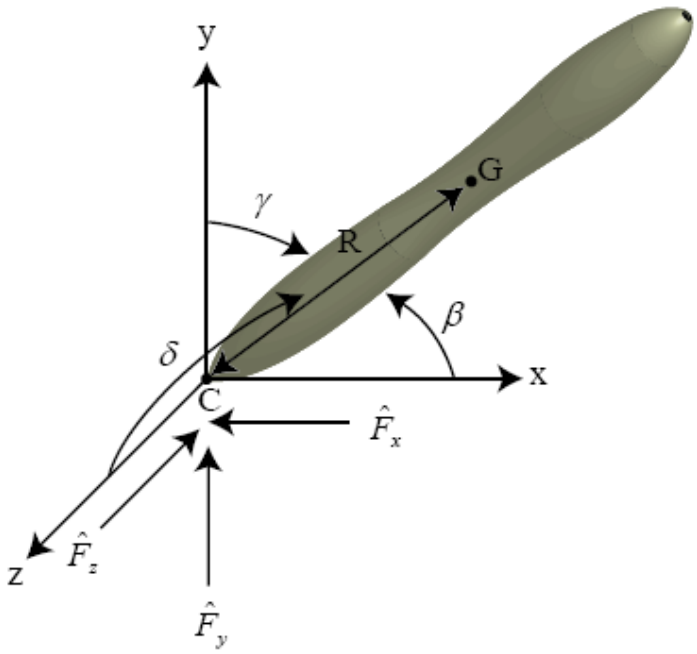

***Figure 2.10**: Orientation of the impacting body in three dimensions.*

The magnitude of the position vector from the contact point to the center of mass will be defined as R and assumed to remain constant. We can now express the position vector in terms of its components.

$$\vec{R} = R_x\hat{i} + R_y\hat{j} + R_z\hat{k} \tag{2.91a}$$

$$R_x = R\cos(\beta) \tag{2.91b}$$

$$R_y = R\cos(\gamma) \tag{2.91c}$$

$$R_z = R\cos(\delta) \tag{2.91d}$$

Paralleling the formulation for planar impact we can express the initial velocity and angular velocity in terms of their components as follows.

$$\vec{V} = V_x\hat{i} + V_y\hat{j} + V_z\hat{k} \tag{2.92}$$

$$\vec{\omega} = \omega_x\hat{i} + \omega_y\hat{j} + \omega_z\hat{k} \tag{2.93}$$

The initial contact point velocity can be calculated as follows.

$$\vec{V}^C = \vec{V} + \vec{\omega}\times\vec{R} = \left(V_x\hat{i} + V_y\hat{j} + V_z\hat{k}\right) + \left(\omega_x\hat{i} + \omega_y\hat{j} + \omega_z\hat{k}\right)\times\left(R_x\hat{i} + R_y\hat{j} + R_z\hat{k}\right)$$

$$\vec{V}^C = \left(V_x + \omega_y R_z - \omega_z R_y\right)\hat{i} + \left(V_y + \omega_z R_x - \omega_x R_z\right)\hat{j} + \left(V_z + \omega_x R_y - \omega_y R_x\right)\hat{k} \tag{2.94}$$

Similarly we can define the final velocity, angular velocity, and contact point velocity.

$$\vec{V}' = V_x'\hat{i} + V_y'\hat{j} + V_z'\hat{k} \tag{2.95}$$

$$\vec{\omega}' = \omega_x'\hat{i} + \omega_y'\hat{j} + \omega_z'\hat{k} \tag{2.96}$$

$$\vec{V}'^C = \left(V_x' + \omega_y' R_z - \omega_z' R_y\right)\hat{i} + \left(V_y' + \omega_z' R_x - \omega_x' R_z\right)\hat{j} + \left(V_z' + \omega_x' R_y - \omega_y' R_x\right)\hat{k} \tag{2.97}$$

Figure 2.10 illustrates the impulsive forces acting at the contact point during impact. Note that the selected direction of the tangential impact forces, $\hat{F}_x$ and $\hat{F}_z$, is somewhat arbitrary since they both depend on the direction of the contact point velocity.

Recall the general principle of linear momentum conservation $m\vec{V} + \int_{t_1}^{t_2} \vec{F} dt = m\vec{V}'$. Using this we can write down the following equations.

$$mV_x - \hat{F}_x = mV_x' \tag{2.98}$$

$$mV_y + \hat{F}_y = mV_y' \tag{2.99}$$

$$mV_z - \hat{F}_z = mV_z' \tag{2.100}$$

The general expression for the conservation of angular momentum for three dimensional motion is $\frac{d}{dt}\vec{H}_G = \vec{M}_G = \vec{R} \times \vec{F}$, where $\vec{F}$ is the impact force. We can also express the conservation of angular momentum as follows

$$\vec{H}_G - \vec{H}_G' = \int_{t_1}^{t_2} \left(\vec{R} \times \vec{F}\right) dt = \vec{R} \times \hat{\vec{F}}$$

where now $\hat{\vec{F}}$ is the impulsive force. The general expression of angular momentum will be cumbersome, therefore we will calculate the terms separately. Let us first consider the $\vec{R} \times \hat{\vec{F}}$ term.

$$\vec{R} \times \hat{\vec{F}} = \left(R_x \hat{i} + R_y \hat{j} + R_z \hat{k}\right) \times \left(\hat{F}_x \hat{i} + \hat{F}_y \hat{j} + \hat{F}_z \hat{k}\right)$$

$$\vec{R} \times \hat{\vec{F}} = \left(R_y \hat{F}_z - R_z \hat{F}_y\right)\hat{i} + \left(R_z \hat{F}_x - R_x \hat{F}_z\right)\hat{j} + \left(R_x \hat{F}_y - R_y \hat{F}_x\right)\hat{k} \tag{2.101}$$

The initial angular momentum of a rigid body in general three dimensional motion can be shown to be as follows, where I_{pq} for $p, q = x, y, z$ defines the inertia matrix for the body.

$$\vec{H}_G = \left(I_{xx}\omega_x - I_{xy}\omega_y - I_{xz}\omega_z\right)\hat{i} + \left(-I_{yx}\omega_x + I_{yy}\omega_y - I_{yz}\omega_z\right)\hat{j} + \left(-I_{zx}\omega_x - I_{zy}\omega_y + I_{zz}\omega_z\right)\hat{k}$$

(2.102)

Similarly the final angular momentum is

$$\vec{H}'_G = \left(I_{xx}\omega'_x - I_{xy}\omega'_y - I_{xz}\omega'_z\right)\hat{i} + \left(-I_{yx}\omega'_x + I_{yy}\omega'_y - I_{yz}\omega'_z\right)\hat{j} + \left(-I_{zx}\omega'_x - I_{zy}\omega'_y + I_{zz}\omega'_z\right)\hat{k} \tag{2.103}$$

Substituting (2.101), (2.102), and (2.103) into the conservation of angular momentum we arrive at the relation

$$\left[\left(I_{xx}\omega_x - I_{xy}\omega_y - I_{xz}\omega_z\right)\hat{i} + \left(-I_{yx}\omega_x + I_{yy}\omega_y - I_{yz}\omega_z\right)\hat{j} + \left(-I_{zx}\omega_x - I_{zy}\omega_y + I_{zz}\omega_z\right)\hat{k}\right] -$$
$$\left[\left(I_{xx}\omega'_x - I_{xy}\omega'_y - I_{xz}\omega'_z\right)\hat{i} + \left(-I_{yx}\omega'_x + I_{yy}\omega'_y - I_{yz}\omega'_z\right)\hat{j} + \left(-I_{zx}\omega'_x - I_{zy}\omega'_y + I_{zz}\omega'_z\right)\hat{k}\right] =$$
$$\left(R_y\hat{F}_z - R_z\hat{F}_y\right)\hat{i} + \left(R_z\hat{F}_x - R_x\hat{F}_z\right)\hat{j} + \left(R_x\hat{F}_y - R_y\hat{F}_x\right)\hat{k}$$

Equating components and separating known and unknown quantities

$$\left(I_{xx}\omega_x - I_{xy}\omega_y - I_{xz}\omega_z\right) = \left(I_{xx}\omega'_x - I_{xy}\omega'_y - I_{xz}\omega'_z\right) + \left(R_y\hat{F}_z - R_z\hat{F}_y\right) \tag{2.104a}$$

$$\left(-I_{yx}\omega_x + I_{yy}\omega_y - I_{yz}\omega_z\right) = \left(-I_{yx}\omega'_x + I_{yy}\omega'_y - I_{yz}\omega'_z\right) + \left(R_z\hat{F}_x - R_x\hat{F}_z\right) \tag{2.104b}$$

$$\left(-I_{zx}\omega_x - I_{zy}\omega_y + I_{zz}\omega_z\right) = \left(-I_{zx}\omega'_x - I_{zy}\omega'_y + I_{zz}\omega'_z\right) + \left(R_x\hat{F}_y - R_y\hat{F}_x\right) \tag{2.104c}$$

Using the basic concepts of rigid body dynamics we derived six equations (2.98), (2.99), (2.100), and (104a), (104b), and (104c), but have total of nine unknowns: $V'_x, V'_y, V'_z, \omega'_x,$ $\omega'_y, \omega'_z, \hat{F}_x, \hat{F}_y,$and $\hat{F}_z$. Therefore we need three more equations which will come from considering restitution and friction.

The coefficient of restitution will once again be introduced in order to describe the change in vertical velocity of the contact point through impact. Recall equation (2.17)

$$e_n = -\frac{\vec{V}'^C \cdot \hat{j}}{\vec{V}^C \cdot \hat{j}} \tag{2.17}$$

Substituting equations (2.94) and (2.97) into (2.17) we arrive at the following definition:

$$e_n = -\frac{\left(V_y' + \omega_z' R_x - \omega_x' R_z\right)}{\left(V_y + \omega_z R_x - \omega_x R_z\right)} \tag{2.105}$$

or

$$\left(V_y' + \omega_z' R_x - \omega_x' R_z\right) = -e_n\left(V_y + \omega_z R_x - \omega_x R_z\right) \tag{2.106}$$

We have introduced one more equation which will be utilized in obtaining the solution to a three dimensional impact problem. This inclusion gives us a total of seven equations. The last two equations will depend on whether the object slides or pivots through impact.

2.8.1 No Sliding Case in Three Dimensions

As was discussed in previous sections, if the impacting body does not slide during impact its final velocity components of the contact point, tangential to the impact surface, will be zero. For the three dimensional case this can be stated as

$$\vec{V}'^{C} \cdot \hat{i} = 0 \tag{2.107a}$$

$$\vec{V}'^{C} \cdot \hat{k} = 0 \tag{2.107b}$$

Substituting equation (2.97) into equations (2.107)

$$\left(V_x' + \omega_y' R_z - \omega_z' R_y\right) = 0 \tag{2.108a}$$

$$\left(V_z' + \omega_x' R_y - \omega_y' R_x\right) = 0 \tag{2.108b}$$

The system of equations for three dimensional impacts for the case when no sliding occurs is now closed. The nine equations are: (2.98), (2.99), (2.100), (2.104a), (2.104b), (2.104c), (2.106), (2.108a), and (2.108b). We can put these equations in matrix form.

$$\begin{bmatrix} m & 0 & 0 & 0 & 0 & 0 & 1 & 0 & 0 \\ 0 & m & 0 & 0 & 0 & 0 & 0 & -1 & 0 \\ 0 & 0 & m & 0 & 0 & 0 & 0 & 0 & 1 \\ 0 & 0 & 0 & I_{xx} & -I_{xy} & -I_{xz} & 0 & -R_z & R_y \\ 0 & 0 & 0 & -I_{yx} & I_{yy} & -I_{yz} & R_z & 0 & -R_x \\ 0 & 0 & 0 & -I_{zx} & -I_{zy} & I_{zz} & -R_y & R_x & 0 \\ 1 & 0 & 0 & 0 & R_z & -R_y & 0 & 0 & 0 \\ 0 & 1 & 0 & -R_z & 0 & R_x & 0 & 0 & 0 \\ 0 & 0 & 1 & R_y & -R_x & 0 & 0 & 0 & 0 \end{bmatrix} \begin{bmatrix} V_x' \\ V_y' \\ V_z' \\ \omega_x' \\ \omega_y' \\ \omega_z' \\ \hat{F}_x \\ \hat{F}_y \\ \hat{F}_z \end{bmatrix} = \begin{bmatrix} mV_x \\ mV_y \\ mV_z \\ \left(I_{xx}\omega_x - I_{xy}\omega_y - I_{xz}\omega_z\right) \\ \left(-I_{yx}\omega_x + I_{yy}\omega_y - I_{yz}\omega_z\right) \\ \left(-I_{zx}\omega_x - I_{zy}\omega_y + I_{zz}\omega_z\right) \\ 0 \\ -e_n\left(V_y + \omega_z R_x - \omega_x R_z\right) \\ 0 \end{bmatrix}$$

(2.109)

System (2.109) can be inverted to obtain the post-impact quantities for this type of impact. We can also express system (2.109) as follows

$$\begin{bmatrix} m & 0 & 0 & 0 & 0 & 0 & 1 & 0 & 0 \\ 0 & m & 0 & 0 & 0 & 0 & 0 & -1 & 0 \\ 0 & 0 & m & 0 & 0 & 0 & 0 & 0 & 1 \\ 0 & 0 & 0 & I_{xx} & -I_{xy} & -I_{xz} & 0 & -R_z & R_y \\ 0 & 0 & 0 & -I_{yx} & I_{yy} & -I_{yz} & R_z & 0 & -R_x \\ 0 & 0 & 0 & -I_{zx} & -I_{zy} & I_{zz} & -R_y & R_x & 0 \\ 1 & 0 & 0 & 0 & R_z & -R_y & 0 & 0 & 0 \\ 0 & 1 & 0 & -R_z & 0 & R_x & 0 & 0 & 0 \\ 0 & 0 & 1 & R_y & -R_x & 0 & 0 & 0 & 0 \end{bmatrix} \begin{bmatrix} V_x' \\ V_y' \\ V_z' \\ \omega_x' \\ \omega_y' \\ \omega_z' \\ \hat{F}_x \\ \hat{F}_y \\ \hat{F}_z \end{bmatrix} = \begin{bmatrix} m & 0 & 0 & 0 & 0 & 0 \\ 0 & m & 0 & 0 & 0 & 0 \\ 0 & 0 & m & 0 & 0 & 0 \\ 0 & 0 & 0 & I_{xx} & -I_{xy} & -I_{xz} \\ 0 & 0 & 0 & -I_{yx} & I_{yy} & -I_{yz} \\ 0 & 0 & 0 & -I_{zx} & -I_{zy} & I_{zz} \\ 0 & 0 & 0 & 0 & 0 & 0 \\ 0 & -e_n & 0 & e_n R_z & 0 & -e_n R_x \\ 0 & 0 & 0 & 0 & 0 & 0 \end{bmatrix} \begin{bmatrix} V_x \\ V_y \\ V_z \\ \omega_x \\ \omega_y \\ \omega_z \end{bmatrix}$$

(2.110)

In matrix notation, system (2.110) can be expressed as

$$\underset{9\times 9}{[A]}\underset{9\times 1}{\{V'\}} = \underset{9\times 6}{[B]}\underset{6\times 1}{\{V\}} \tag{2.111}$$

where the coefficient matrices $[A]$ and $[B]$ are seen in equation (2.110) and the column matrices $\{V'\}$ and $\{V\}$ contain the final and initial quantities, respectively. Therefore the solution can be expressed as

$$\underset{9\times 1}{\{V'\}} = \underset{9\times 9}{[A]^{-1}}\underset{9\times 6}{[B]}\underset{6\times 1}{\{V\}} \tag{2.112}$$

In the general case the coefficient matrix $\underset{9\times9}{[A]}^{-1}\underset{9\times6}{[B]}$ in equation (2.112) provides no physical insight due to its complexity. But, we do obtain a manageable matrix for the three dimensional impact of a sphere. For a sphere, the components of the position vector between points *C* and *G* are $R_x = R_z = 0$, and $R_y = R$, where R is the sphere's radius. The inertia matrix for a solid sphere is diagonal and unaltered by any rotation due to its symmetry. Its components are $I_{xx} = I_{yy} = I_{zz} = \frac{2}{5}mR^2$. Substituting these values into system (2.112), we get the following relationship between the initial and final quantities for the impact of a sphere when no sliding occurs.

$$\begin{bmatrix} V_x' \\ V_y' \\ V_z' \\ \omega_x' \\ \omega_y' \\ \omega_z' \\ \hat{F}_x \\ \hat{F}_y \\ \hat{F}_z \end{bmatrix} = \begin{bmatrix} \frac{5}{7} & 0 & 0 & 0 & 0 & \frac{2}{7}R \\ 0 & -e_n & 0 & 0 & 0 & 0 \\ 0 & 0 & \frac{5}{7} & -\frac{2}{7}R & 0 & 0 \\ 0 & 0 & -\frac{5}{7R} & \frac{2}{7} & 0 & 0 \\ 0 & 0 & 0 & 0 & 1 & 0 \\ \frac{5}{7R} & 0 & 0 & 0 & 0 & \frac{2}{7} \\ \frac{2}{7}m & 0 & 0 & 0 & 0 & -\frac{2}{7}mR \\ 0 & -m(e_n+1) & 0 & 0 & 0 & 0 \\ 0 & 0 & \frac{2}{7}m & \frac{2}{7}mR & 0 & 0 \end{bmatrix} \begin{bmatrix} V_x \\ V_y \\ V_z \\ \omega_x \\ \omega_y \\ \omega_z \end{bmatrix} \qquad (2.113)$$

2.8.2 Sliding Case in Three Dimensions

Now let us consider the impact when the body slides. Using the Coulomb Law of friction we will now define two coefficients of friction, one for each coordinate direction.

$$\mu_x = \left|\frac{\hat{F}_x}{\hat{F}_y}\right| \qquad \mu_z = \left|\frac{\hat{F}_z}{\hat{F}_y}\right| \qquad (2.114a,b)$$

In general, the frictional properties of the impacting surface can be directionally dependent, which is the reason for defining two distinct coefficients of friction. From Fig. 2.10, we see that the vertical component of the impact force will act in the positive direction, while the direction of the two horizontal components will depend on the direction of the initial contact point velocity. We can therefore restate equations (2.114) as

$$\mu_x = \frac{\hat{F}_x}{\hat{F}_y}\,\mathrm{sgn}\left(-\vec{V}^C \cdot \hat{i}\right) \qquad \mu_z = \frac{\hat{F}_z}{\hat{F}_y}\,\mathrm{sgn}\left(-\vec{V}^C \cdot \hat{k}\right) \qquad (2.115a,b)$$

Substituting equation (2.94) into equations (2.115) we obtain

$$\mu_x = \frac{\hat{F}_x}{\hat{F}_y}\,\mathrm{sgn}\left(-\left(V_x + \omega_y R_z - \omega_z R_y\right)\right) \qquad (2.116a)$$

$$\mu_z = \frac{\hat{F}_z}{\hat{F}_y}\,\mathrm{sgn}\left(-\left(V_z + \omega_x R_y - \omega_y R_x\right)\right) \qquad (2.116b)$$

To simplify the algebra let us define the following

$$\bar{\mu}_x = \mu_x\,\mathrm{sgn}\left(-\left(V_x + \omega_y R_z - \omega_z R_y\right)\right) \qquad (2.117a)$$

$$\bar{\mu}_z = \mu_z\,\mathrm{sgn}\left(-\left(V_z + \omega_x R_y - \omega_y R_x\right)\right) \qquad (2.117b)$$

Rearranging equations (2.116) and using equations (2.117) we obtain the following

$$\hat{F}_x - \bar{\mu}_x \hat{F}_y = 0 \qquad (2.118a)$$

$$\hat{F}_z - \bar{\mu}_z \hat{F}_y = 0 \qquad (2.118b)$$

Equations (2.118a) and (2.118b) complete the system of equations required to solve the three dimensional impact problem with sliding, the other seven equations being (2.98), (2.99), (2.100), (2.104a), (2.104b), (2.104c), and (2.106). Putting this system in matrix form we obtain

$$\begin{bmatrix} m & 0 & 0 & 0 & 0 & 0 & 1 & 0 & 0 \\ 0 & m & 0 & 0 & 0 & 0 & 0 & -1 & 0 \\ 0 & 0 & m & 0 & 0 & 0 & 0 & 0 & 1 \\ 0 & 0 & 0 & I_{xx} & -I_{xy} & -I_{xz} & 0 & -R_z & R_y \\ 0 & 0 & 0 & -I_{yx} & I_{yy} & -I_{yz} & R_z & 0 & -R_x \\ 0 & 0 & 0 & -I_{zx} & -I_{zy} & I_{zz} & -R_y & R_x & 0 \\ 0 & 0 & 0 & 0 & 0 & 0 & 1 & -\overline{\mu}_x & 0 \\ 0 & 1 & 0 & -R_z & 0 & R_x & 0 & 0 & 0 \\ 0 & 0 & 0 & 0 & 0 & 0 & 0 & -\overline{\mu}_z & 1 \end{bmatrix} \begin{bmatrix} V_x' \\ V_y' \\ V_z' \\ \omega_x' \\ \omega_y' \\ \omega_z' \\ \hat{F}_x \\ \hat{F}_y \\ \hat{F}_z \end{bmatrix} = \begin{bmatrix} mV_x \\ mV_y \\ mV_z \\ \left(I_{xx}\omega_x - I_{xy}\omega_y - I_{xz}\omega_z\right) \\ \left(-I_{yx}\omega_x + I_{yy}\omega_y - I_{yz}\omega_z\right) \\ \left(-I_{zx}\omega_x - I_{zy}\omega_y + I_{zz}\omega_z\right) \\ 0 \\ -e_n\left(V_y + \omega_z R_x - \omega_x R_z\right) \\ 0 \end{bmatrix} \tag{2.119}$$

System (2.119) can be used to determine the post-impact quantities for a body that slides during impact. We can also express the above system in the following form

$$\begin{bmatrix} m & 0 & 0 & 0 & 0 & 0 & 1 & 0 & 0 \\ 0 & m & 0 & 0 & 0 & 0 & 0 & -1 & 0 \\ 0 & 0 & m & 0 & 0 & 0 & 0 & 0 & 1 \\ 0 & 0 & 0 & I_{xx} & -I_{xy} & -I_{xz} & 0 & -R_z & R_y \\ 0 & 0 & 0 & -I_{yx} & I_{yy} & -I_{yz} & R_z & 0 & -R_x \\ 0 & 0 & 0 & -I_{zx} & -I_{zy} & I_{zz} & -R_y & R_x & 0 \\ 0 & 0 & 0 & 0 & 0 & 0 & 1 & -\overline{\mu}_x & 0 \\ 0 & 1 & 0 & -R_z & 0 & R_x & 0 & 0 & 0 \\ 0 & 0 & 0 & 0 & 0 & 0 & 0 & -\overline{\mu}_z & 1 \end{bmatrix} \begin{bmatrix} V_x' \\ V_y' \\ V_z' \\ \omega_x' \\ \omega_y' \\ \omega_z' \\ \hat{F}_x \\ \hat{F}_y \\ \hat{F}_z \end{bmatrix} = \begin{bmatrix} m & 0 & 0 & 0 & 0 & 0 \\ 0 & m & 0 & 0 & 0 & 0 \\ 0 & 0 & m & 0 & 0 & 0 \\ 0 & 0 & 0 & I_{xx} & -I_{xy} & -I_{xz} \\ 0 & 0 & 0 & -I_{yx} & I_{yy} & -I_{yz} \\ 0 & 0 & 0 & -I_{zx} & -I_{zy} & I_{zz} \\ 0 & 0 & 0 & 0 & 0 & 0 \\ 0 & -e_n & 0 & e_n R_z & 0 & -e_n R_x \\ 0 & 0 & 0 & 0 & 0 & 0 \end{bmatrix} \begin{bmatrix} V_x \\ V_y \\ V_z \\ \omega_x \\ \omega_y \\ \omega_z \end{bmatrix} \tag{2.120}$$

System (2.120) can be written in matrix notation as

$$\underset{9\times 9}{[C]}\underset{9\times 1}{\{V'\}} = \underset{9\times 6}{[D]}\underset{6\times 1}{\{V\}} \tag{2.121}$$

where $[C]$ and $[D]$ are the coefficient matrices, $\{V\}$ is the column matrix of initial quantities, and $\{V'\}$ is the column matrix of post-impact quantities seen in equation (2.120). The solution for the final quantities is given by

$$\underset{9\times 1}{\{V'\}} = \underset{9\times 9}{[C]^{-1}}\underset{9\times 6}{[D]}\underset{6\times 1}{[V]} \tag{2.122}$$

Once again the matrix $\underset{9\times9}{[C]}^{-1}\underset{9\times6}{[D]}$ is very cumbersome for the general case, but it does simplify for the impact of a sphere. Recall that for a sphere $R_x = R_z = 0$, $R_y = R$, and $I_{xx} = I_{yy} = I_{zz} = \frac{2}{5}mR^2$, where R is the sphere's radius. Substituting these values into the system (2.122) we obtain

$$\begin{bmatrix} V_x' \\ V_y' \\ V_z' \\ \omega_x' \\ \omega_y' \\ \omega_z' \\ \hat{F}_x \\ \hat{F}_y \\ \hat{F}_z \end{bmatrix} = \begin{bmatrix} 1 & \bar{\mu}_x(e_n+1) & 0 & 0 & 0 & 0 \\ 0 & -e_n & 0 & 0 & 0 & 0 \\ 0 & \bar{\mu}_z(e_n+1) & 1 & 0 & 0 & 0 \\ 0 & \frac{5}{2}\frac{\bar{\mu}_z}{R}(e_n+1) & 0 & 1 & 0 & 0 \\ 0 & 0 & 0 & 0 & 1 & 0 \\ 0 & -\frac{5}{2}\frac{\bar{\mu}_x}{R}(e_n+1) & 0 & 0 & 0 & 1 \\ 0 & -\bar{\mu}_x m(e_n+1) & 0 & 0 & 0 & 0 \\ 0 & m(e_n+1) & 0 & 0 & 0 & 0 \\ 0 & -\bar{\mu}_z m(e_n+1) & 0 & 0 & 0 & 0 \end{bmatrix} \begin{bmatrix} V_x \\ V_y \\ V_z \\ \omega_x \\ \omega_y \\ \omega_z \end{bmatrix} \qquad (2.123)$$

Equation (2.123) is the relationship between the initial and final quantities for the three dimensional impact of a sphere if siding occurs.

In this study we will consider contact surfaces which can be defined by a single, constant-valued, coefficient of friction μ. We can also say that for this problem, sliding will occur if the maximum tangential impulse $\hat{F}_R$ is large enough to overcome friction, which is defined by its components $\hat{F}_x$ and $\hat{F}_z$.

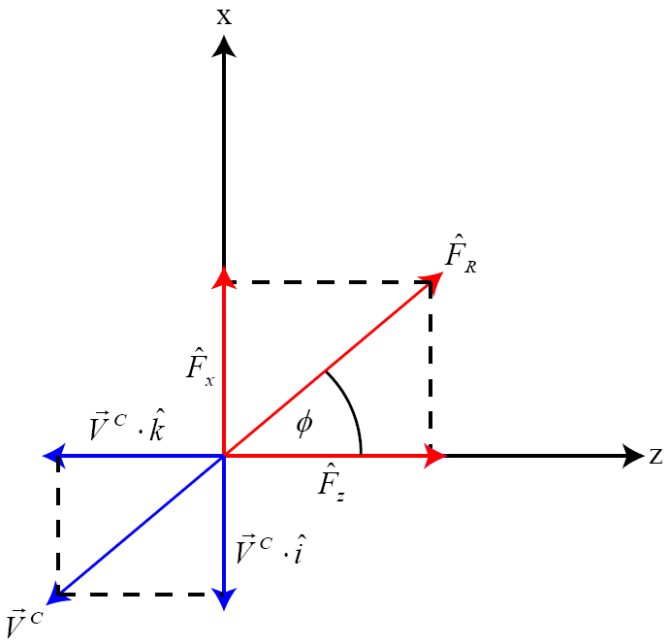

***Figure 2.11**: Tangential impulses.*

From Fig. 2.11 we can see that the components, magnitude, and orientation of the maximum tangential impulse are

$$\hat{\vec{F}}_R = \hat{F}_R\left(\sin(\phi)\hat{i} + \cos(\phi)\hat{k}\right) = \hat{F}_x\hat{i} + \hat{F}_z\hat{k} \tag{2.124}$$

$$\hat{F}_R = \sqrt{\hat{F}_x{}^2 + \hat{F}_z{}^2} \tag{2.125}$$

$$\phi = \tan^{-1}\left(\frac{\vec{V}^C \cdot \hat{i}}{\vec{V}^C \cdot \hat{k}}\right) \tag{2.126}$$

Therefore if the object slides, the ratio of the maximum tangential impulse to the vertical impulse is equivalent to the coefficient of friction μ.

$$\mu = \left|\frac{\hat{F}_R}{\hat{F}_y}\right| \tag{2.127}$$

Using equation (2.124) we can state the following

$$\hat{F}_R = \frac{\hat{F}_x}{\sin(\phi)} \tag{2.128a}$$

$$\hat{F}_R = \frac{\hat{F}_y}{\cos(\phi)} \tag{2.128b}$$

Note from Fig. 2.11 and equation (2.124) we see that the angle ϕ has a range of $0 \le \phi \le \pi/2$, and therefore the $\cos(\phi)$ and $\sin(\phi)$ terms cannot take on negative values. Substituting equations (2.128) into (2.127)

$$\mu = \frac{1}{\sin(\phi)}\left|\frac{\hat{F}_x}{\hat{F}_y}\right| \tag{2.129a}$$

$$\mu = \frac{1}{\cos(\phi)}\left|\frac{\hat{F}_z}{\hat{F}_y}\right| \tag{2.129b}$$

Comparing equations (2.129) to equations (2.114) we can define the following values for the directional coefficients of friction μ_x and μ_z.

$$\mu_x = \mu\sin(\phi) \tag{2.130a}$$

$$\mu_z = \mu\cos(\phi) \tag{2.130b}$$

To summarize, when dealing with a problem having a single-valued coefficient of friction, equations (2.128) should be substituted into equations (2.114) in order to obtain the solution.

We have now derived the systems of equations required to solve both the sliding and no sliding cases. But we must once again determine when to use which set of equations. As was stated earlier, if a single valued coefficient of friction can be used, the sliding regime will be initiated by the maximum tangential impulse. The sliding condition becomes

$$\mu < \frac{\sqrt{\hat{F}_x^{\,2} + \hat{F}_z^{\,2}}}{\hat{F}_y} \tag{2.131}$$

The object will slide if the force ratio exceeds the value of the prescribed coefficient of friction.

2.9 Three Dimensional Impact of a Rod

As an example of a three dimensional impact we will solve the problem for a cylindrical rod. The ends of the rod will be assumed to have a property such that the radius between the contact point and the center of mass is constant.

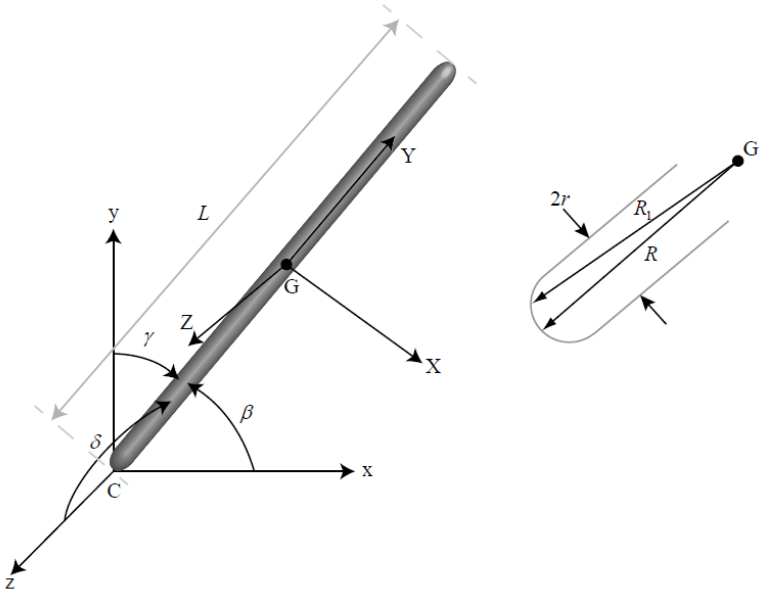

***Figure 2.12**: Three dimensional impact of a rod.*

From the above figure we see that that this assertion is equivalent to saying $R_1 \approx R$. Also note that in the figure, the XYZ coordinate system is attached to the body, while the xyz coordinate system is inertial. This distinction will be required in the calculation of the inertia matrix. The problem is to determine the post-impact quantities for this impact if the rod's mass m, length L, radius r are

$m = 1\text{kg}$

$L = 1\,\text{m}$

$r = \frac{L}{20}\,\text{m}$

and the orientation, initial velocity, and angular velocity are

$\beta = 45^\circ$, $\gamma = 45^\circ$, and $\delta = 90^\circ$

$\vec{V} = 3\hat{i} - 7\hat{j} + 2\hat{k}$

$\vec{\omega} = 12\hat{i} + \hat{j} + 4\hat{k}$

Also the coefficient of restitution and the coefficient of friction are

$e_n = 0.4$

$\mu = 0.7$

Beginning the solution by using equation (2.91), the components of the position vector between the contact point and the center of mass are

$R_x = \frac{\sqrt{2}}{4}$, $R_y = \frac{\sqrt{2}}{4}$, and $R_z = 0$

The inertia matrix for a rod in its principal, XYZ, coordinate system is

$$[I_G] = m\begin{bmatrix} \frac{1}{4}r^2 + \frac{1}{12}L^2 & 0 & 0 \\ 0 & \frac{1}{2}r^2 & 0 \\ 0 & 0 & \frac{1}{4}r^2 + \frac{1}{12}L^2 \end{bmatrix} = \begin{bmatrix} \frac{403}{4800} & 0 & 0 \\ 0 & \frac{1}{800} & 0 \\ 0 & 0 & \frac{403}{4800} \end{bmatrix}$$

Due to their small relative size we are neglecting the contribution of the spherical caps on the ends of the rod to the inertia properties of the rod. From the figure above we see that the inertia matrix must be rotated by an angle γ about the z-axis to coincide with the inertial coordinate system. The rotation matrix is therefore

$$[Q]=\begin{bmatrix}\cos(\gamma) & \sin(\gamma) & 0\\ -\sin(\gamma) & \cos(\gamma) & 0\\ 0 & 0 & 1\end{bmatrix}=\begin{bmatrix}\frac{\sqrt{2}}{2} & \frac{\sqrt{2}}{2} & 0\\ -\frac{\sqrt{2}}{2} & \frac{\sqrt{2}}{2} & 0\\ 0 & 0 & 1\end{bmatrix}$$

The rotated inertia matrix $[I'_G]$ is calculated by

$$[I'_G]=[Q][I_G][Q]^T$$

$$[I'_G]=m\begin{bmatrix}\frac{\sqrt{2}}{2} & \frac{\sqrt{2}}{2} & 0\\ -\frac{\sqrt{2}}{2} & \frac{\sqrt{2}}{2} & 0\\ 0 & 0 & 1\end{bmatrix}\begin{bmatrix}\frac{1}{4}r^2+\frac{1}{12}L^2 & 0 & 0\\ 0 & \frac{1}{2}r^2 & 0\\ 0 & 0 & \frac{1}{4}r^2+\frac{1}{12}L^2\end{bmatrix}\begin{bmatrix}\frac{\sqrt{2}}{2} & -\frac{\sqrt{2}}{2} & 0\\ \frac{\sqrt{2}}{2} & \frac{\sqrt{2}}{2} & 0\\ 0 & 0 & 1\end{bmatrix}$$

and the resulting matrix is

$$[I'_G]=\begin{bmatrix}\left(\frac{409}{9600}\right) & \left(-\frac{197}{2400}\right) & 0\\ \left(-\frac{197}{2400}\right) & \left(\frac{409}{9600}\right) & 0\\ 0 & 0 & \left(\frac{403}{4800}\right)\end{bmatrix}$$

We can now solve the no sliding case. Substituting all pertinent values into matrix (2.109)

$$\begin{bmatrix} 1 & 0 & 0 & 0 & 0 & 0 & 1 & 0 & 0 \\ 0 & 1 & 0 & 0 & 0 & 0 & 0 & -1 & 0 \\ 0 & 0 & 1 & 0 & 0 & 0 & 0 & 0 & 1 \\ 0 & 0 & 0 & \frac{409}{9600} & \frac{197}{2400} & 0 & 0 & 0 & \frac{\sqrt{2}}{4} \\ 0 & 0 & 0 & \frac{197}{2400} & \frac{409}{9600} & 0 & 0 & 0 & -\frac{\sqrt{2}}{4} \\ 0 & 0 & 0 & 0 & 0 & \frac{403}{4800} & -\frac{\sqrt{2}}{4} & \frac{\sqrt{2}}{4} & 0 \\ 1 & 0 & 0 & 0 & 0 & -\frac{\sqrt{2}}{4} & 0 & 0 & 0 \\ 0 & 1 & 0 & 0 & 0 & \frac{\sqrt{2}}{4} & 0 & 0 & 0 \\ 0 & 0 & 1 & \frac{\sqrt{2}}{4} & -\frac{\sqrt{2}}{4} & 0 & 0 & 0 & 0 \end{bmatrix} \begin{bmatrix} V_x' \\ V_y' \\ V_z' \\ \omega_x' \\ \omega_y' \\ \omega_z' \\ \hat{F}_x \\ \hat{F}_y \\ \hat{F}_z \end{bmatrix} = \begin{bmatrix} 3 \\ -7 \\ 2 \\ \left(\frac{409}{800} - \frac{197}{2400}\right) \\ \left(-\frac{197}{200} + \frac{409}{9600}\right) \\ \left(\frac{403}{1200}\right) \\ 0 \\ -0.4\left(-7 + \sqrt{2}\right) \\ 0 \end{bmatrix}$$

The solution to the above system is shown below.

$$\begin{bmatrix} V_x' \\ V_y' \\ V_z' \\ \omega_x' \\ \omega_y' \\ \omega_z' \\ \hat{F}_x \\ \hat{F}_y \\ \hat{F}_z \end{bmatrix} = \begin{bmatrix} -7.868 \\ 10.102 \\ 0.072 \\ -2.159 \\ -1.957 \\ -22.253 \\ 10.868 \\ 17.102 \\ 1.928 \end{bmatrix}$$

Substituting the calculated impulsive forces into the slip condition (2.131)

$$\frac{\sqrt{\hat{F}_x{}^2 + \hat{F}_z{}^2}}{\hat{F}_y} = \frac{\sqrt{(10.868)^2 + (1.928)^2}}{\hat{F}_y} = \frac{11.038}{17.102} = 0.645 < 0.7$$

The impulse ratio does not exceed the value of the coefficient of friction; therefore the rod will not slide during impact and our solution is correct. Note that if now we change the initial vertical velocity from $V_y = -7$ m/s to $V_y = -4$ m/s, the matrix (2.109) would look like

$$\begin{bmatrix} 1 & 0 & 0 & 0 & 0 & 0 & 1 & 0 & 0 \\ 0 & 1 & 0 & 0 & 0 & 0 & 0 & -1 & 0 \\ 0 & 0 & 1 & 0 & 0 & 0 & 0 & 0 & 1 \\ 0 & 0 & 0 & \frac{409}{9600} & \frac{197}{2400} & 0 & 0 & 0 & \frac{\sqrt{2}}{4} \\ 0 & 0 & 0 & \frac{197}{2400} & \frac{409}{9600} & 0 & 0 & 0 & -\frac{\sqrt{2}}{4} \\ 0 & 0 & 0 & 0 & 0 & \frac{403}{4800} & -\frac{\sqrt{2}}{4} & \frac{\sqrt{2}}{4} & 0 \\ 1 & 0 & 0 & 0 & 0 & -\frac{\sqrt{2}}{4} & 0 & 0 & 0 \\ 0 & 1 & 0 & 0 & 0 & \frac{\sqrt{2}}{4} & 0 & 0 & 0 \\ 0 & 0 & 1 & \frac{\sqrt{2}}{4} & -\frac{\sqrt{2}}{4} & 0 & 0 & 0 & 0 \end{bmatrix} \begin{bmatrix} V_x' \\ V_y' \\ V_z' \\ \omega_x' \\ \omega_y' \\ \omega_z' \\ \hat{F}_x \\ \hat{F}_y \\ \hat{F}_z \end{bmatrix} = \begin{bmatrix} 3 \\ -4 \\ 2 \\ \left(\frac{409}{800} - \frac{197}{2400}\right) \\ \left(-\frac{197}{200} + \frac{409}{9600}\right) \\ \left(\frac{403}{1200}\right) \\ 0 \\ -0.4\left(-4 + \sqrt{2}\right) \\ 0 \end{bmatrix}$$

and the solution will be

$$\begin{bmatrix} V_x' \\ V_y' \\ V_z' \\ \omega_x' \\ \omega_y' \\ \omega_z' \\ \hat{F}_x \\ \hat{F}_y \\ \hat{F}_z \end{bmatrix} = \begin{bmatrix} -1.615 \\ 2.649 \\ 0.072 \\ -2.159 \\ -1.957 \\ -4.567 \\ 4.615 \\ 6.649 \\ 1.928 \end{bmatrix}$$

Substituting the impulses into equation (2.131) we get

$$\frac{\sqrt{\hat{F}_x^{\,2} + \hat{F}_z^{\,2}}}{\hat{F}_y} = \frac{\sqrt{(4.615)^2 + (1.928)^2}}{\hat{F}_y} = \frac{5.002}{6.649} = 0.752 > 0.7$$

Now the force ratio exceeds the value of the coefficient of friction, hence the object will slide during impact. This tells us that we must resolve the problem using the appropriate equations, system (2.119). We begin by calculating the components of the initial contact point velocity by equation (2.94).

$$\vec{V}^{C} = \left(3-\sqrt{2}\right)\hat{i} + \left(-4+\sqrt{2}\right)\hat{j} + \left(2+\frac{11}{4}\sqrt{2}\right)\hat{k}$$

From equation (2.124) the angle defining the maximum tangential impulse is

$$\phi = \tan^{-1}\left(\frac{\left(3-\sqrt{2}\right)}{\left(2+\frac{11}{4}\sqrt{2}\right)}\right) = 15.071^{\circ}$$

The directional coefficients of friction are calculated by equations (2.130)

$\mu_x = 0.182$ $\mu_z = 0.676$

From equations (2.117)

$\bar{\mu}_x = -\mu_x = -0.182$ $\bar{\mu}_z = -\mu_z = -0.676$

We are now ready to substitute the directional coefficients of friction along with all other impact parameters into matrix (2.119).

$$\begin{bmatrix} 1 & 0 & 0 & 0 & 0 & 0 & 1 & 0 & 0 \\ 0 & 1 & 0 & 0 & 0 & 0 & 0 & -1 & 0 \\ 0 & 0 & 1 & 0 & 0 & 0 & 0 & 0 & 1 \\ 0 & 0 & 0 & \frac{409}{9600} & \frac{197}{2400} & 0 & 0 & 0 & \frac{\sqrt{2}}{4} \\ 0 & 0 & 0 & \frac{197}{2400} & \frac{409}{9600} & 0 & 0 & 0 & -\frac{\sqrt{2}}{4} \\ 0 & 0 & 0 & 0 & 0 & \frac{403}{4800} & -\frac{\sqrt{2}}{4} & \frac{\sqrt{2}}{4} & 0 \\ 0 & 0 & 0 & 0 & 0 & 0 & 1 & 0.182 & 0 \\ 0 & 1 & 0 & 0 & 0 & \frac{\sqrt{2}}{4} & 0 & 0 & 0 \\ 0 & 0 & 0 & 0 & 0 & 0 & 0 & 0.676 & 1 \end{bmatrix} \begin{bmatrix} V_x' \\ V_y' \\ V_z' \\ \omega_x' \\ \omega_y' \\ \omega_z' \\ \hat{F}_x \\ \hat{F}_y \\ \hat{F}_z \end{bmatrix} = \begin{bmatrix} 3 \\ -4 \\ 2 \\ \left(\frac{409}{800}-\frac{197}{2400}\right) \\ \left(-\frac{197}{200}+\frac{409}{9600}\right) \\ \left(\frac{403}{1200}\right) \\ 0 \\ -0.4\left(-4+\sqrt{2}\right) \\ 0 \end{bmatrix}$$

Solving the above system we obtain the post impact quantities for this impact.

$$\begin{bmatrix} V_x' \\ V_y' \\ V_z' \\ \omega_x' \\ \omega_y' \\ \omega_z' \\ \hat{F}_x \\ \hat{F}_y \\ \hat{F}_z \end{bmatrix} = \begin{bmatrix} 2.133 \\ -8.765 \\ -1.221 \\ 9.415 \\ -13.531 \\ 27.715 \\ 0.867 \\ -4.765 \\ 3.221 \end{bmatrix}$$

If we now check the maximum ratio of the impulses using equation (2.131) we see that it is equal to the coefficient of friction.

$$\frac{\sqrt{\hat{F}_x^{\,2} + \hat{F}_z^{\,2}}}{\hat{F}_y} = \frac{3.336}{4.765} = 0.700$$

One might be concerned about the validity of the last solution because the vertical component of the post-impact velocity of the center of mass is negative. How can the rod's center of mass be going down after impact? We will answer this question by considering the final velocity of the contact point. The post-impact contact point velocity is obtained from equation (2.97).

$$\vec{V}'^{C} = \left(V_x' + \omega_y' R_z - \omega_z' R_y\right)\hat{i} + \left(V_y' + \omega_z' R_x - \omega_x' R_z\right)\hat{j} + \left(V_z' + \omega_x' R_y - \omega_y' R_x\right)\hat{k}$$

Substituting the values form our solution

$$\vec{V}'^{C} = -7.666\hat{i} + 1.034\,\hat{j} + 6.892\hat{k}$$

From the above expression we see that there is no reason for concern since the final vertical velocity of the contact point is positive which reassures the correctness of our solution.

Now that we have solved the problem of a rod impacting a surface in three dimensions, we can formulate the general procedure of solving a three dimensional impact problem. Assuming that the object's orientation and physical parameters are known, one can begin the analysis by determining the inertia matrix in the coordinate system of the impact point. In the previous example, this was done using one rotation, but in the general case two rotations might be needed. The components of the position vector can be calculated by using equation (2.91). All of these parameters as well as the initial velocities and rotations should then be substituted into matrix (2.109). Once the solution is obtained, the components of the impact impulses should be substituted into equation (2.131) in order to check the validity of the no sliding assumption. If this criterion is satisfied the solution is valid, otherwise we must resolve the problem using the equations for the sliding case. If the sliding condition is not satisfied we need to calculate the directional coefficients of friction. This will be done by calculating the direction of the maximum tangential impulse using equation (2.126) and then substituting these values together with the value of the coefficient of friction into equations (2.130). After using equation (2.116), the directional coefficients of friction can then be substituted into the system (2.119). This system gives the solution for the three dimensional impact when sliding occurs during impact. In the general case, the solution to the problem of the three dimensional impact is not simple to obtain by hand. However, the use of computational software renders the problem much easier to manage.

2.10 Three Dimensional Impact of a Rectangular Container

In this section we will analyze the three dimensional impact of a rectangular container. The container will impact the surface with some initial velocity and angular velocity. The solution will be obtained by following the procedure outlined in previous sections. The main goal of this example is to ascertain whether it is adequate to use the two dimensional impact model to solve certain three dimensional problems.

Let us begin the analysis by defining the dimensions and orientation of the container. The side lengths of the container along the x, y, and z axes are L_1, L_2, and L_3, respectively. Figure 2.13 shows the container, where the (x,y,z) coordinate system is fixed to the container and the (X,Y,Z) coordinate system is at the contact point such that the Y axis is normal to the impact plane.

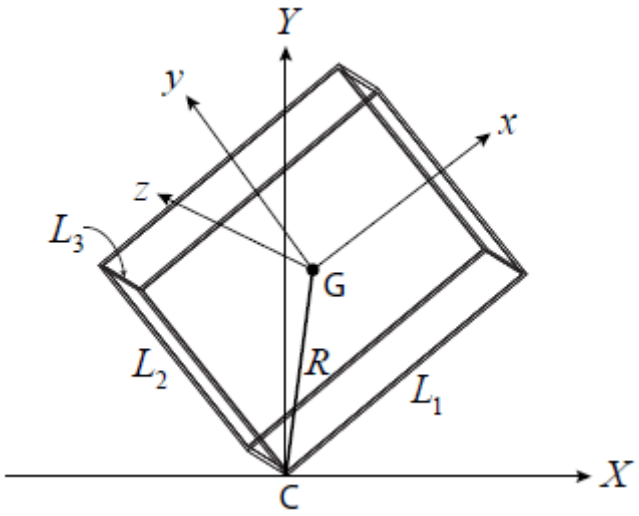

***Figure 2.13**: Three dimensional impact of a rectangular container.*

The distance from the contact point to the center of gravity, R is

$$R = \frac{1}{2}\sqrt{L_1^{\,2} + L_2^{\,2} + L_3^{\,2}}$$

Let us also define the following face angles for the container, which will be used later.

$$\psi_f = \tan^{-1}\left(\frac{L_2}{L_1}\right)$$

$$\psi_s = \tan^{-1}\left(\frac{L_3}{L_2}\right)$$

The orientation of the container will be defined using two rotations. These rotations are shown in Fig. 2.14. The first rotation will be by an angle χ_f about the z-axis, and the second will be by an angle χ_s about the new x-axis denoted as the X'-axis.

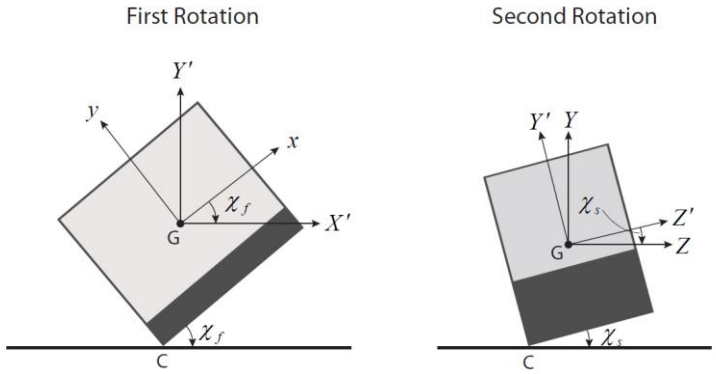

***Figure 2.14**: Rotations of the rectangular container.*

The purpose of the second rotation is to effectively tilt the container back such that impact occurs at a corner rather than a side.

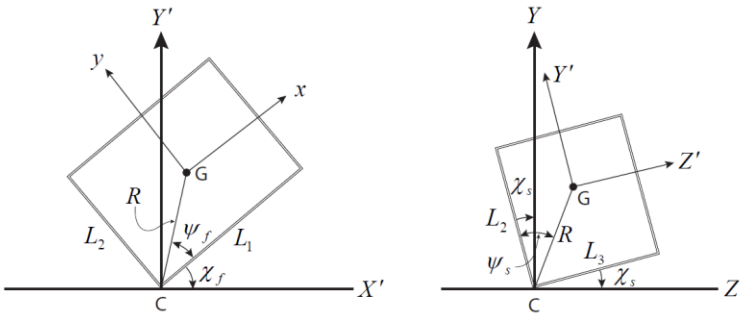

***Figure 2.15**: Calculations of the components of $\vec{R}$.*

Now that we know the magnitude of $\vec{R}$ we need to determine its components. Figure 2.15 shows both rotations as well as the relevant angles. We will begin by projecting $\vec{R}$ onto the (X,Y) plane, via a rotation by an angle $(\psi_s - \chi_s)$. Then we can express the components in the (X,Y) plane using the angle $(\psi_f + \chi_f)$. The resulting components are

$$R_x = R\cos(\psi_s - \chi_s)\cos(\psi_f + \chi_f)$$

$$R_y = R\cos(\psi_s - \chi_s)\sin(\psi_f + \chi_f)$$

$$R_z = R\sin(\psi_s - \chi_s)$$

Note that these expressions are only valid for the following ranges of the angles

$$\chi_s \le \psi_s$$

$$\chi_f \le \pi/2 - \psi_f$$

We are now ready to formulate the two rotation matrices denoted as $[Q_z]$ and $[Q_x]$.

$$[Q_z] = \begin{bmatrix} \cos(-\chi_f) & -\sin(-\chi_f) & 0 \\ \sin(-\chi_f) & \cos(-\chi_f) & 0 \\ 0 & 0 & 1 \end{bmatrix}$$

$$[Q_x] = \begin{bmatrix} 1 & 0 & 0 \\ 0 & \cos(\chi_s) & -\sin(\chi_s) \\ 0 & \sin(\chi_s) & \cos(\chi_s) \end{bmatrix}$$

The inertia matrix for this container is as follows

$$[I_G] = \begin{bmatrix} I_{xx} & 0 & 0 \\ 0 & I_{yy} & 0 \\ 0 & 0 & I_{zz} \end{bmatrix}$$

where $I_{xx} = (m/12)(L_2{}^2 + L_3{}^2)$, $I_{yy} = (m/12)(L_1{}^2 + L_3{}^2)$, and $I_{zz} = (m/12)(L_1{}^2 + L_2{}^2)$.

Since all calculations are carried out in the coordinate system of the contact point, the inertia matrix must be rotated. The rotated inertia matrix is given by

$$[I'_G] = [Q_x][Q_z][I_G][Q_z]^T[Q_x]^T$$

We are now ready to solve the impact problem. The dimensions of the container will be

$L_1 = 32\,\text{in}$

$L_2 = 25\,\text{in}$

$L_3 = 22.5\,\text{in}$

The weight of the container will be specified as 100 lb. Also, the coefficients of restitution and friction are $e_n = 0.32$ and $\mu = 0.7$, respectively. We can substitute the defined values into the above equations to obtain

$\psi_f = 38^0$

$\psi_s = 42^0$

$$[I_G] = \begin{bmatrix} 2.0331 & 0 & 0 \\ 0 & 2.7502 & 0 \\ 0 & 0 & 2.9636 \end{bmatrix} slug \cdot ft^2$$

Next we need to specify the initial velocities and angular velocities and solve for the final quantities. From here on, the analysis will be identical to that of the previous section. We will use the matrix equation (2.109) to solve for the final quantities for the case when no sliding occurs. Then, we need to check whether the sliding condition given by equation (2.131) is satisfied. If it is not, the matrix equation (2.119) needs to be solved for the final velocities. Matrix equation (2.119) uses the directional coefficients of friction, which should be calculated using equations (2.94), (2.124), (3.130) and (2.117).

We will begin the impact analysis of this container by specifying the initial velocity and angular velocity as follows

$\vec{V} = 60\hat{i} - 75\hat{j} - 1\hat{k}$

$\vec{\omega} = \vec{0}$

The X and Y components of the initial velocity are representative of those observed during drop tests of such a container. The Z component is assumed to be small and can be attributed to the effects of wind since the container is released from an altitude above the impacting surface. We will study the aerodynamics of free fall in Chapter 4. In Fig. 2.16 we plot the Z component of velocity after impact while varying the angles χ_f and χ_s.

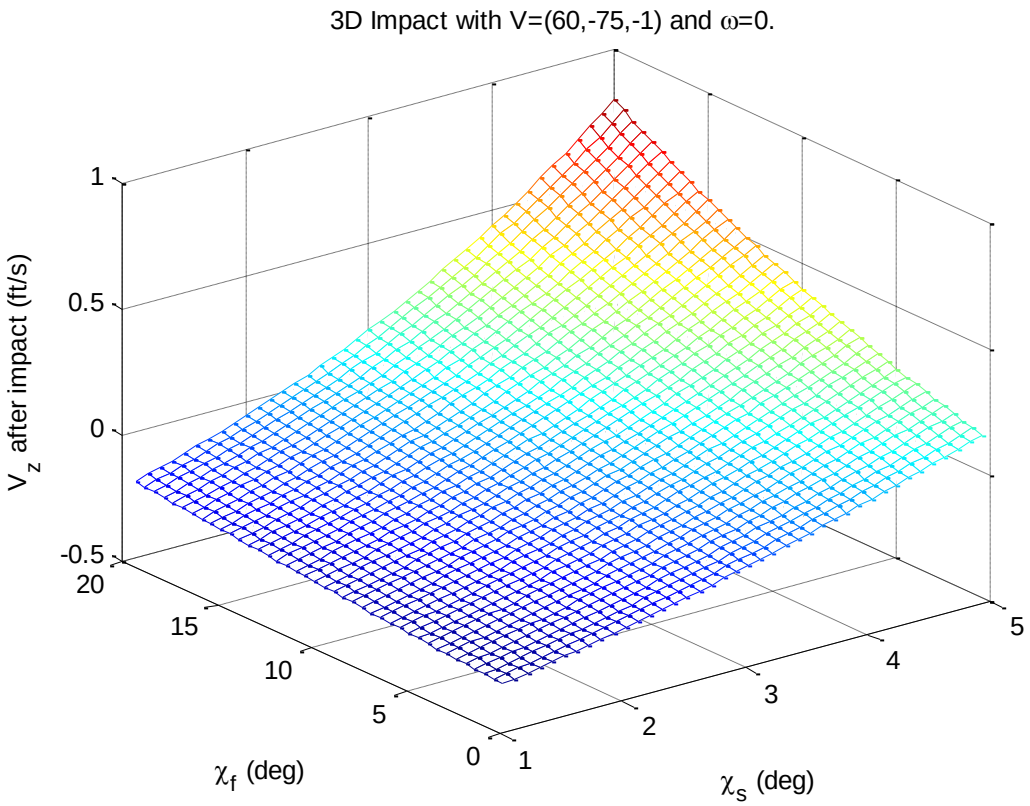

***Figure 2.16**: V_z' as a function of χ_f and χ_s; $\vec{V} = 60\hat{i} - 75\hat{j} - 1\hat{k}$, $\vec{\omega} = \vec{0}$.*

The above figure shows that for various values of χ_s, the Z component of velocity after impact, remains small, and can be neglected when compared to the other components of velocity. This validates the analysis of three dimensional impact using the two dimensional formulation when the container impacts the surface almost on a side, meaning that the angle χ_s is small. Note that the final velocity in the Z direction increases with an increasing χ_s. This tells us that if the angle χ_s is large, the three dimensional formulation must be used.

We would also like to determine how the existence of an initial angular velocity not perpendicular to the general plane of motion, (X,Y) plane, affects the post-impact velocities. Consider the following initial velocities

$$\vec{V} = 60\hat{i} - 75\hat{j} - 1\hat{k}$$

$$\vec{\omega} = \frac{\vec{V}}{10R} = \frac{\vec{V}}{193.44}$$

The resulting variation of the post-impact Z component of velocity is shown in the following figure. We see that the resulting Z component of velocity remains on the order of the initial velocity of the contact point in the Z direction. Therefore, if this component of velocity is small, then the two dimensional approximation remains valid. Just like Fig. 2.16, Fig. 2.17 also shows an increase in the Z component of the post-impact velocity with an increasing χ_s. Therefore the second criteria for using the two dimensional formulation remains the condition that χ_s is small. These results agree with experiment. For the quasi-planar impact of such a container, drop test have shown that the container continues to travel along the direction of the velocity at release. This will be studied in

greater detail in Chapter 5, where we will analyze the subsequent impacts of a rectangular container and use the two dimensional formulation in the analysis.

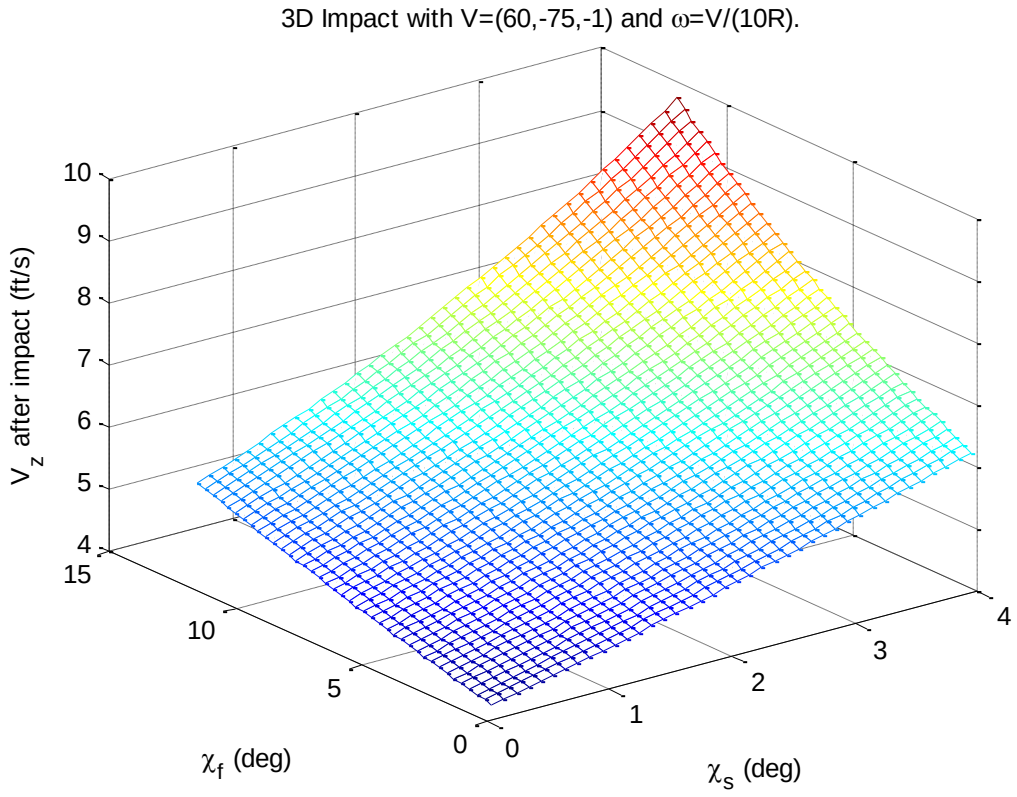

Figure 2.17: V_z' as a function of χ_f and χ_s; $\vec{V} = 60\hat{i} - 75\hat{j} - 1\hat{k}$, $\vec{\omega} = \dfrac{\vec{V}}{193.44}$.

Lastly, it should be noted that the range of χ_s analyzed in this section produces sliding during impact.

We have hereby concluded our discussion of rigid body impact and will now turn our attention to other models. In the following chapter we will study vibrational impact models and their applications.

Chapter 3

Vibrational Impact Mechanics

So far in our discussion of impact mechanics we have resorted to describing the energy dissipation during impact with the coefficient of restitution. The way it has been presented, this coefficient is more of a kinematical convenience rather than a material property of the impacting body. This chapter will be devoted to presenting material models for which the coefficient of restitution will be determined. These models will be viewed as linear and nonlinear vibratory systems. We will begin the analysis by looking at linear single degree of freedom oscillator, which will render a first approximation of the transient impact force. Multi-degree of freedom linear systems will also be used to model the interaction of cargo with its cushioning material. The stiffness properties between the cushion and cargo play a vital role in how the energy is absorbed during impact. The chapter will conclude with the analysis of a nonlinear vibratory model which will produce a more accurate representation of the impact force.

3.1 One Degree of Freedom Linear Oscillator

The aim of this section is to analyze a one degree of freedom linear mass spring damper system as it undergoes impact. The material modeled by this system is assumed to behave as a linear spring and damper in parallel. The coefficient of restitution will be obtained by first determining the governing differential equation and solving it subject to specified pre-impact conditions. The resulting solution will give the post-impact velocity and the impact duration as functions of the system parameters.

Consider the one degree of freedom system shown in Fig. 3.1, where m is the mass of the body, c is the damping coefficient, and k is the stiffness coefficient. The displacement of the mass is denoted by $y(t)$. We know that the spring force is ky and the damping force is $c\dot{y}$, where $\dot{y}$ indicates the first time derivative of the displacement.

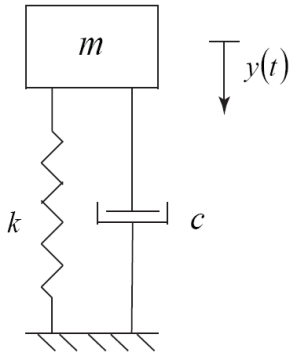

Figure 3.1*: One degree of freedom oscillator.*

Summing the forces acting on the on the mass we arrive at the following equation of motion

$$m\ddot{y} + c\dot{y} + ky = 0 \qquad (3.1)$$

where $\ddot{y}$ is the second derivative of the displacement with respect to time or the acceleration. To obtain a solution to (3.1), let us assume a solution of the form

$$y(t) = Ce^{vt} \qquad (3.2)$$

and substitute it into the differential equation leading to

$$mv^2Ce^{vt} + cvCe^{vt} + kCe^{vt} = 0$$

Simplifying we get the following characteristic equation

$$mv^2 + cv + k = 0$$

Therefore the two roots are

$$v_{1,2} = \frac{-c \pm \sqrt{c^2 - 4km}}{2m} \tag{3.3}$$

Since we are interested in determining the coefficient of restitution, we will not consider the over damped and critically damped cases. For the under damped case ($c^2 < 4km$) the roots of the characteristic equation are of the form:

$$v_{1,2} = -\varsigma \pm i\omega \tag{3.4}$$

$$\varsigma = \frac{c}{2m} \qquad \omega = \frac{\sqrt{4km - c^2}}{2m} \tag{3.5a,b}$$

Substituting equation (3.4) into solution (3.2) we get the following solution

$$y(t) = e^{-\varsigma t}\left[C_1 \cos(\omega t) + C_2 \sin(\omega t)\right] \tag{3.6}$$

The two constants C_1 and C_2 are determined using the initial conditions on position and velocity. The initial condition on position is

$$y(0) = 0 \tag{3.7}$$

Applying equation (3.7) to equation (3.6) we get

$$C_1 = 0 \tag{3.8}$$

The solution (3.6) now becomes

$$y(t) = e^{-\varsigma t} C_2 \sin(\omega t) \tag{3.9}$$

The initial velocity of the impacting body is specified as

$$\dot{y}(0) = V_0 \tag{3.10}$$

In order to apply equation (3.10) to equation (3.9), we first need to differentiate it.

$$\dot{y}(t) = e^{-\varsigma t} C_2 \left[\omega \cos(\omega t) - \varsigma \sin(\omega t)\right] \tag{3.11}$$

Apply the initial condition on velocity we get

$$C_2 = \left(\frac{V_0}{\omega} \right) \tag{3.12}$$

The final expressions for the position, velocity, and after differentiating again, acceleration are:

$$y(t) = e^{-\varsigma t} \left(\frac{V_0}{\omega} \right) \sin(\omega t) \tag{3.13a}$$

$$\dot{y}(t) = e^{-\varsigma t} \left(\frac{V_0}{\omega} \right) \left[\omega \cos(\omega t) - \varsigma \sin(\omega t) \right] \tag{3.13b}$$

$$\ddot{y}(t) = e^{-\varsigma t} \left(\frac{V_0}{\omega} \right) \left[\left(\varsigma^2 - \omega^2 \right) \sin(\omega t) - 2\varsigma\omega \cos(\omega t) \right] \tag{3.13c}$$

In order to determine the coefficient of restitution we have to specify when the restitution phase ends. One way of doing this is by allowing the system to go through one half of an oscillation and analyzing it afterwards. A different approach is to define the end of impact as the time when the impact force reaches a zero value. The first approach seems more appropriate since the inherent problem with the linear mass spring damper model is that the initial velocity causes a nonzero initial impact force. This can be seen from the governing equation (3.1) where the initial damping force is non-zero.

Let us begin by considering the first approach. If we allow the mass spring damper system to go through one half of an oscillation the resulting impact duration is

$$t^* = \frac{\pi}{\omega} \tag{3.14}$$

where ω is the damped natural frequency given by equation (3.5b). In order to obtain the coefficient of restitution we need to determine the velocity at time t^*. Substituting equation (3.14) into equation (3.13b) we get

$$\dot{y}(t^*) = -e^{-\varsigma\frac{\pi}{\omega}}V_0 \tag{3.15}$$

The coefficient if restitution is defined as the negative ratio of final to initial impact velocities

$$e_n = -\frac{\dot{y}(t^*)}{V_0} \tag{3.16}$$

Substituting equation (3.15) into equation (3.16)

$$e_n = e^{-\frac{\pi\varsigma}{\omega}} \tag{3.17}$$

Using expressions (3.5a,b) we get the coefficient of restitution in terms of stiffness coefficient and the damping coefficient.

$$e_n = \exp\left(\frac{-\pi c}{\sqrt{4km - c^2}}\right) \tag{3.18}$$

Note that the coefficient of restitution is not a function of the initial velocity but only depends on the stiffness and damping coefficients. The next figures demonstrate the variation of the impact duration and the coefficient of restitution with respect to the impact parameters.

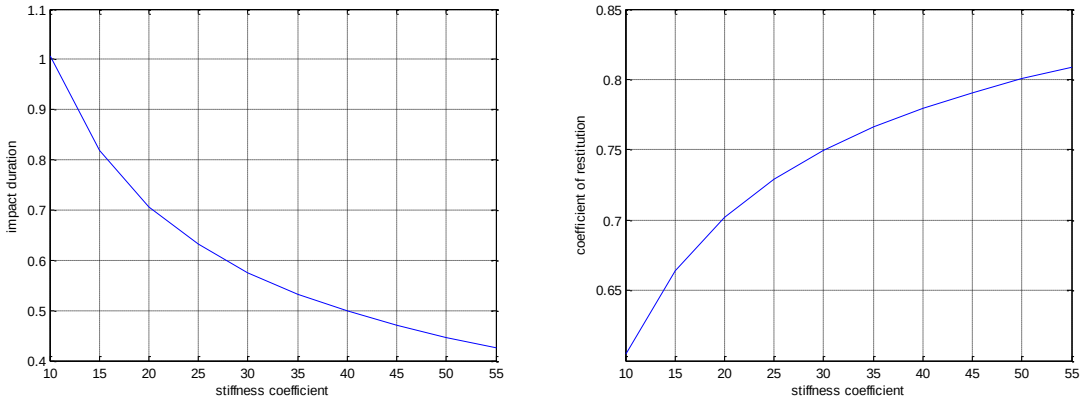

***Figure 3.2**: Impact duration and coefficient of restitution for* $m = 1$, $V_i = 1$, *and* $c = 1$.

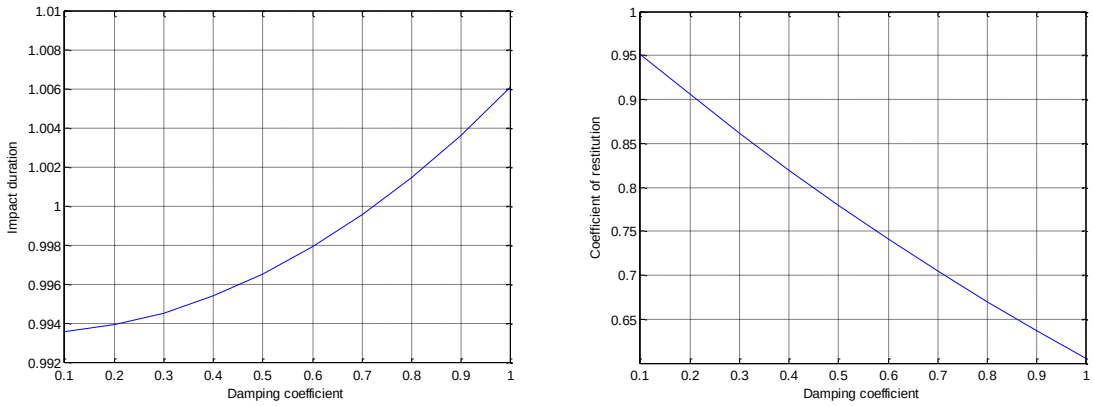

***Figure 3.3**: Impact duration and coefficient of restitution for* $m=1$, $V_i=1$, *and* $k=10$.

From Fig. 3.2 we see that an increase in the stiffness coefficient decreases the impact duration and increases the coefficient of restitution. An increasing damping coefficient slightly increases the impact duration, leaving it essentially unchanged, and decreases the coefficient of restitution seen in Fig. 3.3. This is intuitive since a larger value of the damping coefficient corresponds to more energy loss and hence a smaller coefficient of restitution. Smaller, more realistic, impact duration is presented in the following figure.

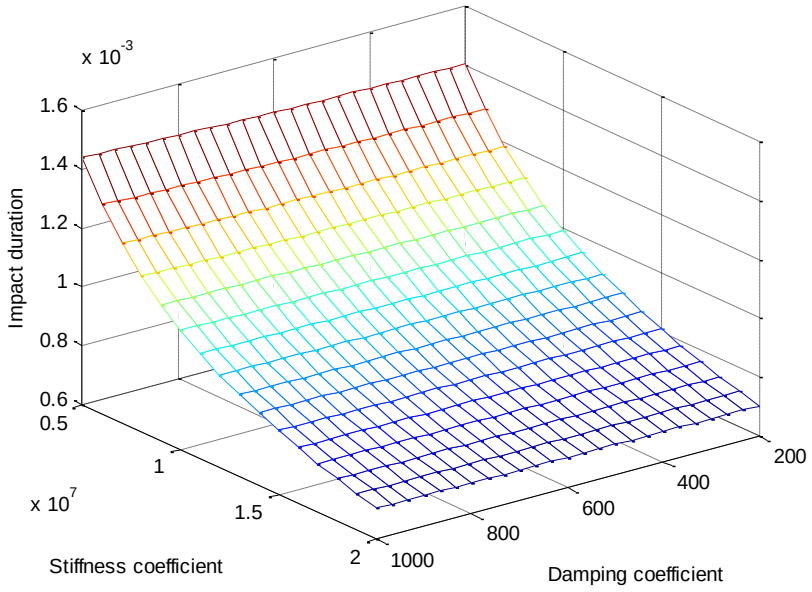

***Figure 3.4**: Impact duration as a function of stiffness and damping coefficients.*

The value of the damping coefficient has less of an effect on the impact duration. The stiffness coefficient has a more profound affect. Let us conduct a thought experiment to see why an increase of the stiffness coefficient causes the impact duration to drop. A stiffer material will have a larger natural frequency and therefore a smaller period of oscillation, which is essentially the impact duration.

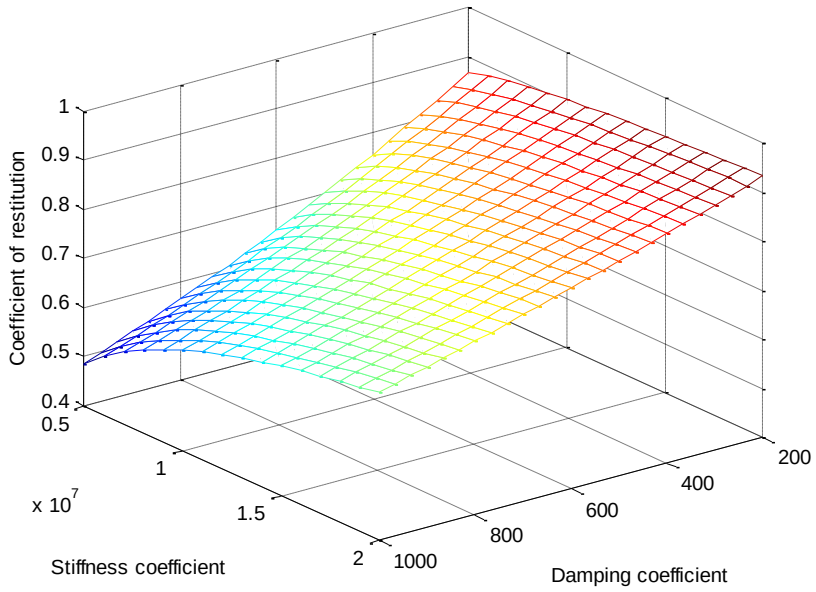

Figure 3.5*: Coefficient of restitution as a function of stiffness and damping coefficients.*

Figure 3.5 shows the expected behavior of the coefficient of restitution, namely its decrease with increasing damping. The thing to note is that the coefficient of restitution increases at a decreasing rate with an increasing stiffness coefficient. This tells us that in impact scenarios where the stiffness coefficient is substantially large varying its value will have little effect on the coefficient of restitution. This behavior will be more evident at higher damping coefficients.

For the sake of comparison let us now solve for the impact duration and the coefficient of restitution for the one degree of freedom linear oscillator using the second

approach. This method is different because rather than considering a half oscillation of the system, we define the end of impact as the instant when the impact force goes to zero. Since this model is presented with a purely vertical impact, the impact force is equal to the inertial force of mass times the acceleration. Note that we have neglected the contribution of the gravitational acceleration because its magnitude is miniscule in comparison with the impact force. A similar discussion which includes gravitational effects was done by Benaroya [2]. Let us begin our analysis by setting the acceleration given by equation (3.13c) equal to zero and solving for the impact duration.

$$t^* = \frac{1}{\omega}\arctan\left(\frac{2\varsigma\omega}{\left(\varsigma^2 - \omega^2\right)}\right) \tag{3.19}$$

Substituting the expressions (3.5a) and (3.5b) into above we get

$$t^* = \frac{2m}{\sqrt{4km - c^2}}\arctan\left(\sqrt{4km - c^2}\left(\frac{c}{c^2 - 2km}\right)\right) \tag{3.20}$$

The coefficient is obtained by using equations (3.13b) and (3.16).

$$e_n = -e^{-\varsigma t^*}\left[\cos\left(\omega t^*\right) - \frac{\varsigma}{\omega}\sin\left(\omega t^*\right)\right] \tag{3.21}$$

This will not be done in this thesis, but equation (3.20) can now be substituted into equation (3.21) in order to obtain the coefficient of restitution in terms of the system parameters. The following figures compare the zero force model to the half oscillation model discussed earlier in this section.

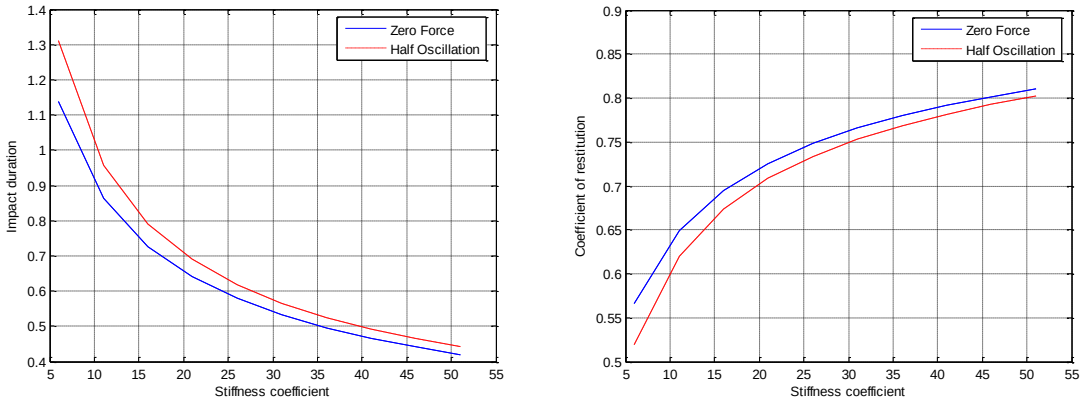

***Figure 3.6**: Comparison of the models varying stiffness, with* $m=1$, $V_0=1$, *and* $c=1$.

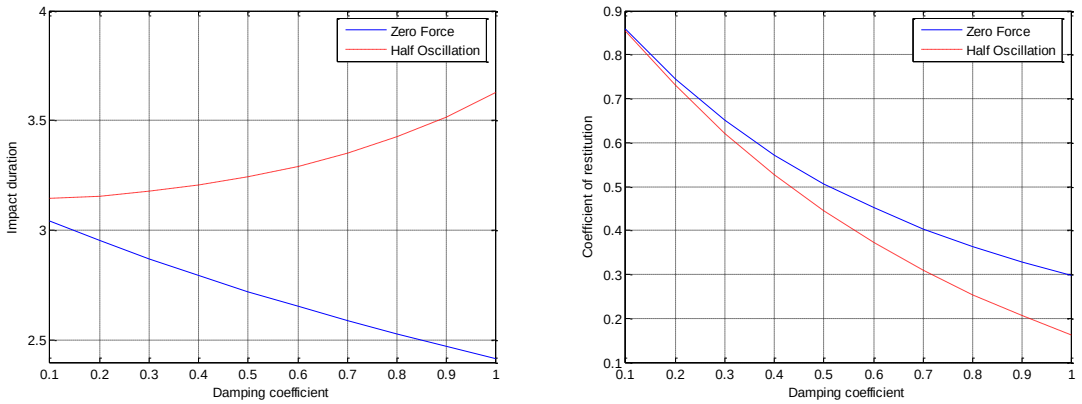

***Figure 3.7**: Comparison of the models varying damping, with* $m=1$, $V_0=1$, *and* $k=10$.

Figure 3.6 shows that the impact duration and the coefficient of restitution only differ by a small offset between the two models. From Fig. 3.7 we also see that the curves of the coefficient of restitution are very close, but the impact duration curves deviate from each other with an increasing damping coefficient. Let us now consider the force versus displacement curves for the impact scenarios discussed in this section.

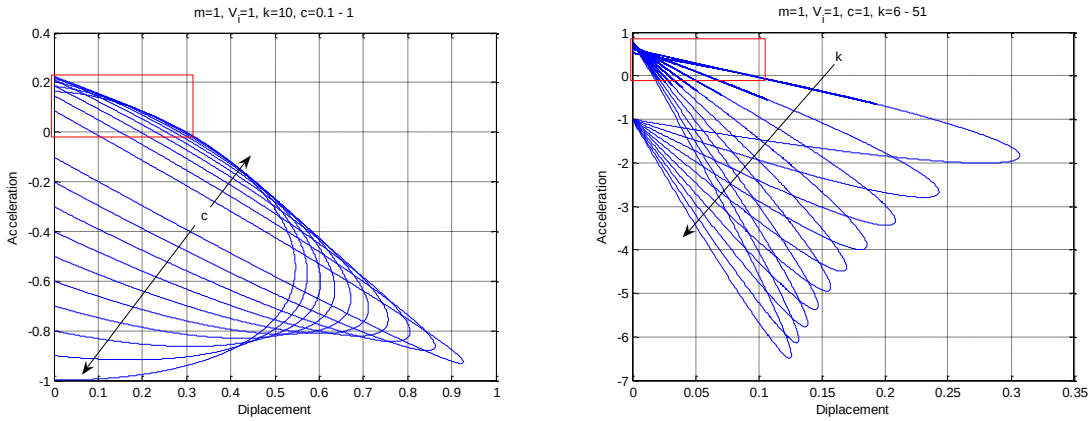

***Figure 3.8**: Hysteresis curves for the impacts analyzed in section 3.1.*

The hysteresis curves presented in Fig. 3.8 show the impact force being negative; this is because the direction of positive displacement was taken downwards in Fig. 3.1. The zero force model having a larger coefficient of restitution can be explained by looking at Fig. 3.8 (displacement vs. force) which shows that the energy loss (enclosed area) will of course be larger for the half oscillation model. This difference in the energy loss of the two models is outlined by a red rectangle. Now that we have obtained a topical understanding of the impact behavior of the one degree of freedom linear oscillator we can turn our attention to multi degree of freedom systems.

3.2 Two Degree of Freedom Linear Oscillator

In this section we will consider a two degree of freedom mass spring damper system. This model can be useful in analyzing the response for impacts when the material properties of the cargo and the cushion are different. The cushion will be modeled by having a mass, stiffness, and damping properties similar to the cargo. One should keep in mind that this is a linear model as opposed to most impact phenomena which tend to be highly nonlinear. Consider the schematic of the cushion-cargo system shown in Fig. 3.9.

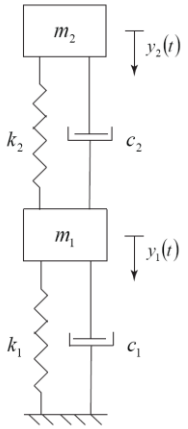

***Figure 3.9**: Two degree of freedom oscillator.*

The mass, damping coefficient, stiffness coefficient, and the displacement of the cushion are m_1, c_1, k_1, and $y_1(t)$, while for the cargo they are m_2, c_2, k_2, and $y_2(t)$. The kinetic diagram for both masses is shown below.

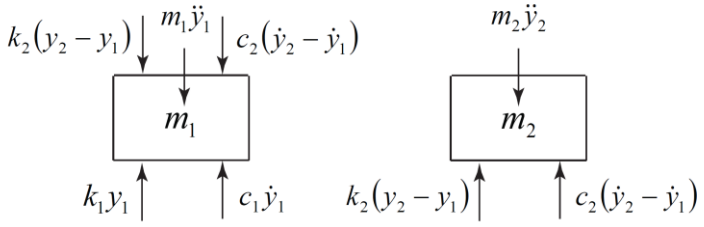

***Figure 3.10**: Kinetic diagram of the two degree of freedom oscillator.*

Summing the forces for both masses we get

$$m_1\ddot{y}_1 = c_2(\dot{y}_2 - \dot{y}_1) + k_2(y_2 - y_1) - c_1\dot{y}_1 - k_1 y_1 \tag{3.22a}$$

$$m_2\ddot{y}_2 = -c_2(\dot{y}_2 - \dot{y}_1) - k_2(y_2 - y_1) \tag{3.22b}$$

Note that we have once again disregarded the contribution of the gravitational force because it is non-impulsive and therefore its contribution is negligible. Rearranging and putting equation (3.22) into matrix form we arrive at

$$\begin{bmatrix} m_1 & 0 \\ 0 & m_2 \end{bmatrix}\begin{Bmatrix} \ddot{y}_1 \\ \ddot{y}_2 \end{Bmatrix} + \begin{bmatrix} (c_1 + c_2) & -c_2 \\ -c_2 & c_2 \end{bmatrix}\begin{Bmatrix} \dot{y}_1 \\ \dot{y}_2 \end{Bmatrix} + \begin{bmatrix} (k_1 + k_2) & -k_2 \\ -k_2 & k_2 \end{bmatrix}\begin{Bmatrix} y_1 \\ y_2 \end{Bmatrix} = \begin{Bmatrix} 0 \\ 0 \end{Bmatrix} \tag{3.23a}$$

$$[m]\{\ddot{y}\}+[c]\{\dot{y}\}+[k]\{y\}=\{0\} \tag{3.23b}$$

, where $[m]$, $[c]$, and $[k]$ are the mass, damping and stiffness matrices. In this model we are interested in analyzing the effects of the stiffness and mass ratios on the behavior of the system; therefore we will assume that the damping is proportional to the stiffness. This is a special case of proportional damping, or more accurately Rayleigh Damping [5], and can be stated mathematically as

$$[c]=\sigma[k] \tag{3.24}$$

, where σ is the proportionality constant.

Substituting equation (3.24) into (3.23) we get

$$\begin{bmatrix} m_1 & 0 \\ 0 & m_2 \end{bmatrix}\begin{Bmatrix} \ddot{y}_1 \\ \ddot{y}_2 \end{Bmatrix}+\sigma\begin{bmatrix} (k_1+k_2) & -k_2 \\ -k_2 & k_2 \end{bmatrix}\begin{Bmatrix} \dot{y}_1 \\ \dot{y}_2 \end{Bmatrix}+\begin{bmatrix} (k_1+k_2) & -k_2 \\ -k_2 & k_2 \end{bmatrix}\begin{Bmatrix} y_1 \\ y_2 \end{Bmatrix}=\begin{Bmatrix} 0 \\ 0 \end{Bmatrix} \tag{3.25a}$$

$$[m]\{\ddot{y}\}+\sigma[k]\{\dot{y}\}+[k]\{y\}=\{0\} \tag{3.25b}$$

In other words what we are saying is

$$c_1=\sigma k_1 \qquad\qquad c_2=\sigma k_2 \tag{3.26a,b}$$

We will use modal analysis to solve the system of differential equations given by (3.25). We therefore need to first solve the undamped problem. The problem to be solved is now

$$\begin{bmatrix} m_1 & 0 \\ 0 & m_2 \end{bmatrix}\begin{bmatrix} \ddot{y}_1 \\ \ddot{y}_2 \end{bmatrix}+\begin{bmatrix} (k_1+k_2) & -k_2 \\ -k_2 & k_2 \end{bmatrix}\begin{bmatrix} y_1 \\ y_2 \end{bmatrix}=\begin{bmatrix} 0 \\ 0 \end{bmatrix} \tag{3.27a}$$

$$[m]\{\ddot{y}\}+[k]\{y\}=\{0\} \tag{3.27b}$$

Assuming a solution of the form

$$\{y(t)\}=\{Y\}e^{rt} \tag{3.28}$$

Substituting equation (3.28) into equation (3.27b) we get

$$\left([m]r^2+[k]\right)\{Y\}=\{0\} \tag{3.29}$$

In order to render the matrix linearly dependent we require that the determinant is zero.

$$\det\left(\left[m\right]r^2+\left[k\right]\right)=0 \tag{3.30}$$

Using equation (3.27a) the determinant in equation (3.30) becomes

$$\begin{vmatrix} m_1r^2+\left(k_1+k_2\right) & -k_2 \\ -k_2 & m_2r^2+k_2 \end{vmatrix}=0$$

Working out the above determinant we get the following characteristic equation.

$$m_1m_2r^4+\left(m_1k_2+m_2\left(k_1+k_2\right)\right)r^2+\left(k_1k_2\right)=0 \tag{3.31}$$

For arbitrary values of mass and stiffness, equation (3.31) is used to determine r_i in our undamped solution given by (3.28). The corresponding modal vectors are obtained by substituting the values of r_i back into equation (3.29).

$$Y_2^{(i)}=\frac{m_1r_i^{\,2}+\left(k_1+k_2\right)}{k_2}Y_1^{(i)} \tag{3.32}$$

Note that the superscript specifies the modal vector, while the subscript denotes the components of the modal vector. The modal vector can now be arranged in column form into a matrix as follows:

$$\left[T\right]=\left[\left\{Y^{(1)}\right\}\quad\left\{Y^{(2)}\right\}\right]=\begin{bmatrix} Y_1^{(1)} & Y_1^{(2)} \\ Y_2^{(1)} & Y_2^{(2)} \end{bmatrix} \tag{3.33}$$

To reiterate, the reason for obtaining the undamped solution first was to be able to construct the $\left[T\right]$ transformation matrix. This matrix will now be used to diagonalize the mass and stiffness matrices as follows

$$\left[\tilde{m}\right]=\left[T\right]^T\left[m\right]\left[T\right] \tag{3.34a}$$

$$\left[\tilde{k}\right]=\left[T\right]^T\left[k\right]\left[T\right] \tag{3.34b}$$

Let us also define the modal displacement variable as

$$\{y(t)\} = [T]\{\eta(t)\} \tag{3.35}$$

Pre-multiplying equation (3.25b) by $[T]^T$ and substituting equation (3.35) we get

$$[T]^T [m][T]\{\ddot{\eta}(t)\} + \sigma[T]^T [k][T]\{\dot{\eta}(t)\} + [T]^T [k][T]\{\eta(t)\} = \{0\}$$

Applying equations (3.34) to the above equation, we get

$$[\tilde{m}]\{\ddot{\eta}(t)\} + \sigma[\tilde{k}]\{\dot{\eta}(t)\} + [\tilde{k}]\{\eta(t)\} = \underline{0} \tag{3.36}$$

The modal mass and stiffness matrices in equation (3.36) are diagonal; we have therefore just decoupled the governing equations. Defining the position along the diagonal of the matrix as j, we get the following equation to solve as many times as there are degrees of freedom, in this case twice.

$$\tilde{m}_j \ddot{\eta}_j(t) + \sigma\tilde{k}_j \dot{\eta}_j(t) + \tilde{k}_j \eta_j(t) = 0 \tag{3.37}$$

We will now assume a solution of the form

$$\eta(t) = Ce^{\varepsilon t} \tag{3.38}$$

Substituting equation (3.38) into equation (3.37) we arrive at

$$\tilde{m}_j \varepsilon^2 + \sigma\tilde{k}_j \varepsilon + \tilde{k}_j = 0 \tag{3.39}$$

The roots of equation (3.39) are

$$\varepsilon_j = \frac{-\sigma\tilde{k}_j}{2\tilde{m}_j} \pm \frac{\sqrt{\tilde{k}_j\left(\sigma^2\tilde{k}_j - 4\tilde{m}_j\right)}}{2\tilde{m}_j} \tag{3.40}$$

Once again we are interested in the underdamped case, because in this model it corresponds to the restitution phase of impact. The necessary condition for this case becomes $\tilde{m}_j \geq \left(\sigma^2 \big/ 4\right)\tilde{k}_j$, therefore equation (3.40) can be rewritten as follows.

$$\varepsilon_i = -\varsigma_i \pm i\omega_i \tag{3.41}$$

$$\varsigma_j = \frac{\sigma\tilde{k}_j}{2\tilde{m}_j} \qquad \omega_j = \frac{\sqrt{\tilde{k}_j\left(4\tilde{m}_j - \sigma^2\tilde{k}_j\right)}}{2\tilde{m}_j} \tag{3.42a,b}$$

Using Euler's formula the modal solution is

$$\eta_j(t) = e^{-\varsigma_j t}\left[C_j\cos(\omega_j t) + D_j\sin(\omega_j t)\right] \tag{3.43}$$

, where C_j and D_j are constants. In order to obtain the response of the system we have to transform the above solution back to the original displacement coordinates $\underline{y}(t)$.

Substituting equation (3.33) into equations (3.35) we have

$$\{y(t)\} = [T]\{\eta(t)\} = \begin{bmatrix} Y_1^{(1)} & Y_1^{(2)} \\ Y_2^{(1)} & Y_2^{(2)} \end{bmatrix}\begin{Bmatrix}\eta_1(t)\\ \eta_2(t)\end{Bmatrix}$$

Multiplying out the above equation

$$y_1(t) = Y_1^{(1)}\eta_1(t) + Y_1^{(2)}\eta_2(t) \tag{3.44a}$$

$$y_2(t) = Y_2^{(1)}\eta_1(t) + Y_2^{(2)}\eta_2(t) \tag{3.44b}$$

Substituting the solution (3.43) into above

$$y_1(t) = Y_1^{(1)}e^{-\varsigma_1 t}\left[C_1\cos(\omega_1 t) + D_1\sin(\omega_1 t)\right] + Y_1^{(2)}e^{-\varsigma_2 t}\left[C_2\cos(\omega_2 t) + D_2\sin(\omega_2 t)\right]$$

$$y_2(t) = Y_2^{(1)}e^{-\varsigma_1 t}\left[C_1\cos(\omega_1 t) + D_1\sin(\omega_1 t)\right] + Y_2^{(2)}e^{-\varsigma_2 t}\left[C_2\cos(\omega_2 t) + D_2\sin(\omega_2 t)\right]$$

(3.45a,b)

Besides the displacements, we will also need the velocities and accelerations of both masses, which are obtained by differentiating equations (3.45) with respect to time.

$$\begin{aligned}\dot{y}_1(t) = {} & e^{-\varsigma_1 t}Y_1^{(1)}\left[\left(-\varsigma_1 C_1 + \omega_1 D_1\right)\cos(\omega_1 t) + \left(-\varsigma_1 D_1 - \omega_1 C_1\right)\sin(\omega_1 t)\right] \\ & + e^{-\varsigma_2 t}Y_1^{(2)}\left[\left(-\varsigma_2 C_2 + \omega_2 D_2\right)\cos(\omega_2 t) + \left(-\varsigma_2 D_2 - \omega_2 C_2\right)\sin(\omega_2 t)\right]\end{aligned} \tag{3.45c}$$

$$\begin{aligned}\dot{y}_2(t) = {} & e^{-\varsigma_1 t}Y_2^{(1)}\left[\left(-\varsigma_1 C_1 + \omega_1 D_1\right)\cos(\omega_1 t) + \left(-\varsigma_1 D_1 - \omega_1 C_1\right)\sin(\omega_1 t)\right] \\ & + e^{-\varsigma_2 t}Y_2^{(2)}\left[\left(-\varsigma_2 C_2 + \omega_2 D_2\right)\cos(\omega_2 t) + \left(-\varsigma_2 D_2 - \omega_2 C_2\right)\sin(\omega_2 t)\right]\end{aligned} \tag{3.45d}$$

$$\ddot{y}_1(t) = e^{-\varsigma_1 t} Y_1^{(1)} \left[\left({\varsigma_1}^2 C_1 - 2\varsigma_1 \omega_1 D_1 - {\omega_1}^2 C_1 \right) \cos(\omega_1 t) + \left({\varsigma_1}^2 D_1 + 2\varsigma_1 \omega_1 C_1 - {\omega_1}^2 D_1 \right) \sin(\omega_1 t) \right]$$
$$+ e^{-\varsigma_2 t} Y_1^{(2)} \left[\left({\varsigma_2}^2 C_2 - 2\varsigma_2 \omega_2 D_2 - {\omega_2}^2 C_2 \right) \cos(\omega_2 t) + \left({\varsigma_2}^2 D_2 + 2\varsigma_2 \omega_2 C_2 - {\omega_2}^2 D_2 \right) \sin(\omega_2 t) \right]$$

$$\ddot{y}_2(t) = e^{-\varsigma_1 t} Y_2^{(1)} \left[\left({\varsigma_1}^2 C_1 - 2\varsigma_1 \omega_1 D_1 - {\omega_1}^2 C_1 \right) \cos(\omega_1 t) + \left({\varsigma_1}^2 D_1 + 2\varsigma_1 \omega_1 C_1 - {\omega_1}^2 D_1 \right) \sin(\omega_1 t) \right]$$
$$+ e^{-\varsigma_2 t} Y_2^{(2)} \left[\left({\varsigma_2}^2 C_2 - 2\varsigma_2 \omega_2 D_2 - {\omega_2}^2 C_2 \right) \cos(\omega_2 t) + \left({\varsigma_2}^2 D_2 + 2\varsigma_2 \omega_2 C_2 - {\omega_2}^2 D_2 \right) \sin(\omega_2 t) \right]$$

(3.45e,f)

We still need to determine the constants C_j and D_j. This will be done by specifying the initial conditions on position and velocity. Without loss of generality let us take the initial displacements as zero and the initial velocity of both masses to be the same, such that there is no relative motion between the masses prior to impact. Applying these conditions to equations (3.45) we arrive at the following

$$y_1(0) = 0 = Y_1^{(1)} C_1 + Y_1^{(2)} C_2$$

$$y_2(0) = 0 = Y_2^{(1)} C_1 + Y_2^{(2)} C_2$$

$$\dot{y}_1(0) = V_0 = -\varsigma_1 Y_1^{(1)} C_1 + \omega_1 Y_1^{(1)} D_1 - \varsigma_2 Y_1^{(2)} C_2 + \omega_2 Y_1^{(2)} D_2$$

$$\dot{y}_2(0) = V_0 = -\varsigma_1 Y_2^{(1)} C_1 + \omega_1 Y_2^{(1)} D_1 - \varsigma_2 Y_2^{(2)} C_2 + \omega_2 Y_2^{(2)} D_2$$

Putting the four equations above into matrix form we get

$$\begin{bmatrix} 0 \\ 0 \\ V_0 \\ V_0 \end{bmatrix} = \begin{bmatrix} Y_1^{(1)} & 0 & Y_1^{(2)} & 0 \\ Y_2^{(1)} & 0 & Y_2^{(2)} & 0 \\ -\varsigma_1 Y_1^{(1)} & \omega_1 Y_1^{(1)} & -\varsigma_2 Y_1^{(2)} & \omega_2 Y_1^{(2)} \\ -\varsigma_1 Y_2^{(1)} & \omega_1 Y_2^{(1)} & -\varsigma_2 Y_2^{(2)} & \omega_2 Y_2^{(2)} \end{bmatrix} \begin{bmatrix} C_1 \\ D_1 \\ C_2 \\ D_2 \end{bmatrix} \tag{3.46}$$

In matrix notation equation (3.46) becomes

$$\{y_0\} = [G]\{C\} \tag{3.47}$$

, where $\{y_0\}$ is the vector of initial conditions, $\{C\}$ is the vector of the constants to be determined, and $[G]$ is the matrix seen in equation (3.46). The unknown constants are therefore

$$\{C\} = [G]^{-1}\{y_0\} \tag{3.48}$$

We have now solved the problem of a two degree of freedom linear oscillator impacting a surface with an initial velocity. A question which still needs to be answered is what marks the end of impact. For a two mass system there is no single frequency which can be used to obtain the period of half of an oscillation as we have done in the previous section. Instead we take the end of impact as the time when the acceleration of m_1 reaches its initial value. Recall that the initial accelerations of the masses are non-zero in this linear model due to the initial condition on velocity. The initial accelerations can be obtained from equations (3.45e,f) as follows

$$\ddot{y}_1(0) = Y_1^{(1)}\left(\varsigma_1{}^2 C_1 - 2\varsigma_1\omega_1 D_1 - \omega_1{}^2 C_1\right) + Y_1^{(2)}\left(\varsigma_2{}^2 C_2 - 2\varsigma_2\omega_2 D_2 - \omega_2{}^2 C_2\right)$$

$$\ddot{y}_2(0) = Y_2^{(1)}\left(\varsigma_1{}^2 C_1 - 2\varsigma_1\omega_1 D_1 - \omega_1{}^2 C_1\right) + Y_2^{(2)}\left(\varsigma_2{}^2 C_2 - 2\varsigma_2\omega_2 D_2 - \omega_2{}^2 C_2\right)$$

(3.49a,b)

The end of impact, t^*, is defined as the time when the acceleration of the cushion is

$$\ddot{y}_1(t^*) = \ddot{y}_1(0) \tag{3.50}$$

This definition of the impact termination time might seem random, but other definitions do not differ by much because of the large amplitude of the maximum acceleration compared to the value of the initial acceleration.

In order to analyze the behavior of this system in a dimensionless manner we need to define the mass and stiffness ratios as follows.

$$\hat{m} = \frac{m_2}{m_1} \qquad \hat{k} = \frac{k_2}{k_1} \qquad (3.51a,b)$$

The following figures depict the variation of the impact duration as well as the coefficient of restitution with the mass and stiffness ratios. The reference mass and stiffness of m_1 were taken as unity. The impact duration shown in Fig. 3.11 decreases with an increasing stiffness ratio, while the mass ratio, in the range shown, has little effect on it.

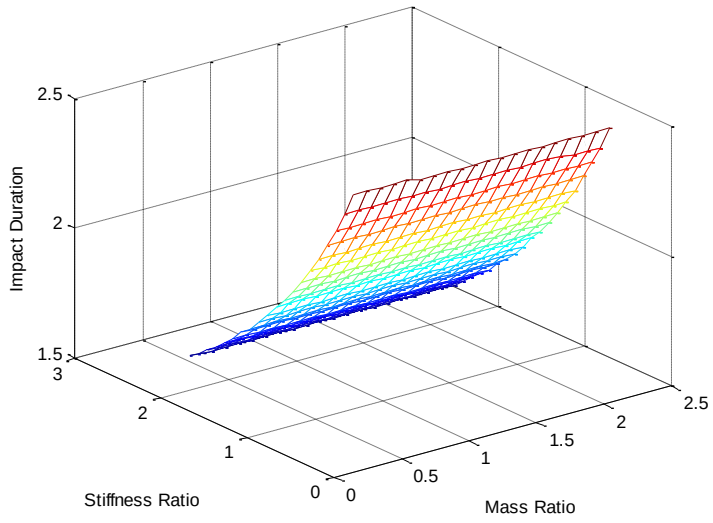

***Figure 3.11**: Impact duration for* $\sigma = 0.2$.

As was shown in the previous section, the coefficient of restitution plotted in Fig. 3.12 increases with increasing stiffness coefficient. This might not look so from the figures, but that is because they are plotted as a function of the ratio of stiffness coefficients. The figure showing the coefficients of restitution of both masses is the key in understanding the interaction between the cushion and the cargo, which is what we are trying to model by this system. The coefficient of restitution of the cargo, mass m_2, is calculated using the impact duration defined by the cushion, mass m_1, meaning that the value of the final

velocity is taken at the end of impact defined earlier. We see that the coefficients of restitution of the cargo and the cushion are quite different for small values of the stiffness ratio. This is undesirable since the acceleration experienced by the cargo will be larger than that of the cushion. We therefore want the stiffness of the cushion to be smaller than the stiffness of the cargo.

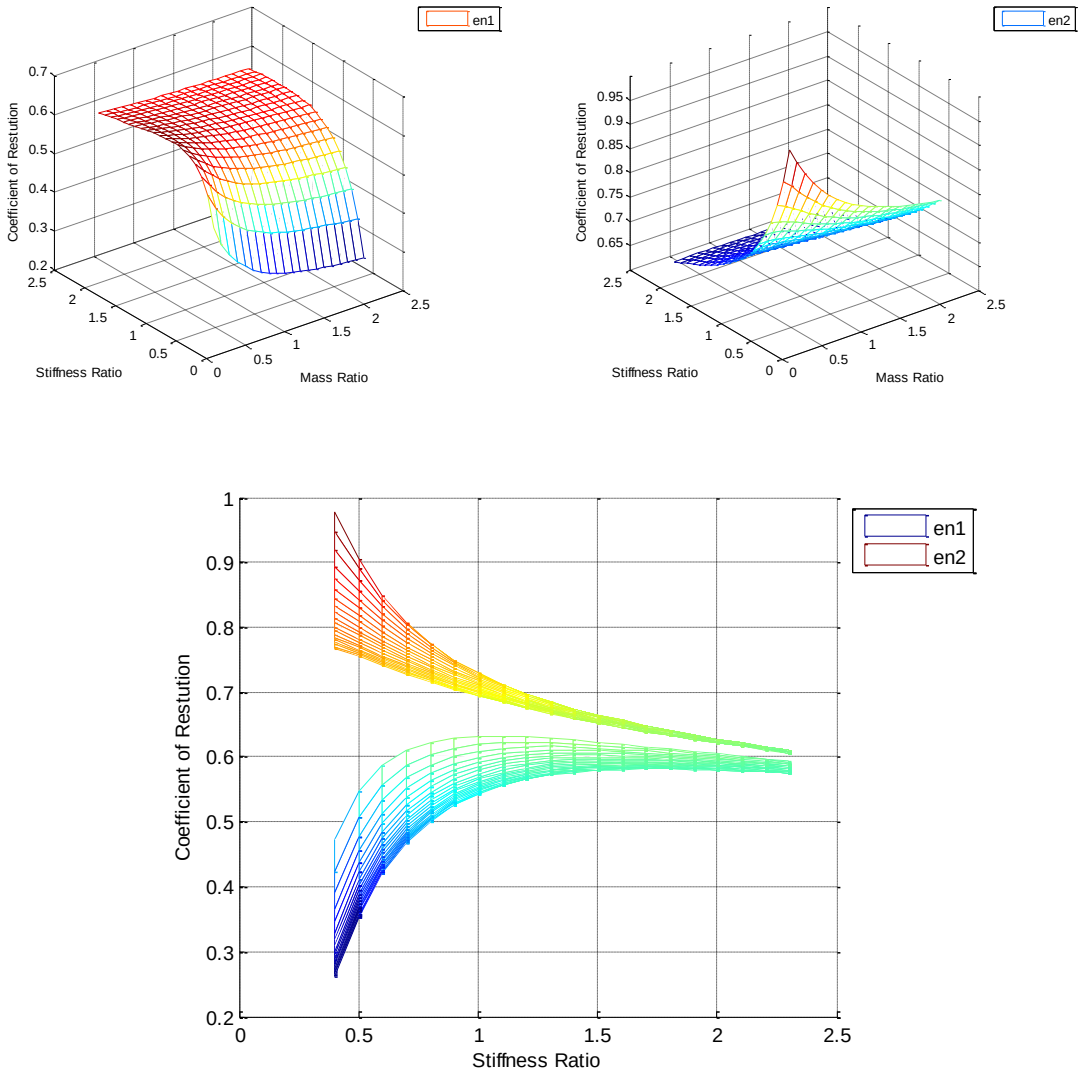

***Figure 3.12**: Coefficient of restitution for* $\sigma = 0.2$.

The cushion-cargo interaction depends on the difference in the coefficients of restitution. If this difference is large then one of the masses must have experienced a larger

acceleration because the release velocities are the same. This means that a lower stiffness of the cargo causes it to oscillate faster than the cushion and absorb more energy than the cushion. For comparison, the next two figures show the same plots with proportionality constant of $\sigma = 0.7$ rather than $\sigma = 0.2$ used previously.

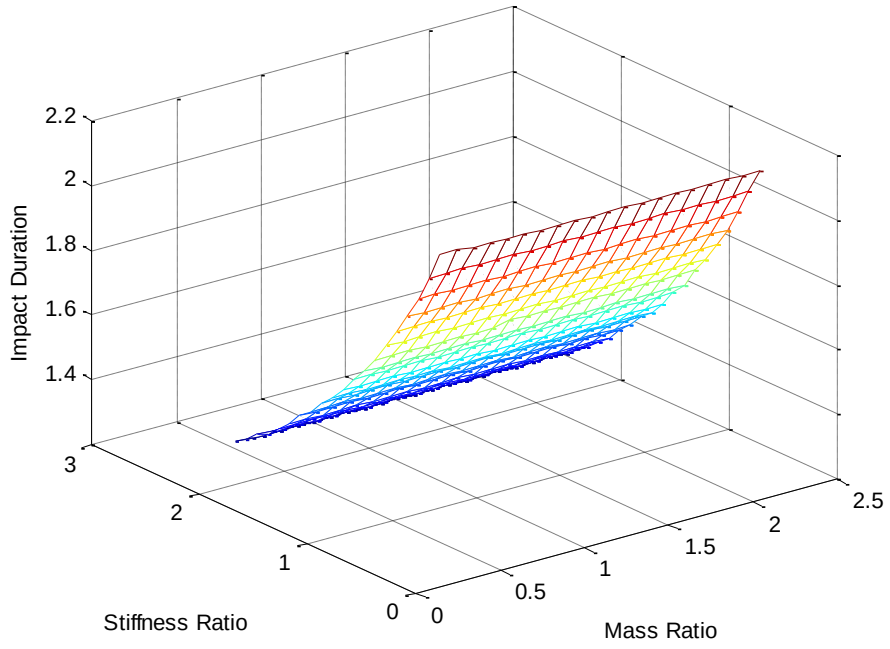

***Figure 3.13**: Impact duration for $\sigma = 0.7$.*

Comparing Fig. 3.13 to Fig. 3.11 we see a decrease in the impact duration for a larger value of σ. Figure 3.14 shows the plots of the coefficient of restitution for both the cargo and the cushion when $\sigma = 0.7$. We see that overall behavior has not changed by increasing the proportionality constant. However, the value of the coefficient of restitution for the same values of mass and stiffness ratios has decreased. This is expected since a larger damping coefficient corresponds to more energy absorbed during the impact. We once again see that the behavior of the two masses is more synchronized for larger values of the stiffness ratio. These results are supported by experimental evidence.

Experiments have shown that a cushion which is designed to soften the impact of a slightly stiffer metallic object, does not fare well in cushioning a softer plastic object. Also note the decrease in the similar values of the coefficients of restitution in the combined figure for a ratio of stiffness larger than 1.5.

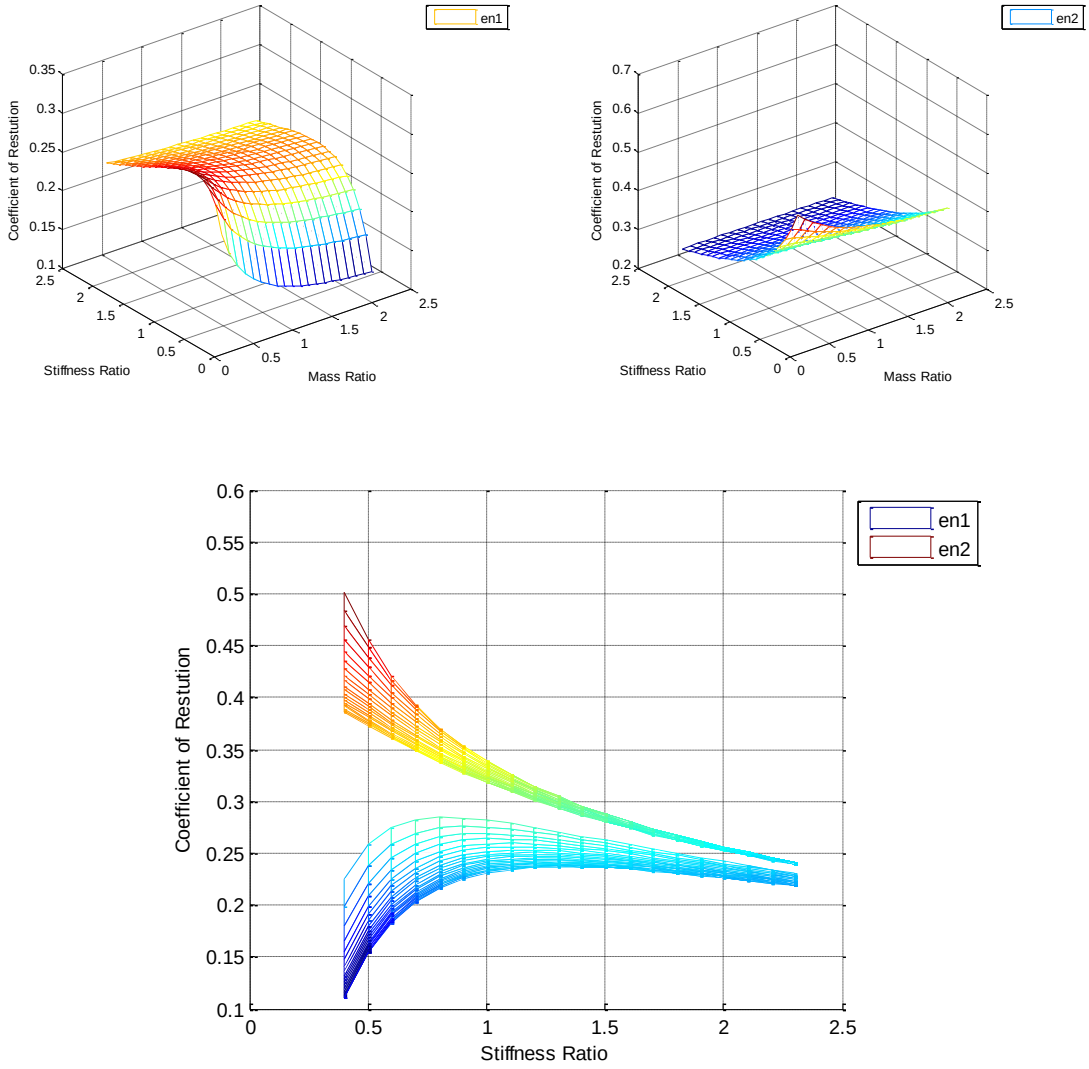

***Figure 3.14**: Coefficient of restitution for* $\sigma = 0.7$.

We have hereby completed our discussion of linear vibratory systems and their applications. The coefficient of restitution as defined in Chapter 2 has a more physical meaning now. If the object has material properties which can be modeled as a linear

spring damper system, then the coefficient of restitution can be determined form these properties and be applied to the impact analysis presented in the previous chapter. In the next section we will discuss a nonlinear model used to describe the impact phenomenon.

3.3 Nonlinear Oscillator, Hunt-Crossley Model

As we stated earlier, most impact phenomena are highly nonlinear, but so far we have only analyzed linear models. In this section we will investigate a commonly used nonlinear impact model. This impact model was proposed by K.H. Hunt and F.R.E. Crossley [15] and has the following governing equation

$$m\ddot{y} + \left(\xi y^n\right)\dot{y} + \kappa y^n = 0 \qquad (3.52)$$

where ξ, κ, and n are constants and m is the mass.

The model is derived analytically by assuming a nonlinear stiffness force and a coefficient of restitution which decreases linearly with initial velocity. A typical power used in equation (3.52) is $n = 3/2$, because then the stiffness force is identical to the Hertz's Law of Contact of two spheres [6, 13, 19]. But, of course, the main advantage of this model is that the impact force is zero at the beginning of impact. This is because the damping term involves not only the velocity, but also the displacement which is zero at the beginning of impact.

Equation (3.52) is highly nonlinear and must be solved numerically. We used MATLAB's ordinary differential equation solver, ode45, but we will discuss solutions to such equations in much more detail later in this thesis. For this model, the end of impact is simply the time when the impact force decreases to a value of zero. This time gives us the impact duration, the final velocity, and therefore the coefficient of restitution. Just as

we have done for the linear system, we will now analyze the behavior of this system subject to varying the model parameters ξ, κ, and n.

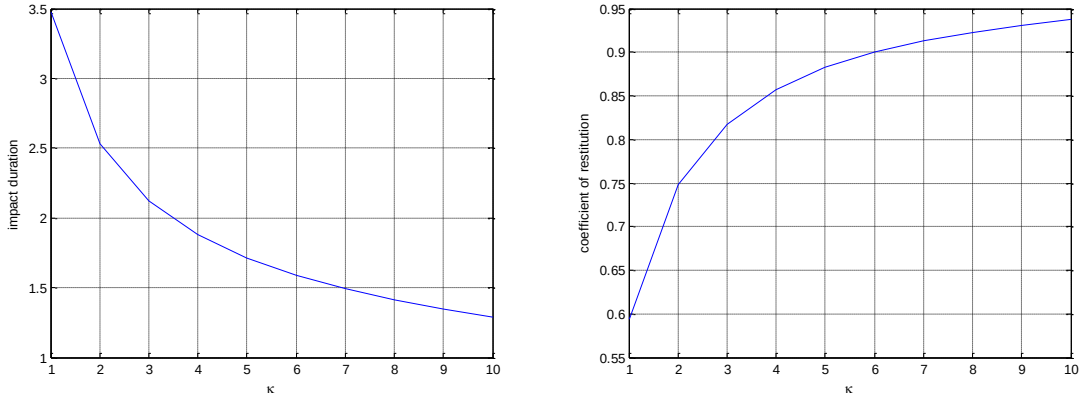

***Figure 3.15**: Impact duration and coefficient of restitution;* $m=1,\ V_0=1,\ n=3/2,$ $\xi=1.$

The above figure shows the decrease of the impact duration and the increase of the coefficient of restitution with an increase in the value of κ. We therefore know that κ must be a measure of stiffness because the stiffness coefficient for the linear model produced the same results in Fig. 3.2. One must keep in mind that the units of κ will depend on the exponent n. Figure 3.16 shows that the impact duration increases and the coefficient of restitution decreases with increasing ξ. This behavior is similar to that of the linear system to the damping coefficient in Fig. 3.3.

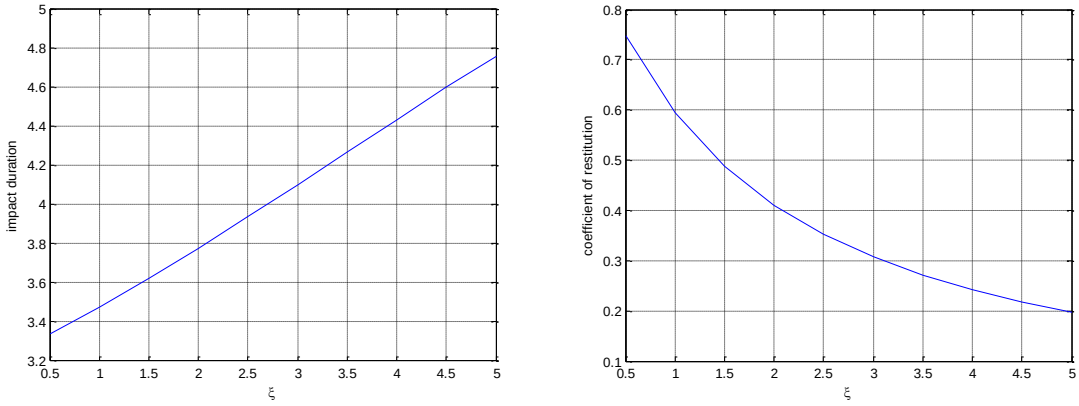

***Figure 3.16**: Impact duration and coefficient of restitution;* $m=1, V_0=1,\ n=3/2,$ $\kappa=1.$

However, calling ξ the effective damping coefficient would be misleading. The damping coefficient leads the $\dot{y}$ term and is therefore $\left(\xi y^n\right)$. We now see that the actual damping coefficient is not constant but changes with the displacement. Similarly the stiffness coefficient is defined as leading the y term and is therefore $\left(\kappa y^{n-1}\right)$, as can be seen in equation (3.52). These two coefficients are plotted for a typical impact as functions of time in Fig. 3.17. Looking at the damping and stiffness coefficients, their maximum values are achieved at maximum deflection.

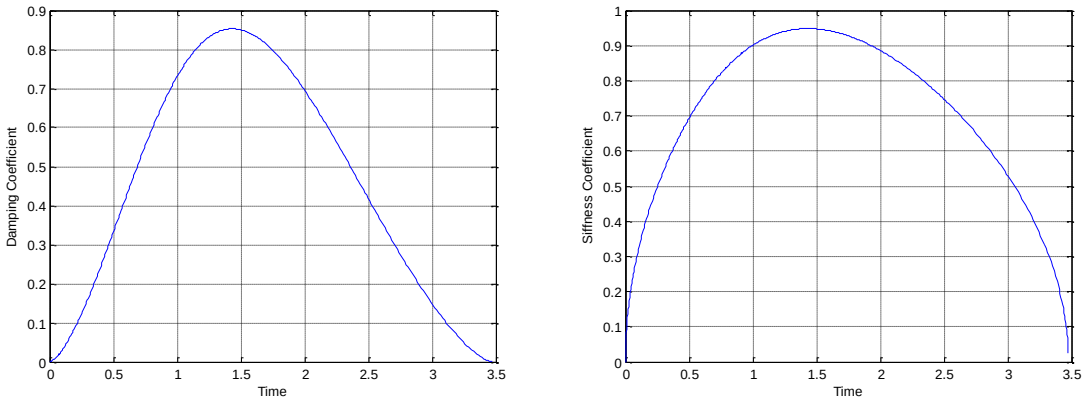

***Figure 3.17**: Damping and stiffness coefficients for* $m=1,\ V_0=1,\ n=3/2, \kappa=1,\ \xi=1.$

We also need to look at the dependence of the impact duration and the coefficient of restitution on the exponent n. This exponent is the third parameter of this nonlinear model, which is quite different from the linear model where only two parameters needed to be specified. The dependence of the impact outcome on n is plotted in Fig. 3.18, which shows an increase in the impact duration with an increase in the value of n. Aside from this, Fig. 3.18 also shows that the value of the coefficient of restitution is unaffected by the power n. This behavior of the model will become clearer when we analyze the hysteresis curves.

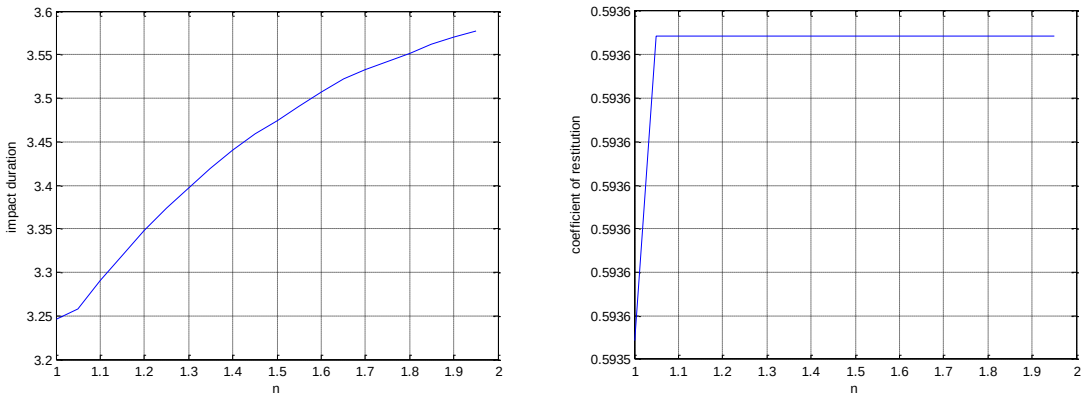

***Figure 3.18**: Damping and stiffness coefficients for* $m=1$, $V_0=1$, $\kappa=1$, *and* $\xi=1$.

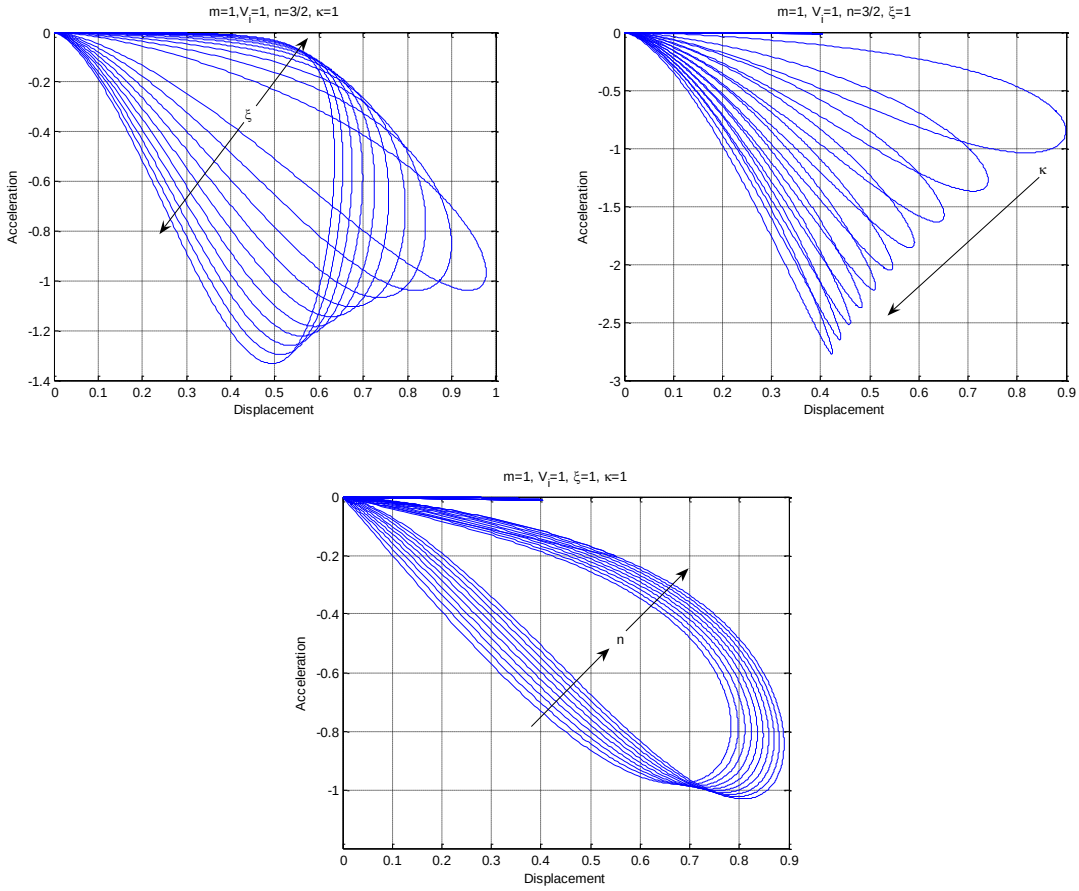

***Figure 3.19**: Hysteresis curves for the impacts analyzed in section 3.3.*

The above figure shows the hysteresis curves for the impacts presented in this section as functions of ξ, κ, and n. From Fig. 3.19 we see the expected increase in the area encompassed by the hysteresis curve with an increasing ξ. This correlates with an increasing energy loss and a decreasing coefficient of restitution seen in Fig. 3.16. On the other hand, increasing the coefficient κ does not have such a dramatic effect on the area encompassed by the hysteresis curve, but it does substantially decrease the maximum deflection and increase the maximum acceleration. The last figure above shows the effect of varying the value of n on the hysteresis curve. We see that the curve moves up in a way that increases the maximum deflection and acceleration. But the interesting fact is

that the value of n has no influence on the area encompassed; this was already seen in the plot of the coefficient of restitution in Fig. 3.18.

Typical applications of this model require that the coefficients be determined experimentally. This will, of course, only happen if the behavior of the material analyzed is similar to that discussed in this section. If this model is fitted to one's impact scenario, they gain a transient model of the impact which can be used to describe and, more importantly, predict all impact outcomes. If it so happens that this model cannot be fitted, there are other material models that one can try, such as the Maxwell model or the Kelvin-Voigt model. These, as well as other nonlinear models, are discussed in some detail by Polushko, Jiba, Krononova, and Sokolova [32]. But the Hunt-Crossley model does seem to remain a popular choice because it has three parameters allowing for a more accurate fit to the experimental results.

Chapter 4

Aerodynamics of Free Fall

Now that we have analyzed the mechanics of rigid body impact and considered vibrational impact we realize that the solutions we obtained depend strongly on the initial parameters, such as the velocity. We now need to consider the general case when the body travels along a trajectory prior to impacting the surface. Ascertaining this path and the pre-impact velocity requires the analysis of the aerodynamic drag experienced by the object. This chapter is dedicated to determining the pre-impact parameters for a body that travels through air prior to impact.

4.1 Two Dimensional Formulation

The goal of this section is to determine how aerodynamic effects, during free fall, influence the initial impact parameters. Let us first define the orientation and the direction of motion for the object. Note that in Fig. 4.1 the coordinate system is setup such that the plane of motion coincides with a coordinate plane, in this case the (x,y) plane.

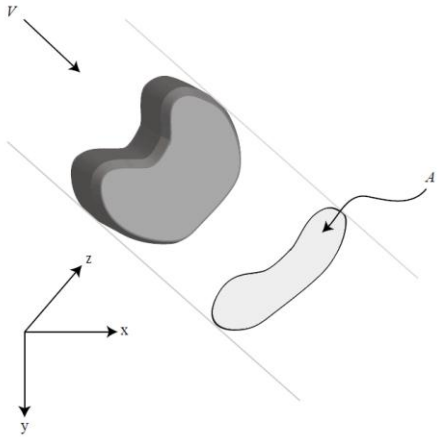

***Figure 4.1**: Formulation of aerodynamics.*

Also, the y-axis is selected as positive downwards because the forcing is gravitational and it will prove advantageous when we set up the governing equations of motion. Figure 4.1 also shows the projected area, that is orthogonal to the direction of motion, which we will assume remains constant throughout the fall. This assumption is valid for blunt bodies as well as small angular velocities. We will actually assume that the angular velocity is unaffected by the aerodynamics throughout the descent, effectively treating our object as a particle. This assumption has been validated through experiment by observing drop tests of large blunt bodies. The direction of motion will be defined by an angle θ relating the velocity components as follows.

$$\vec{V} = V_x \hat{i} + V_y \hat{j} \tag{4.1}$$

$$\vec{V} = V\left(\cos(\theta)\hat{i} + \sin(\theta)\hat{j}\right) \tag{4.2}$$

$$V = \sqrt{V_x{}^2 + V_y{}^2} \tag{4.3}$$

The angle θ is a function of time and its trigonometric functions can be expressed as

$$\cos(\theta) = \frac{V_x}{V} \tag{4.4a}$$

$$\sin(\theta) = \frac{V_y}{V} \tag{4.4b}$$

Substituting equation (4.3) into (4.4a) and (4.4b) we obtain

$$\cos(\theta) = \frac{V_x}{\sqrt{V_x{}^2 + V_y{}^2}} \tag{4.5a}$$

$$\sin(\theta) = \frac{V_y}{\sqrt{V_x{}^2 + V_y{}^2}} \tag{4.5b}$$

Let us now formulate the kinetics of this problem, which will be used to determine the equations of motion for a body falling through air. Since we are once again dealing with a planar problem, Fig. 4.2 depicts all of the forces acting on the body during free fall without loss of generality.

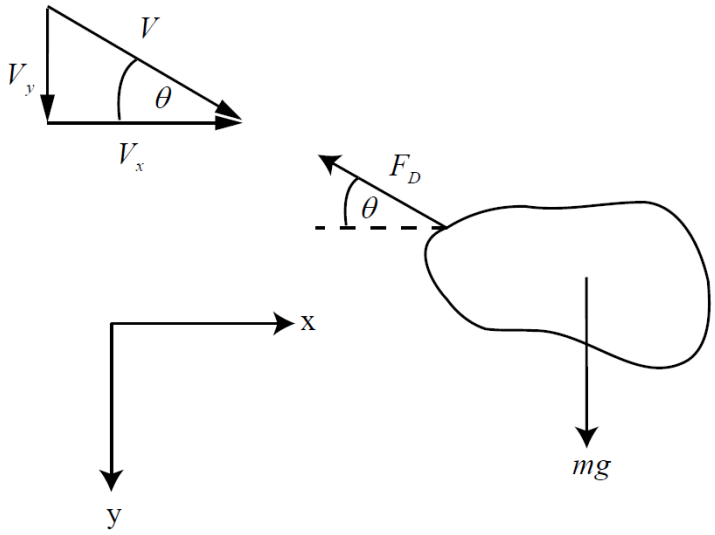

***Figure 4.2**: Kinetics of free fall.*

The drag force retards motion and acts in the direction opposite the direction of motion. The direction of motion depends on time and will be defined by the velocity components which will change during the descent.

From the literature we know that, for high Reynolds numbers flows, the drag force varies with the square of the velocity [22]. This relationship also depends on a number of constants and can be expressed as

$$F_D = \frac{1}{2}\rho_{air} C_D A V^2 \qquad (4.6)$$

where ρ_{air} is the density of air, C_D is the coefficient of drag, and A is the projected area perpendicular to the direction of motion called the *planform area*. In this study, we are considering drops from a relatively low altitude, therefore we can safely neglect changes

in density during the fall. Generally, the coefficient of drag depends on the object's geometry, surface roughness and even the free stream air velocity. We will assume that we are dealing with a blunt object and therefore neglect any changes in projected area, A, or the coefficient of drag, C_D, during the descent. This assumption is valid since it has been shown [4, 22] that, for a wide range of Reynolds numbers, the coefficient of drag on basic geometries such as a sphere or a cylinder remains constant.

We can separate the drag force into its components along the *x* and *y* axes, using the angle θ.Writing Newton's second law along both coordinate directions, for an object of mass m, we obtain

$$\sum F_x = -F_D \cos(\theta) = ma_x \tag{4.7a}$$

$$\sum F_y = -F_D \sin(\theta) + mg = ma_y \tag{4.7b}$$

The components of acceleration can be described in terms of the velocity components as

$$a_x = \frac{dV_x}{dt} \tag{4.8a}$$

$$a_y = \frac{dV_y}{dt} \tag{4.8b}$$

Turning our attention to the drag force, we can substitute equation (4.3) into equation (4.6) to obtain

$$F_D = \frac{1}{2}\rho_{air} C_D A\left(V_x{}^2 + V_y{}^2\right) \tag{4.9}$$

We can now put everything together. Substituting equations (4.4), (4.8) and (4.9) into equations (4.7) we obtain the following:

$$-\frac{1}{2}\rho_{air} C_D A\left(V_x{}^2 + V_y{}^2\right)\frac{V_x}{\sqrt{V_x{}^2 + V_y{}^2}} = m\frac{dV_x}{dt} \tag{4.10a}$$

$$-\frac{1}{2}\rho_{air}C_D A\left(V_x{}^2+V_y{}^2\right)\frac{V_y}{\sqrt{V_x{}^2+V_y{}^2}}+mg=m\frac{dV_y}{dt} \qquad (4.10b)$$

Dividing through by the mass and simplifying we get the following set of coupled nonlinear differential equations relating the transient velocity components.

$$\frac{dV_x}{dt}+\left(\frac{\rho_{air}C_D A}{2m}\right)V_x\sqrt{V_x{}^2+V_y{}^2}=0 \qquad (4.11a)$$

$$\frac{dV_y}{dt}+\left(\frac{\rho_{air}C_D A}{2m}\right)V_y\sqrt{V_x{}^2+V_y{}^2}-g=0 \qquad (4.11b)$$

We can see from equation (4.11a) that the horizontal velocity V_x decreases with time, and, if allowed to continue indefinitely, will approach zero. On the other hand, equation (4.11b) states that the vertical component of velocity increases with time, but eventually reaches a limit. This limit is known as the *terminal velocity* and it is reached when the drag force and the weight are in equilibrium. We will determine the terminal velocity V_{term} by setting the acceleration in equation (4.11b) equal to zero. As we have just mentioned, the horizontal velocity approaches zero after a long time. We will therefore, set it equal to zero as well. Hence,

$$\left(\frac{\rho_{air}C_D A}{2m}\right)\left(V_{term}\right)\sqrt{\left(V_{term}\right)^2}-g=0$$

Solving the above for V_{term} gives

$$V_{term}{}^2=\frac{2mg}{\rho_{air}C_D A} \qquad (4.12)$$

$$V_{term}=\sqrt{\frac{2mg}{\rho_{air}C_D A}} \qquad (4.13)$$

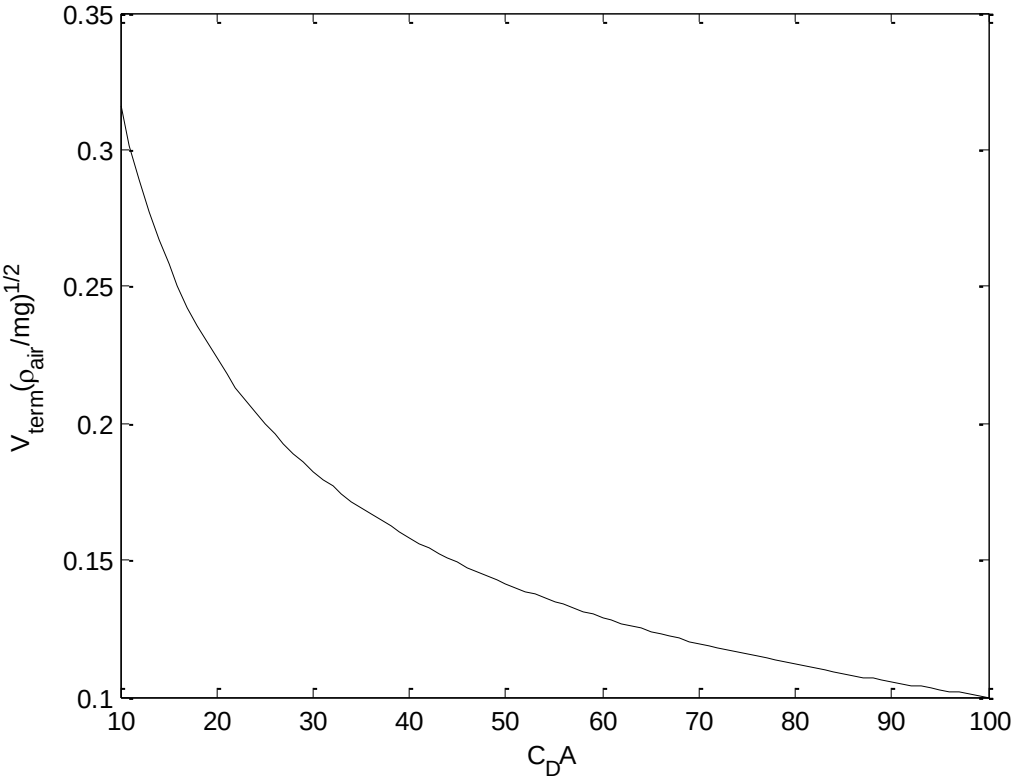

***Figure 4.3**: Terminal velocity.*

Equation (4.13) is plotted in Fig. 4.3, which shows that the terminal velocity decreases with an increasing coefficient of drag and projected area. This is intuitive since a large value of the coefficient of drag corresponds to a larger drag force which decreases the terminal velocity. Similarly a large projected area increases the resistance to motion, thereby decreasing the terminal velocity.

We can obtain a more compact form of the differential equations (4.11) by using equation (4.12). This gives

$$\frac{dV_x}{dt} + \left(\frac{g}{V_{term}^{\ 2}}\right) V_x \sqrt{V_x^{\ 2} + V_y^{\ 2}} = 0 \qquad (4.14a)$$

$$\frac{dV_y}{dt} + \left(\frac{g}{V_{term}^{\ 2}}\right) V_y \sqrt{V_x^{\ 2} + V_y^{\ 2}} - g = 0 \qquad (4.14b)$$

Now that we have determined the differential equations relating the velocity components, we also want to express them in terms of the position variables x and y.

The components of velocity can be expressed as

$$\frac{dx}{dt} = V_x \tag{4.15a}$$

$$\frac{dy}{dt} = V_y \tag{4.15b}$$

Substituting equation (4.15) into equations (4.16) results in

$$\frac{d^2x}{dt^2} + \left(\frac{g}{V_{term}^{\ 2}}\right)\frac{dx}{dt}\sqrt{\left(\frac{dx}{dt}\right)^2 + \left(\frac{dy}{dt}\right)^2} = 0 \tag{4.16a}$$

$$\frac{d^2y}{dt^2} + \left(\frac{g}{V_{term}^{\ 2}}\right)\frac{dy}{dt}\sqrt{\left(\frac{dx}{dt}\right)^2 + \left(\frac{dy}{dt}\right)^2} - g = 0 \tag{4.16b}$$

Equations (4.14) and (4.16) can be solved to obtain the velocity and the position of the object as a function of time. The solution to these coupled nonlinear differential equations will be obtained numerically using the Runge-Kutta method later in this chapter. Solution of these equations requires that we specify a set of initial conditions. Since equations (4.16) are second order, we will need to define at least two initial conditions for each. These will be the initial position and velocity. Thus,

$$x(t=0) = x_0 \tag{4.17a}$$

$$y(t=0) = y_0 \tag{4.17b}$$

$$V_x(t=0) = \frac{dx(t=0)}{dt} = V_x^0 \tag{4.17c}$$

$$V_y(t=0) = \frac{dy(t=0)}{dt} = V_y^0 \tag{4.17d}$$

where x_0 and y_0 define the initial position, and V_x^0 and V_y^0 define the initial velocity.

An interesting solution to the differential equations governing free fall can be obtained by making some simplifications. Let us consider the case when the object falls vertically, which corresponds to the case when $V_x = 0$ throughout the descent. Upon substituting $V_x = 0$ into equations (4.14) we see that equation (4.14a) is identically zero, while equation (4.14b) becomes

$$\frac{dV_y}{dt} + \left(\frac{g}{V_{term}^{\ 2}} \right) V_y^{\ 2} - g = 0 \qquad (4.18)$$

We can now drop the subscript on the vertical velocity component and just keep in mind that the problem is one dimensional. Simplifying equation (4.18) gives

$$\frac{dV}{dt} + g\left(\frac{V}{V_{term}} \right)^2 - g = 0 \qquad (4.19)$$

Similarly we can substitute $V_x = 0$ into equations (4.16). Once again equation (4.16a) is satisfied identically and equation (4.16b) becomes

$$\frac{d^2 y}{dt^2} + \left(\frac{g}{V_{term}^{\ 2}} \right) \left(\frac{dy}{dt} \right)^2 - g = 0 \qquad (4.20)$$

We now have our equations of motion for an object that free falls vertically. As we said previously, we are mostly interested in the velocity of the object prior to impact. Due to the complexity of the calculations we will not go through the exercise of solving for the impact velocity, but rather discuss the procedure and present the solution. We begin the solution by first solving equation (4.20) for the position of the object as a function of time. This will be done by incorporating the initial conditions (4.17b) and (4.17d). The solution was obtained by using a symbolic manipulator and is given below as

$$y(t) = y_0 - V_{term}t + \left(\frac{V_{term}^{\,2}}{2g}\right)\ln\left[\left(\frac{V_{term}^{\,4}}{4g^{3}}\right)\left\{\left(\frac{g^{3/2}}{V_{term}^{\,2}}\right)\left(e^{\frac{2g}{V_{term}}t}+1\right)+\left(\frac{V_0}{V_{term}}\right)\left(\frac{g^{3/2}}{V_{term}^{\,2}}\right)\left(e^{\frac{2g}{V_{term}}t}-1\right)\right\}^{2}\right] \tag{4.21}$$

where V_{term} is the terminal velocity, g is the gravitational constant, y_0 is the drop height and V_0 is the initial velocity. From the position of the object as a function of time, equation (4.21), we can determine the time when impact occurs since we know the initial drop height y_0. Solving the parallel differential equation (4.18) and using the initial condition (4.17d) we obtain the velocity as a function of time,

$$V(t) = V_{term}\tanh\left[\left(\frac{g}{V_{term}}\right)t + \tanh^{-1}\left(\frac{V_0}{V_{term}}\right)\right] \tag{4.22}$$

Substituting the impact time obtained from solving equation (4.21) into the velocity solution of equation (4.22) we arrive at the impact velocity, V_{impact}, for an object released from rest from a height of y_0 and an initial velocity V_0. Thus,

$$V_{impact} = V_{term}\tanh\left[\left(\frac{1}{2}\right)\ln\left\{\frac{\left(\left(\frac{V_0}{V_{term}}\right)^{2}-1\right)e^{\frac{2gy_0}{V_{term}^{\,2}}}+2+2\sqrt{1+\left(\left(\frac{V_0}{V_{term}}\right)^{2}-1\right)e^{\frac{2gy_0}{V_{term}^{\,2}}}}}{\left(\left(\frac{V_0}{V_{term}}\right)+1\right)^{2}e^{\frac{2gy_0}{V_{term}^{\,2}}}}\right\}+a\tanh\left(\frac{V_0}{V_{term}}\right)\right] \tag{4.23}$$

Note that we have defined the positive y-axis downward with the origin fixed at the release point. Therefore, the drop height, y_0, in equation (4.23) should be a negative quantity. This equation is the general solution, and is quite cumbersome. Note that all ratios inside the parenthesis are dimensionless quantities, which is expected when dealing

with natural logarithms. The following figure shows the dependence of the impact velocity on the dimensionless initial parameters.

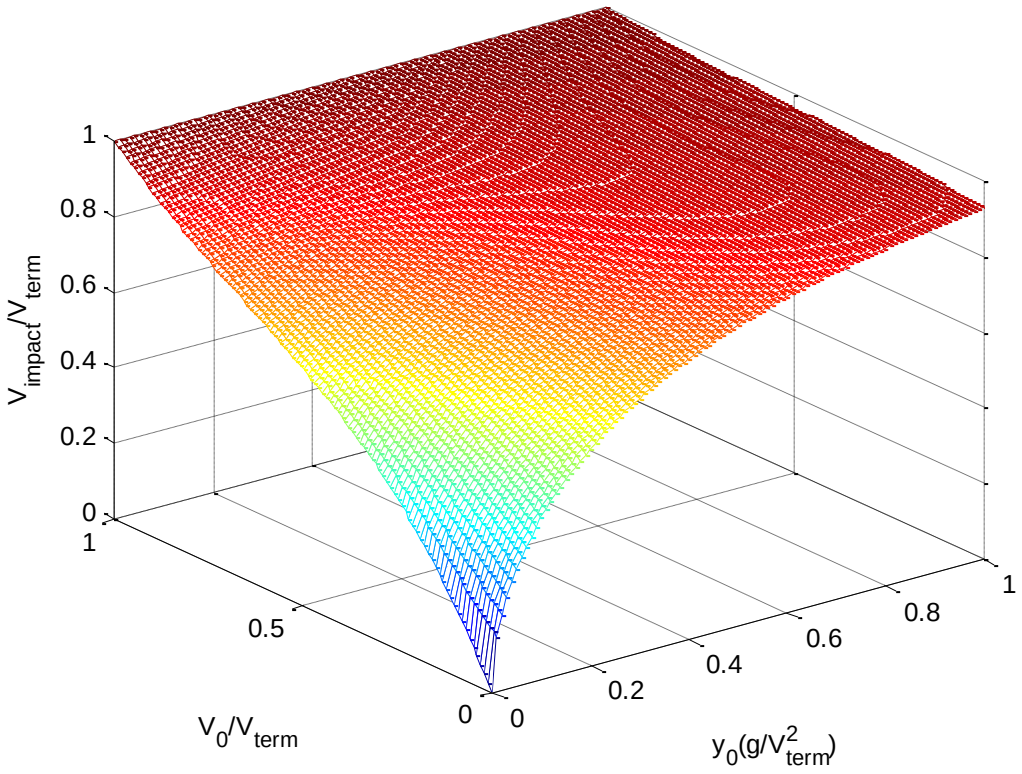

***Figure 4.4**: Impact velocity for vertical free fall.*

From Fig. 4.4 we see that if the object is released with an initial velocity equal to the terminal velocity it will impact with that velocity regardless of the drop height. Also, as the drop height is increased, the impact velocity approaches the terminal velocity. Note that in plotting equation (4.23) we have defined the drop height as $-y_0$, but it is presented as a positive quantity in the figure. Lastly, if we state that the object is released from rest, we can set $V_0 = 0$ arriving at

$$V_{impact} = V_{term} \tanh\left[\left(\frac{1}{2}\right)\ln\left\{2\left(\frac{1+\sqrt{1-e^{\frac{2gy_0}{V_{term}^2}}}}{e^{\frac{2gy_0}{V_{term}^2}}}\right)-1\right\}\right] \qquad (4.24)$$

where, once again, y_0 must be a negative quantity according to our convention.

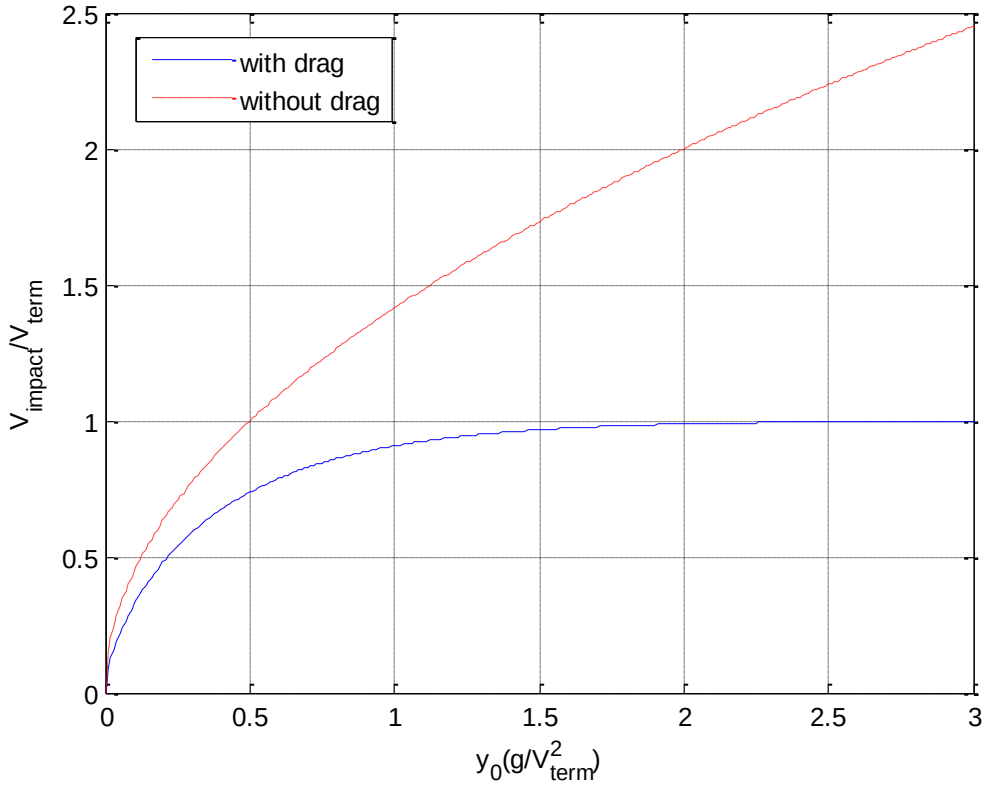

***Figure 4.5**: Impact velocity for an object released from rest.*

The figure above shows the dimensionless impact velocity as a function of the dimensionless drop height for an object which is released from rest. This is compared to the case with no aerodynamic drag where the impact velocity is given by the following

$$\frac{V_{impact}}{V_{term}} = \sqrt{\frac{-2gy_0}{V_{term}{}^2}}$$

For the case where a drag force acts on the object we once again see that the impact velocity approaches the terminal velocity as the drop height is increased while, for the case without drag, the impact velocity increases indefinitely with increasing drop height.

4.2 General Solution Via The Runge-Kutta Method

The governing equations for an object which falls freely though air were derived earlier where we constructed a system of coupled nonlinear ordinary differential equations. This system of equations cannot be solved analytically; therefore we must turn to numerical methods. A useful method for solving such a system is the Runge-Kutta method. We will use a fourth order Runge-Kutta (RK4) method due to its accuracy and stability [14, 26]. This method approximates the value of a function at a subsequent time $t + \Delta t$ by using the functions value at time t and the variation of the function with time.

Let us now present the general method and then extend it to a system of equations. If we have a function $s(t)$ whose value is known at some time t, then according to the RK4 method, its value at time $t + \Delta t$ will be given by the following.

$$s_{i+1} = s_i + \frac{1}{6}(u_1 + 2u_2 + 2u_3 + u_4)h \tag{4.25}$$

where i is the iterative variable, $s_{i+1} = s(t_i + \Delta t)$, $s_i = s(t_i)$, $h = \Delta t$, and u_i are defined as

$$u_1 = s'(t_i, s_i) \tag{4.26a}$$

$$u_2 = s'\left(t_i + \frac{h}{2}, s_i + \frac{h}{2}k_1\right) \tag{4. 26b}$$

$$u_3 = s'\left(t_i + \frac{h}{2}, s_i + \frac{h}{2}k_2\right) \tag{4. 26c}$$

$$u_4 = s'(t_i + h, s_i + hk_3) \tag{4. 26d}$$

with $s'(t, s) = \dfrac{ds(t, s)}{dt}$

The general solution is obtained by repeating the calculation, where for the second iteration $s(t+h)$ becomes the new reference value and we march out the solution in order to calculate $s(t+2h)$ and so on.

This methodology is designed for first order differential equations; we must therefore restate the governing equations as a system of first order differential equations. Using equations equation (4.14) and (4.15) we obtain

$$\frac{dx(t)}{dt} = V_x(t) \tag{4.27a}$$

$$\frac{dy(t)}{dt} = V_y(t) \tag{4.27b}$$

$$\frac{dV_x(t)}{dt} = -C_1 V_x(t)\sqrt{V_x(t)^2 + V_y(t)^2} \tag{4.27c}$$

$$\frac{dV_y(t)}{dt} = -C_1 V_y(t)\sqrt{V_x(t)^2 + V_y(t)^2} + C_2 \tag{4.27d}$$

where $C_1 = \left(\frac{g}{V_{term}^{\ 2}}\right)$ and $C_2 = g$.

Using the RK4 method, the values of position and velocity at time $t+h$ will be given by

$$V_x(t+h) = V_x(t) + \breve{k} \tag{4.28a}$$

$$V_y(t+h) = V_y(t) + \breve{l} \tag{4.28b}$$

$$x(t+h) = x(t) + \breve{m} \tag{4.28c}$$

$$y(t+h) = y(t) + \breve{n} \tag{4.28d}$$

where

$$\breve{k} = \frac{1}{6}\left(\breve{k}_1 + 2\breve{k}_2 + 2\breve{k}_3 + \breve{k}_4\right) \tag{4.29a}$$

$$\breve{k}_1 = \left(-C_1 V_x(t) \sqrt{V_x(t)^2 + V_y(t)^2} \right) h \tag{4.29b}$$

$$\breve{k}_2 = \left(-C_1 \left\langle V_x(t) + \frac{1}{2}\breve{k}_1 \right\rangle \sqrt{\left\langle V_x(t) + \frac{1}{2}\breve{k}_1 \right\rangle^2 + \left\langle V_y(t) + \frac{1}{2}\breve{l}_1 \right\rangle^2} \right) h \tag{4.29c}$$

$$\breve{k}_3 = \left(-C_1 \left\langle V_x(t) + \frac{1}{2}\breve{k}_2 \right\rangle \sqrt{\left\langle V_x(t) + \frac{1}{2}\breve{k}_2 \right\rangle^2 + \left\langle V_y(t) + \frac{1}{2}\breve{l}_2 \right\rangle^2} \right) h \tag{4.29d}$$

$$\breve{k}_4 = \left(-C_1 \left\langle V_x(t) + \breve{k}_3 \right\rangle \sqrt{\left\langle V_x(t) + \breve{k}_3 \right\rangle^2 + \left\langle V_y(t) + \breve{l}_3 \right\rangle^2} \right) h \tag{4.29e}$$

$$\breve{l} = \frac{1}{6}\left(\breve{l}_1 + 2\breve{l}_2 + 2\breve{l}_3 + \breve{l}_4 \right) \tag{4.20a}$$

$$\breve{l}_1 = \left(C_2 - C_1 V_y(t) \sqrt{V_x(t)^2 + V_y(t)^2} \right) h \tag{4.30b}$$

$$\breve{l}_2 = \left(C_2 - C_1 \left\langle V_y(t) + \frac{1}{2}\breve{l}_1 \right\rangle \sqrt{\left\langle V_x(t) + \frac{1}{2}\breve{k}_1 \right\rangle^2 + \left\langle V_y(t) + \frac{1}{2}\breve{l}_1 \right\rangle^2} \right) h \tag{4.30c}$$

$$\breve{l}_3 = \left(C_2 - C_1 \left\langle V_y(t) + \frac{1}{2}\breve{l}_2 \right\rangle \sqrt{\left\langle V_x(t) + \frac{1}{2}\breve{k}_2 \right\rangle^2 + \left\langle V_y(t) + \frac{1}{2}\breve{l}_2 \right\rangle^2} \right) h \tag{4.30d}$$

$$\breve{l}_4 = \left(C_2 - C_1 \left\langle V_y(t) + \breve{l}_3 \right\rangle \sqrt{\left\langle V_x(t) + \breve{k}_3 \right\rangle^2 + \left\langle V_y(t) + \breve{l}_3 \right\rangle^2} \right) h \tag{4.30e}$$

$$\breve{m} = \frac{1}{6}\left(\breve{m}_1 + 2\breve{m}_2 + 2\breve{m}_3 + \breve{m}_4 \right) \tag{4.31a}$$

$$\breve{m}_1 = V_x(t) h \tag{4.31b}$$

$$\breve{m}_2 = \left(V_x(t) + \breve{k}_2 \right) h \tag{4.31c}$$

$$\breve{m}_3 = \left(V_x(t) + \breve{k}_3\right)h \tag{4.31d}$$

$$\breve{m}_4 = \left(V_x(t) + \breve{k}_4\right)h \tag{4.31e}$$

$$\breve{n} = \frac{1}{6}\left(\breve{n}_1 + 2\breve{n}_2 + 2\breve{n}_3 + \breve{n}_4\right) \tag{4.32a}$$

$$\breve{n}_1 = V_y(t)h \tag{4.32b}$$

$$\breve{n}_2 = \left(V_y(t) + \breve{l}_2\right)h \tag{4.32c}$$

$$\breve{n}_3 = \left(V_y(t) + \breve{l}_3\right)h \tag{4.32d}$$

$$\breve{n}_4 = \left(V_y(t) + \breve{l}_4\right)h \tag{4.32e}$$

A question arises: what is an adequate size of the time step? As a first indicator one can use the fact that the error associated with each step of the RK4 method is on the order of $O\left(h^4\right)$ [26]. But, decreasing the time step will cost a lot of computational power. An alternative way of decreasing the error is to use an adaptive step. These include variations of the RK4 method such as the Fehlberg (RKF45), Cash-Karp (RKCP), as well as the Dormand-Prince (RKDP) methods. These methods approximate the value of the function using both a fourth order method and a fifth order method. The two values are compared and if the difference exceeds some prescribed tolerance the step is decreased and the value of the function is recalculated.

In order to completely grasp the behavior of this system of differential equations we will now turn to graphical means of representing our numerical solution. We must begin by nondimensionalizing the governing differential equations in order to obtain a

parametric solution to the free fall problem. Let us begin by defining the following dimensionless time, position, and velocity variables.

$$\tilde{t} = t\frac{g}{V_{term}} \qquad \tilde{x} = x\frac{g}{V_{term}^2} \qquad \tilde{y} = y\frac{g}{V_{term}^2} \tag{4.33a,b,c}$$

$$\tilde{V}_x = \frac{V_x}{V_{term}} \qquad \tilde{V}_y = \frac{V_y}{V_{term}} \tag{4.34a,b}$$

Substituting equations (4.33) and (4.34) into equations (4.14) and (4.16) we obtain

$$\frac{d\tilde{V}_x}{d\tilde{t}} + \tilde{V}_x\sqrt{\tilde{V}_x^{\,2} + \tilde{V}_y^{\,2}} = 0 \tag{4.35a}$$

$$\frac{d\tilde{V}_y}{d\tilde{t}} + \tilde{V}_y\sqrt{\tilde{V}_x^{\,2} + \tilde{V}_y^{\,2}} = 1 \tag{4.35b}$$

$$\frac{d^2\tilde{x}}{d\tilde{t}^{\,2}} + \frac{d\tilde{x}}{d\tilde{t}}\sqrt{\left(\frac{d\tilde{x}}{d\tilde{t}}\right)^2 + \left(\frac{d\tilde{y}}{d\tilde{t}}\right)^2} = 0 \tag{4.36a}$$

$$\frac{d^2\tilde{y}}{d\tilde{t}^{\,2}} + \frac{d\tilde{y}}{d\tilde{t}}\sqrt{\left(\frac{d\tilde{x}}{d\tilde{t}}\right)^2 + \left(\frac{d\tilde{y}}{d\tilde{t}}\right)^2} = 1 \tag{4.36b}$$

Since we are primarily interested in the pre-impact velocity of the object, we will only seek a solution to equations (4.35). The numerical solution to these equations was obtained using the aforementioned Runge-Kutta method and is displayed in the following figures. Figure 4.6 shows the general behavior of the velocity components of a free falling body for the given initial conditions. As predicted, we see that the horizontal component of velocity decays to zero, while the vertical component of velocity approaches the terminal velocity with increasing time. Note the clearly visible minimum of the resultant velocity, shown by the heavy solid line, which is at a value of about 0.5 on the horizontal axis. In other words, the minimum resultant velocity occurs soon after the release and far from steady state conditions. Theoretically, this is a very powerful

result, which shows that there exists a time at which all forces acting on the object are in equilibrium.

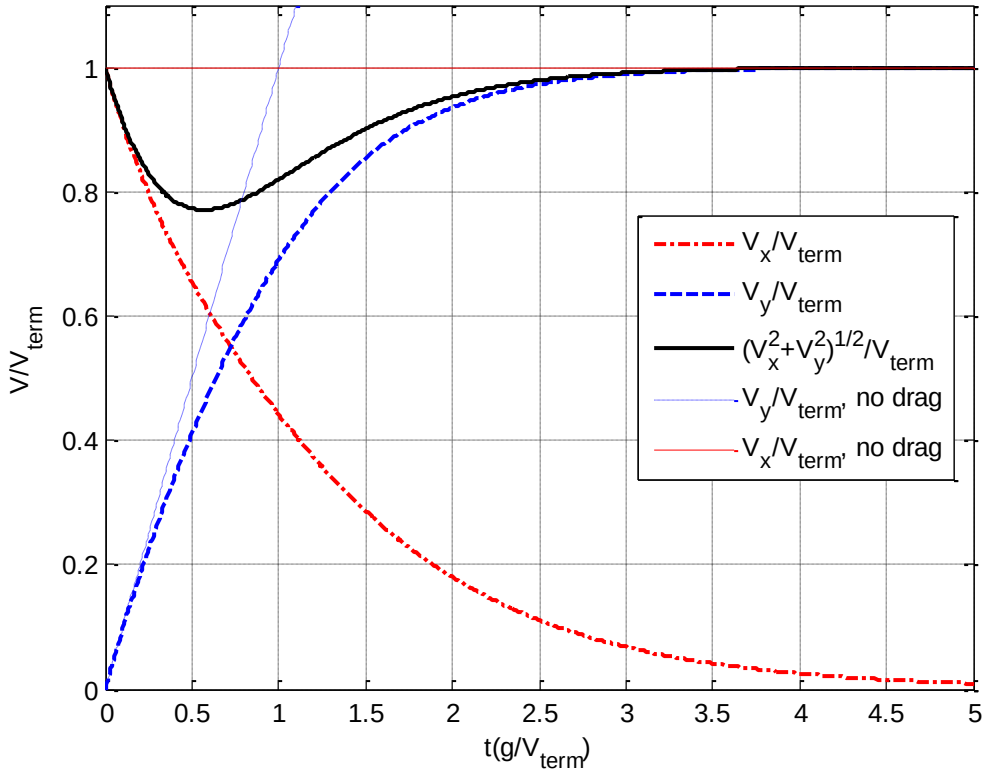

***Figure 4.6**: Behavior of the nonlinear solution for $V_x^0 = V_{term}$ and $V_y^0 = 0$.*

For the given initial conditions, the magnitude of the total velocity at this minimum is about 23% smaller than the value of the terminal velocity. Having the object impact the surface with this minimum velocity would greatly increase its survivability.

Now, let us consider how the initial conditions influence the position and magnitude of the minimum resultant velocity. From Fig. 4.7 and Fig. 4.8, we can see that changing the initial conditions significantly alters the position and magnitude of the minimum resultant velocity. For some initial conditions, this minimum will be essentially at the terminal velocity, thereby losing its significance. In the following section we will

further discuss this result and provide relationships between the velocity components at this extremum.

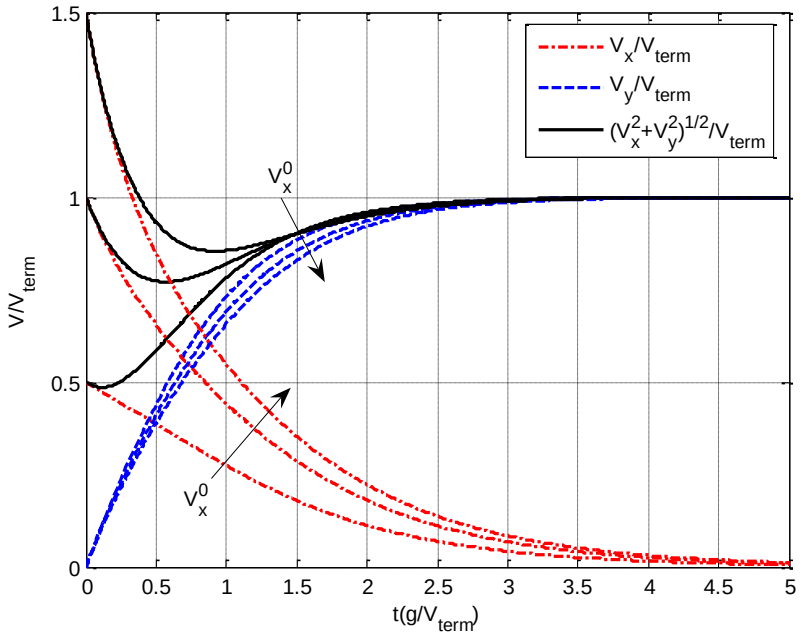

***Figure 4.7**: Effects of increasing the initial vertical velocity V_x^0.*

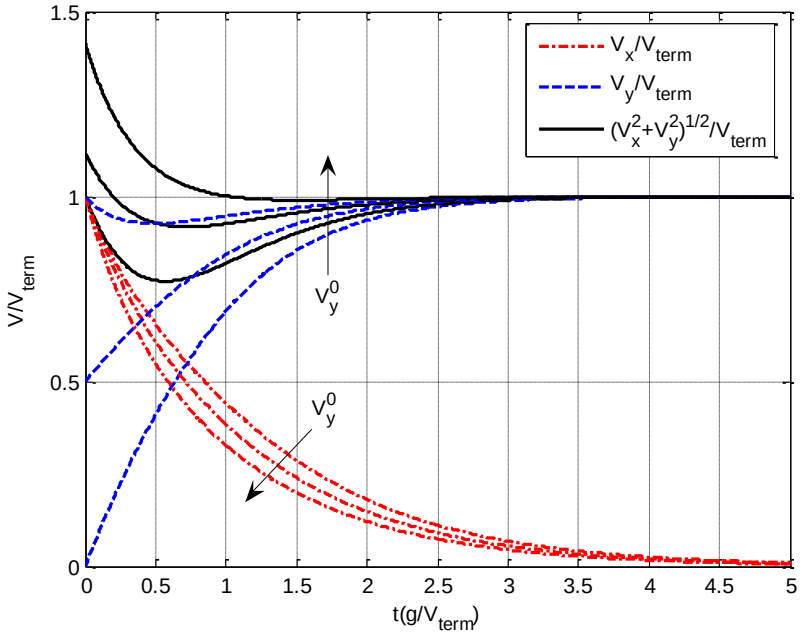

***Figure 4.8**: Effects of increasing the initial vertical velocity V_y^0.*

4.3 Minimum Kinetic Energy

In Chapter 2 we have showed the energy loss for a rigid body impact varies with many parameters. But, we can also make a general statement that if the object has a small pre-impact kinetic energy, then any damage that it suffers should be less than for the same impact with a higher kinetic energy. Since it is assumed in this chapter that the aerodynamic forces do not affect the rotation we will try to minimize the translational kinetic energy. In the previous section, we graphically showed that there exists a favorable minimum of the resultant velocity. We will now derive a relationship between the transient components of velocity V_x and V_y at this minimum. We can begin by restating equation (4.3) which is

$$V = \sqrt{V_x^{\,2} + V_y^{\,2}}$$

Differentiating equation (4.3), with respect to time gives

$$\frac{dV}{dt} = \frac{1}{2}\left[V_x^{\,2} + V_y^{\,2}\right]^{-1/2}\left[2V_x\frac{dV_x}{dt} + 2V_y\frac{dV_y}{dt}\right]$$

Upon rearranging we have

$$\frac{dV}{dt} = \frac{\left[V_x\frac{dV_x}{dt} + V_y\frac{dV_y}{dt}\right]}{\sqrt{V_x^{\,2} + V_y^{\,2}}} \tag{4.37}$$

Solving equations (4.14) for the accelerations yields

$$\frac{dV_x}{dt} = -\left(\frac{g}{V_{term}^{\,2}}\right)V_x\sqrt{V_x^{\,2} + V_y^{\,2}} \tag{4.38a}$$

$$\frac{dV_y}{dt} = -\left(\frac{g}{V_{term}^{\,2}}\right)V_y\sqrt{V_x^{\,2} + V_y^{\,2}} + g \tag{4.38b}$$

Substituting equations (4.38) into equation (4.37)

$$\frac{dV}{dt} = \frac{\left[-\left(\left(\frac{g}{V_{term}^{\ 2}} \right) V_x \sqrt{V_x^{\ 2} + V_y^{\ 2}} \right) V_x + \left(-\left(\frac{g}{V_{term}^{\ 2}} \right) V_y \sqrt{V_x^{\ 2} + V_y^{\ 2}} + g \right) V_y \right]}{\sqrt{V_x^{\ 2} + V_y^{\ 2}}}$$

Dividing through by $\sqrt{V_x^{\ 2} + V_y^{\ 2}}$ and simplifying

$$\frac{dV}{dt} = \left(\frac{g}{V_{term}^{\ 2}} \right) \left(\frac{V_y V_{term}^{\ 2}}{\sqrt{V_x^{\ 2} + V_y^{\ 2}}} - \left(V_x^{\ 2} + V_y^{\ 2} \right) \right) \tag{4.39}$$

Setting the derivative equal to zero we obtain

$$\left(V_x^{\ 2} + V_y^{\ 2} \right)^{3/2} = V_y V_{term}^{\ 2}$$

Lastly, solving for V_x gives

$$V_x = \sqrt{\left(V_y V_{term}^{\ 2} \right)^{2/3} - V_y^{\ 2}} \tag{4.40}$$

Equation (4.40) is the relationship between the components of velocity at an extremum of the transient total velocity.

The most favorable time for impact to take place is when the total velocity of the impacting object is minimal. If the impact is designed such that the object impacts with this minimum velocity, the components of the velocity are related by equation (4.40). Now, we can obtain an expression for the initial velocity ratio, ρ_x, which we defined in our discussion of rigid body impact. Recall equation (2.12a),

$$\rho_x = \frac{V_x}{V_y}$$

Substituting equation (4.40) into the above gives

$$\rho_x = \frac{\sqrt{\left(V_y V_{term}{}^2\right)^{2/3} - V_y{}^2}}{V_y}$$

Simplifying, we get the initial velocity ratio at the minimum resultant velocity as

$$\rho_x = \sqrt{\left(\frac{V_{term}}{V_y}\right)^{4/3} - 1} \tag{4.41}$$

This value can be used to solve the inverse problem, such as that of determining the release parameters which would result in the most favorable value of ρ_x.

4.4 Approximate Model

The behavior of the velocity components and the total velocity with time is similar to that of the thermal resistance of an insulated rod as a function of the radius of insulation [17]. The convection resistance behaves like the horizontal component of velocity and the conduction resistance behaves like the vertical component of velocity. The total thermal resistance has a minimum value analogous to that of the total velocity during free fall. In this section we will show that one can obtain a solution to the free fall problem similar to the known solution for the heat transfer in an insulated rod. This will be done by decoupling the equations of motion.

From the equations of motion (4.14) we note that the coupling term is $\sqrt{V_x{}^2 + V_y{}^2}$. We can rearrange this term as follows,

$$\sqrt{V_x{}^2 + V_y{}^2} = V_x\left(1 + \left(\frac{V_y}{V_x}\right)^2\right)^{\frac{1}{2}} \tag{4.42}$$

Expanding equation (4.42) using the Binomial Theorem we obtain

$$V_x\left(1+\left(\frac{V_y}{V_x}\right)^2\right)^{\frac{1}{2}} = V_x\left(1+\frac{1}{2}\left(\frac{V_y}{V_x}\right)^2-\frac{1}{8}\left(\frac{V_y}{V_x}\right)^4+\ldots\right)$$

Simplifying gives

$$V_x\left(1+\left(\frac{V_y}{V_x}\right)^2\right)^{\frac{1}{2}} = V_x+\frac{1}{2}\frac{{V_y}^2}{V_x}-\frac{1}{8}\frac{{V_y}^4}{{V_x}^3}+\ldots \qquad (4.43a)$$

We can also obtain a similar expression by factoring the V_y term rather that the V_x term in equation (4.42).

$$V_y\left(1+\left(\frac{V_x}{V_y}\right)^2\right)^{\frac{1}{2}} = V_y+\frac{1}{2}\frac{{V_x}^2}{V_y}-\frac{1}{8}\frac{{V_x}^4}{{V_y}^3}+\ldots \qquad (4.43b)$$

If we only retain the first term in expansions (4.43) we obtain the following approximation which effectively decouples the governing equations.

$$V_x\left(1+\left(\frac{V_y}{V_x}\right)^2\right)^{\frac{1}{2}} \approx V_x \qquad (4.44a)$$

$$V_y\left(1+\left(\frac{V_x}{V_y}\right)^2\right)^{\frac{1}{2}} \approx V_y \qquad (4.44b)$$

Substituting equation (4.44a) into equation (4.14a) and equation (4.44b) into equation (4.14b) we obtain the following decoupled governing equations

$$\frac{dV_x}{dt}+\left(\frac{g}{{V_{term}}^2}\right){V_x}^2 = 0 \qquad (4.45a)$$

$$\frac{dV_y}{dt}+\left(\frac{g}{{V_{term}}^2}\right){V_y}^2 - g = 0 \qquad (4.45b)$$

We have already obtained the solution to equation (4.45b) when analyzing vertical free fall. It is as follows,

$$V_y(t) = V_{term} \tanh\left[\left(\frac{g}{V_{term}}\right)t + \tanh^{-1}\left(\frac{V_y^0}{V_{term}}\right)\right] \tag{4.46}$$

The solution to equation (4.45a) subject to boundary condition (4.17c) is

$$V_x(t) = \frac{1}{\left(\frac{g}{V_{term}^{\ 2}}\right)t + \frac{1}{V_x^0}} \tag{4.47}$$

Note that the horizontal velocity varies with inverse of time which is identical to the variation of convection resistance to the insulation radius.

Equations (4.46) and (4.47) should not be used as a means of producing accurate values for the transient velocity components as a function of time. However, these solutions do contain the essence of the behavior and can be used to approximate the velocity of the object soon after release. After a longer time, the lack of coupling effects results in larger deviations from the exact solution. Also, the resultant or total velocity for this decoupled system does exhibit a minimum which is near the actual minimum, but should only be used as a first approximation.

The figure below compares the approximate solution presented in this section to that obtained in a previous section using the Runge-Kutta method. The *y* component of velocity is closely approximated by this solution, while the *x* component deviates drastically. Also note that the resultant velocity for the approximate solution does not approach the terminal velocity from below. It rather overshoots the terminal velocity and then approaches it from above.

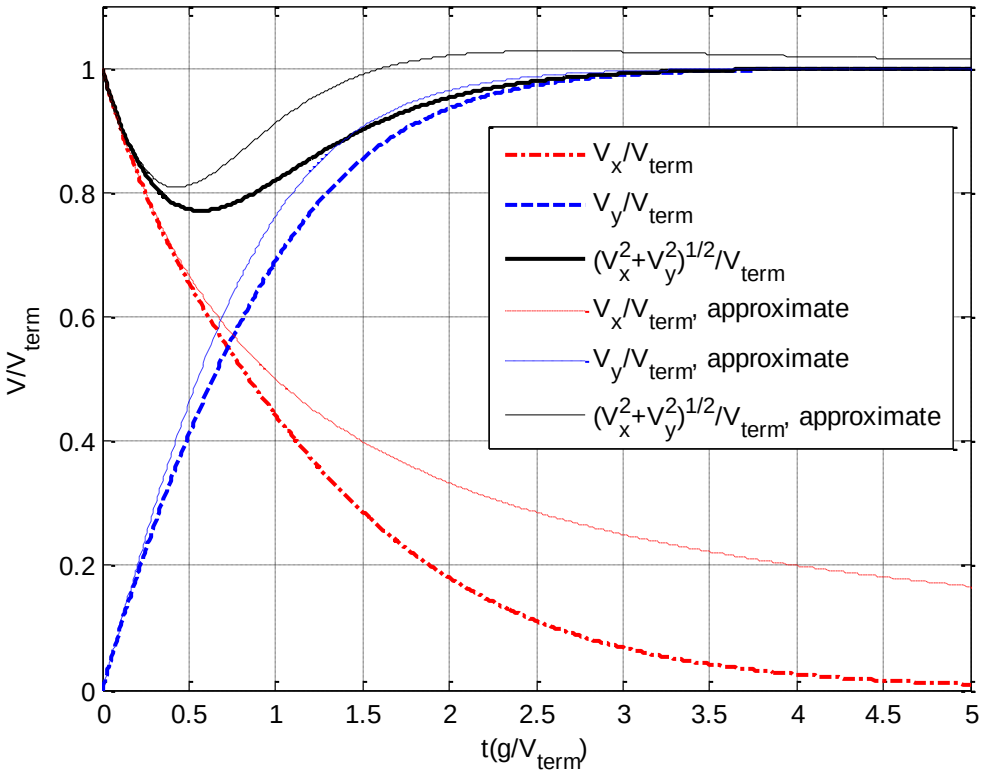

***Figure 4.9**: Comparison of the approximate solution to the exact solution.*

4.5 Three Dimensional Formulation Including Effects of Wind

Up to now, we discussed the planar motion of a body in a viscous fluid, namely air. The equations governing this two dimensional motion were derived and then solved numerically as well as approximately. The question that we will try to answer in this section is what affect wind has on the motion of the body. The velocity vector specifying the direction of the wind will, in general, have components in all three coordinate directions. Therefore, our two-dimensional aerodynamic model will no longer suffice and we must develop a new three-dimensional model.

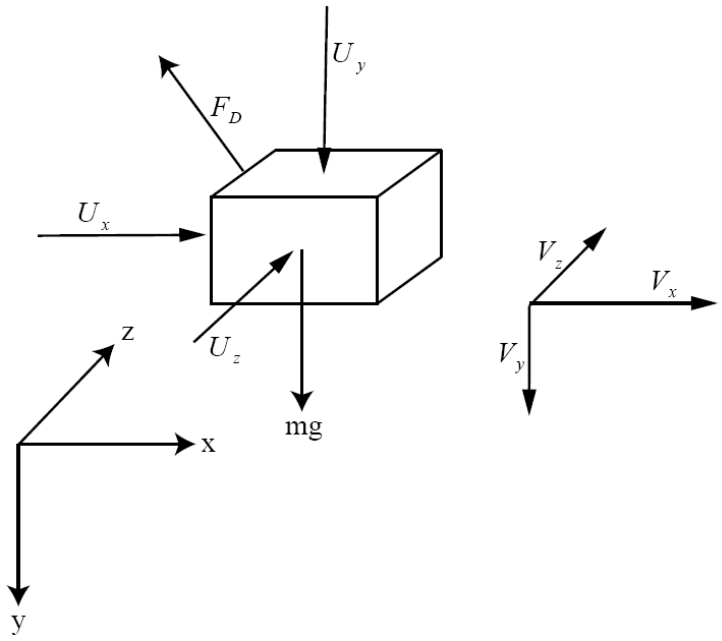

Figure 4.10*: Three dimensional formulation, including wind.*

The wind velocity vector will be defined as $\vec{U} = U_x\hat{i} + U_y\hat{j} + U_z\hat{k}$, which is shown acting on the object in Fig. 4.10. The velocity of the body will now also have three components and take the following form $\vec{V} = V_x\hat{i} + V_y\hat{j} + V_z\hat{k}$. Recall that the drag force depends on the velocity of the air past the container. This relative velocity can be written in vector form as

$$\vec{V}_{rel} = (V_x - U_x)\hat{i} + (V_y - U_y)\hat{j} + (V_z - U_z)\hat{k} \qquad (4.48)$$

where the velocity components of the wind are subtracted because, for example, a tailwind will decrease the relative velocity of the air past the object. We are now ready to define the drag force acting on the body.

As in the two dimensional formulation the magnitude of the drag force is given by

$$F_D = \frac{1}{2}\rho_{air} C_D A V_{rel}^{\ 2} \qquad (4.49)$$

Substituting equation (4.48) into above

$$F_D = \frac{1}{2}\rho_{air} C_D A\left(\sqrt{(V_x - U_x)^2 + (V_y - U_y)^2 + (V_z - U_z)^2}\right)^2 \qquad (4.50)$$

The direction of the drag force is defined by the direction of the relative air velocity vector. We can now sum the forces which act on the body in flight under the action of wind.

$$\sum F_x = -(F_D)_x = ma_x \qquad (4.51a)$$

$$\sum F_y = -(F_D)_y + mg = ma_y \qquad (4.51b)$$

$$\sum F_z = -(F_D)_z = ma_z \qquad (4.51c)$$

Where, for example, $(F_D)_x$ is the component of the drag force along the x-axis and can be expressed using the components of the relative air velocity.

$$(F_D)_x = F_D \frac{(V_x - U_x)}{\sqrt{(V_x - U_x)^2 + (V_y - U_y)^2 + (V_z - U_z)^2}} \qquad (4.52)$$

Using equations (4.48), (4.50), (4.52), and (4.8) we can write equations (4.51) as

$$\frac{dV_x}{dt} + \left(\frac{\rho_{air} C_D A}{2m}\right)(V_x - U_x)\sqrt{(V_x - U_x)^2 + (V_y - U_y)^2 + (V_z - U_z)^2} = 0 \qquad (4.53a)$$

$$\frac{dV_y}{dt} + \left(\frac{\rho_{air} C_D A}{2m}\right)(V_y - U_y)\sqrt{(V_x - U_x)^2 + (V_y - U_y)^2 + (V_z - U_z)^2} = g \qquad (4.53b)$$

$$\frac{dV_z}{dt} + \left(\frac{\rho_{air} C_D A}{2m}\right)(V_z - U_z)\sqrt{(V_x - U_x)^2 + (V_y - U_y)^2 + (V_z - U_z)^2} = 0 \qquad (4.53c)$$

Remember that the coefficient of drag, C_D, and the planform area, A, are assumed to be invariant of the coordinate direction. This assumption is valid for blunt bodies. Equations (4.53) can be expressed in terms of the terminal velocity as follows

$$\frac{dV_x}{dt}+\left(\frac{g}{V_{term}{}^2}\right)(V_x-U_x)\sqrt{(V_x-U_x)^2+(V_y-U_y)^2+(V_z-U_z)^2}=0 \qquad (4.54a)$$

$$\frac{dV_y}{dt}+\left(\frac{g}{V_{term}{}^2}\right)(V_y-U_y)\sqrt{(V_x-U_x)^2+(V_y-U_y)^2+(V_z-U_z)^2}=g \qquad (4.54b)$$

$$\frac{dV_z}{dt}+\left(\frac{g}{V_{term}{}^2}\right)(V_z-U_z)\sqrt{(V_x-U_x)^2+(V_y-U_y)^2+(V_z-U_z)^2}=0 \qquad (4.54c)$$

The position of the container is governed by

$$\frac{dx}{dt}=V_x \qquad (4.54d)$$

$$\frac{dy}{dt}=V_y \qquad (4.54e)$$

$$\frac{dz}{dt}=V_z \qquad (4.54f)$$

The six equations (4.54) can now be solved numerically to obtain the position and velocity of the body during its descent. The required initial conditions are

$$x(t=0)=x_0 \qquad (4.55a)$$

$$y(t=0)=y_0 \qquad (4.55b)$$

$$z(t=0)=z_0 \qquad (4.55c)$$

$$V_x(t=0)=V_x^0 \qquad (4.55d)$$

$$V_y(t=0)=V_y^0 \qquad (4.55e)$$

$$V_z(t=0)=V_z^0 \qquad (4.55f)$$

In order to present the solution in the most general form we will now nondimensionalize equations (4.54) using definitions (4.33) and (4.34). The nondimensional velocity components will be

$$\tilde{V}_x = \frac{V_x}{V_{term}} \qquad \tilde{V}_y = \frac{V_y}{V_{term}} \qquad \tilde{V}_z = \frac{V_z}{V_{term}} \tag{4.55a,b,c}$$

$$\tilde{U}_x = \frac{U_x}{V_{term}} \qquad \tilde{U}_y = \frac{U_y}{V_{term}} \qquad \tilde{U}_z = \frac{U_z}{V_{term}} \tag{4.56a,b,c}$$

The nondimensional time will be defined as

$$\tilde{t} = t\left(\frac{g}{V_{term}}\right) \tag{4.57}$$

Lastly, the dimensionless position variables will take the form

$$\tilde{x} = x\left(\frac{g}{V_{term}^{\ 2}}\right) \qquad \tilde{y} = y\left(\frac{g}{V_{term}^{\ 2}}\right) \qquad \tilde{z} = z\left(\frac{g}{V_{term}^{\ 2}}\right) \tag{4.58a,b,c}$$

Substituting equations (4.55) through (4.58) into equations (4.54) we arrive at

$$\frac{d\tilde{V}_x}{d\tilde{t}} + \left(\tilde{V}_x - \tilde{U}_x\right)\sqrt{\left(\tilde{V}_x - \tilde{U}_x\right)^2 + \left(\tilde{V}_y - \tilde{U}_y\right)^2 + \left(\tilde{V}_z - \tilde{U}_z\right)^2} = 0 \tag{4.59a}$$

$$\frac{d\tilde{V}_y}{d\tilde{t}} + \left(\tilde{V}_y - \tilde{U}_y\right)\sqrt{\left(\tilde{V}_x - \tilde{U}_x\right)^2 + \left(\tilde{V}_y - \tilde{U}_y\right)^2 + \left(\tilde{V}_z - \tilde{U}_z\right)^2} = 1 \tag{4.59b}$$

$$\frac{d\tilde{V}_z}{d\tilde{t}} + \left(\tilde{V}_z - \tilde{U}_z\right)\sqrt{\left(\tilde{V}_x - \tilde{U}_x\right)^2 + \left(\tilde{V}_y - \tilde{U}_y\right)^2 + \left(\tilde{V}_z - \tilde{U}_z\right)^2} = 0 \tag{4.59c}$$

$$\frac{d\tilde{x}}{d\tilde{t}} = \tilde{V}_x \tag{4.59d}$$

$$\frac{d\tilde{y}}{d\tilde{t}} = \tilde{V}_y \tag{4.59e}$$

$$\frac{d\tilde{z}}{d\tilde{t}} = \tilde{V}_z \tag{4.59f}$$

The equations were solved using the techniques presented earlier in this chapter and a typical result is shown in Fig 4.10. This figure clearly depicts the sideways drift due to a crosswind.

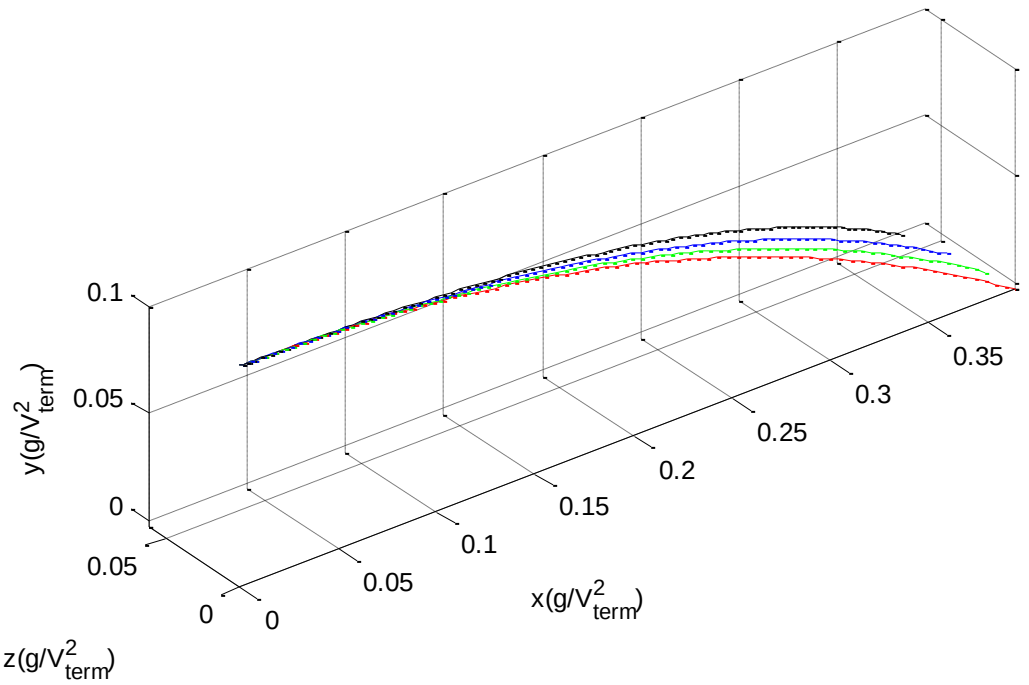

***Figure 4.11**: Position of an object under the action of wind at* $\tilde{U}_z = 0,0.2,0.4,0.6,$ *released from* $\tilde{y} = 0.1$ *with* $\tilde{V}_x = 1.$

Tables 4.1 and 4.2 present the drift for various initial drop heights as well as release speeds. The increase in the amount of drift with increasing initial velocity is nonlinear and increases at an increasing rate.

***Table 4.1**: Drift due to crosswind of magnitude* $\tilde{U}_z = 0.2.$

Drop Height ($\tilde{y}_0$)	Release Velocity ($\tilde{V}_x^0$)	Sideways Drift ($\tilde{z}$)
0.1	0	0.0053
0.2	0	0.0121
0.1	0.5	0.0106
0.2	0.5	0.0218
0.1	1	0.0184
0.2	1	0.0349

***Table 4.2**: Drift due to crosswind of magnitude $\tilde{U}_z = 0.4$.*

Drop Height ($\tilde{y}_0$)	Release Velocity ($\tilde{V}_x^0$)	Sideways Drift ($\tilde{z}$)
0.1	0	0.0169
0.2	0	0.0360
0.1	0.5	0.0244
0.2	0.5	0.0499
0.1	1	0.0382
0.2	1	0.0739

Analyzing sideways drift is of utmost importance in problems where the magnitude of the crosswind is on the order of the terminal velocity.

Chapter 5

Subsequent Impacts

In most impact cases the initial impact is the most damaging, but this is not always true when dealing with non-spherical objects. Subsequent impact of such objects will be investigated in this chapter, especially the presence of velocity components along the plane of impact, where the position of the center of gravity with respect to the contact point plays a crucial role. In such cases, It is possible for more energy to be absorbed during the second impact than during the first, which is the reason why analyzing subsequent impacts is vital in any impact analysis. We are also interested in determining the distance that an object tumbles after the initial impact. This distance is of great importance in designing an impact scenario where the object would have to be retrieved after impact.

5.1 General Formulation

Hitherto in this thesis we have discussed the theory of rigid body impact mechanics as well as aerodynamics of free fall, both of which will be employed when analyzing subsequent impacts. One way of modeling subsequent impacts is to split the problem into aerodynamics and impact mechanics. These will be analyzed separately in order to obtain the object's position and velocity throughout its motion.

A typical impact occurs when the object is released form some initial position above the impacting surface given some initial velocity and angular velocity. These initial conditions have to be used with the equations governing the aerodynamic drag,

which were derived in the third chapter of this study. As was proposed earlier, numerical integration can be used to obtain the velocity as well as the position of the object during its descent. Recall that we assumed that the object's angular velocity is unaffected by the aerodynamics and thereby remains constant. The trajectory of the object through the air is terminated at the first impact. The object's geometry plays an important role in determining the exact time and orientation when impact begins.

Once the initial velocity and orientation of the box have been ascertained, the impact can be analyzed. In this chapter, we will use the rigid body model of impact to describe the impact phenomenon. Therefore according to the formulation in Chapter 2, we must begin by determining whether the object will slide or not slide during impact. This is to be done by evaluating the force ratio and comparing it to some predefined coefficient of friction. Depending on whether the object slides or does not, the appropriate set of equations can then be used to obtain the post-impact components of velocity and the angular velocity. Since the time of impact is typically very small, the position and orientation of the box will be assumed not to change during impact. The analysis is now complete and the post-impact position and velocities can be applied to the aerodynamics equations to calculate the object's path leading to the second impact.

The iterative nature of this problem, and the fact that the aerodynamic equations can only be solved numerically, suggests that the solution can be easily obtained using computational software. In fact, we will formulate and solve the subsequent impacts problem in this manner. One must keep in mind, that because the equations governing the aerodynamics must be solved numerically, an exact position of the body prior to impact cannot be obtained, but we can obtain this position to within an acceptable tolerance.

5.2 Subsequent Planar Impacts of a Rectangular Container

In this section, we will apply the general theory of subsequent impacts to analyze the impact of a rectangular container. The dimensions of the container are defined by the distance from the center of mass to a corner, R, and the angle ψ as seen in the Fig. 5.1.

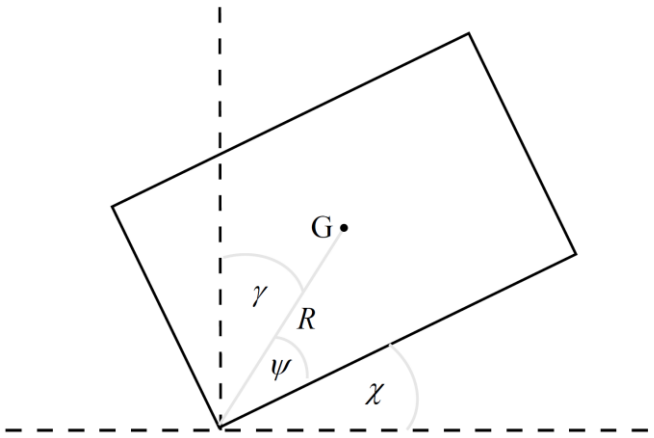

***Figure 5.1**: Orientation angles of the container.*

The orientation of the container is specified by the angle that the longer side makes with the horizontal, which will be denoted by χ. The angle which the line between the contact point and the center of mass makes with the vertical will be denoted by γ. This is all the necessary information to completely describe the orientation of this container. The moment of inertia of this rectangular object about the axis of rotation through the mass center G is

$$I_G = \frac{1}{12} m\left(\left(2R\cos(\psi)\right)^2 + \left(2R\sin(\psi)\right)^2\right) = \frac{2}{3} mR^2 \qquad (5.1)$$

The motion of the container will begin with some initial velocity and angular velocity from a given initial position. The required initial conditions can be expressed as:

$$x(t=0) = x_0 \qquad (5.2a)$$

$$y(t=0)=y_0 \tag{5.2b}$$

$$V_x(t=0)=\frac{dx(t=0)}{dt}=V_x^0 \tag{5.3c}$$

$$V_y(t=0)=\frac{dy(t=0)}{dt}=V_y^0 \tag{5.3d}$$

Using these initial conditions we can now numerically solve the aerodynamic equations which will yield the trajectory of the center of mass of the container. As were derived in Chapter 4, these equations are

$$\frac{d^2x}{dt^2}+\left(\frac{g}{V_{term}{}^2}\right)\frac{dx}{dt}\sqrt{\left(\frac{dx}{dt}\right)^2+\left(\frac{dy}{dt}\right)^2}=0 \tag{5.4a}$$

$$\frac{d^2y}{dt^2}+\left(\frac{g}{V_{term}{}^2}\right)\frac{dy}{dt}\sqrt{\left(\frac{dx}{dt}\right)^2+\left(\frac{dy}{dt}\right)^2}-g=0 \tag{5.4b}$$

$$\frac{dx}{dt}=V_x \tag{5.5a}$$

$$\frac{dy}{dt}=V_y \tag{5.5b}$$

where $V_{term}=\sqrt{\frac{2mg}{\rho_{air}C_DA}}$.

Note that, since we are dealing with a blunt body and short flight duration, we can assume that the planform area and the coefficient of drag remain constant. Once we know the flight path we need to determine when the first impact occurs. Using the path of the center of mass and the angular velocity we can calculate the position of each corner throughout the flight. Figure 5.2 shows the initial trajectory of the falling container, which was released from $50\,ft$ with a horizontal velocity of $80\,ft/s$ and an initial

orientation angle $\chi = 35^o$. The angular velocity was taken to be -1 rad/s and the initial vertical component of velocity was zero.

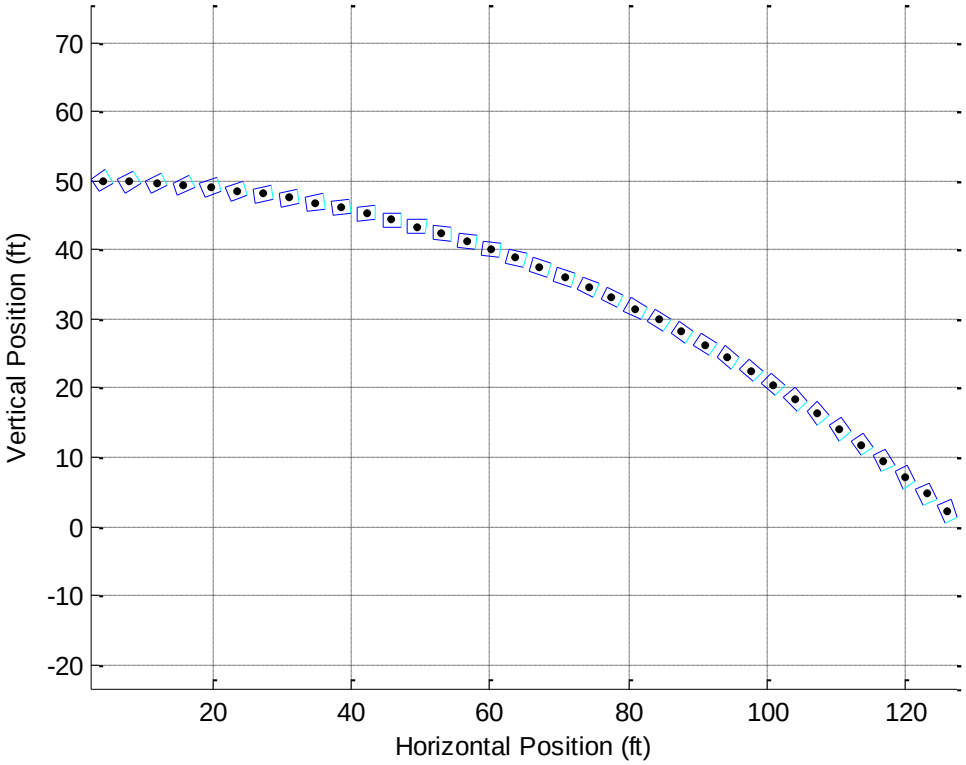

***Figure 5.2**: Initial flight.*

Knowing the position of the corner throughout the trajectory is essential for this analysis. Because the probability of the container impacting on its side is extremely small it is more likely that impact will occur at a corner. It is a bit difficult to obtain the exact position of the impacting corner when it makes contact with the ground due to the iterative nature of the aerodynamic solution. A very close approximation to the position of the container can be determined by re-solving the aerodynamic equations near the point of impact with a smaller time step. The initial solution of the flight path is terminated when one of the corners goes below the impacting surface. In our case, this is

the positive x-axis. The idea is to then take the second to last coordinates of the container in the position array and proceed to recalculate the equations with a smaller time step. Once again this second loop will break once one of the corners passes the impacting surface. An interesting point is that, depending on the magnitude of the angular velocity, the corner of the container that terminated the first loop need not be the same as that of the second; therefore the algorithm must be written to account for this. The following two figures show this procedure.

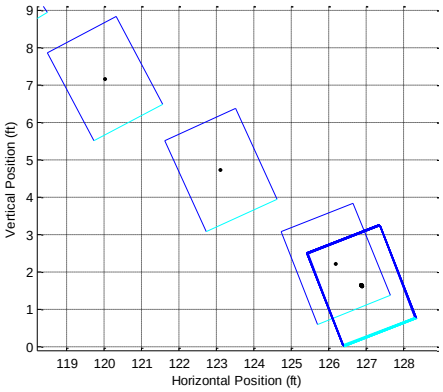

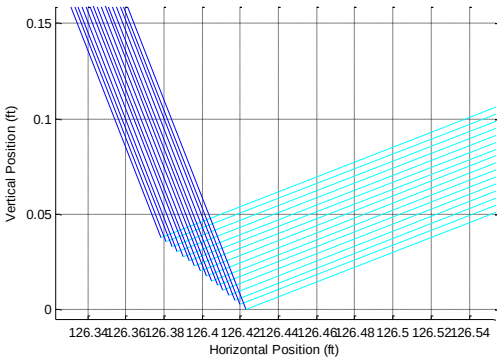

***Figure 5.3**: Initial impact.* ***Figure 5.4**: Recalculation of the corner's position.*

Figure 5.3 shows the larger view of the first impact, while Fig. 5.4 clearly depicts the recalculation of the aerodynamic equations with a substantially smaller time step. This can be done several times until the container is within a tolerable distance from the impact surface. This last position will provide the quantities necessary to conduct the impact analysis.

Now that we have the determined the pre-impact position and velocity, we are ready for the impact analysis. Using the rigid body impact model, we begin by calculating the force ratio which will determine whether the object slides during impact.

This expression for the force ratio was derived in Chapter 2, equation (2.55), and is shown below. Hence,

$$\mu < \frac{\operatorname{sgn}(\rho_x + \lambda_z \cos(\gamma))\left[\rho_x\left(\alpha + \sin^2(\gamma)\right) - (e_n + 1)\cos(\gamma)\sin(\gamma) + \lambda_z\left(\alpha - e_n \sin^2(\gamma)\right)\cos(\gamma)\right]}{\left[\rho_x \cos(\gamma)\sin(\gamma) - (e_n + 1)\left(\alpha + \cos^2(\gamma)\right) - \lambda_z\left(\alpha(e_n + 1) + e_n \cos^2(\gamma)\right)\sin(\gamma)\right]}$$

where $\rho_x = \frac{V_x}{V_y}$ and $\lambda_z = \frac{\omega_z R}{V_y}$ are dimensionless pre-impact parameters. The above condition states that if the force ratio, which is the ratio of the horizontal to vertical components of the impact force, exceeds the value of the coefficient of friction, μ, sliding will occur during impact. Once the impact regime is ascertained, the appropriate set of equations will give the post-impact velocity and angular velocity. If no sliding occurs, the post-impact velocities and angular velocity are given by these equations

$$\omega_z'' = \left(\frac{1}{\alpha + 1}\right)\left[-\rho_x \cos(\gamma) - (e_n + 1)\sin(\gamma) + \lambda_z\left(\alpha - e_n \sin^2(\gamma)\right)\right]$$

$$V_x'' = \left(\frac{1}{\alpha + 1}\right)\left[\rho_x \cos^2(\gamma) + (e_n + 1)\cos(\gamma)\sin(\gamma) - \lambda_z\left(\alpha - e_n \sin^2(\gamma)\right)\cos(\gamma)\right]$$

$$V_y'' = \left(\frac{1}{\alpha + 1}\right)\left[\rho_x \cos(\gamma)\sin(\gamma) + (e_n + 1)\sin^2(\gamma) - \lambda_z\left(\alpha(e_n + 1) + e_n \cos^2(\gamma)\right)\sin(\gamma)\right] - e_n$$

If the container slides through impact, then the post-impact quantities are given by the following equations, which were also derived in Chapter 2:

$$\omega_z'' = \frac{-(e_n + 1)\left(-\bar{\mu}\cos(\gamma) + \sin(\gamma)\right) + \lambda_z\left(-e_n\left(-\bar{\mu}\cos(\gamma) + \sin(\gamma)\right)\sin(\gamma) + \alpha\right)}{\left(\alpha - \bar{\mu}\cos(\gamma)\sin(\gamma) + \sin^2(\gamma)\right)}$$

$$V_x'' = \frac{\rho_x\left(\alpha - \bar{\mu}\cos(\gamma)\sin(\gamma) + \sin^2(\gamma)\right) + \bar{\mu}\alpha(e_n + 1) + \lambda_z \bar{\mu}\alpha(e_n + 1)\sin(\gamma)}{\left(\alpha - \bar{\mu}\cos(\gamma)\sin(\gamma) + \sin^2(\gamma)\right)}$$

$$V_y'' = \frac{\left(-\bar{\mu}\cos(\gamma)\sin(\gamma) + \sin^2(\gamma) - \alpha e_n\right) - \lambda_z \alpha(e_n + 1)\sin(\gamma)}{\left(\alpha - \bar{\mu}\cos(\gamma)\sin(\gamma) + \sin^2(\gamma)\right)}$$

where $\bar{\mu} = \mu \operatorname{sgn}\left(\rho_x - \lambda_z \bar{R}_y\right)$ is the coefficient of friction, the sign of which depends on the direction of the horizontal velocity of the contact point. As we can see, all impact equations require the use of the angle γ introduced in Chapter 2 and shown in Fig. 5.1. Caution should be taken in the calculation of this angle since it plays such a vital role in the impact dynamics. The post-impact quantities now become the initial conditions for the new interval of flight leading to the second impact. The same methodology is to be applied here and for all subsequent impacts. The first seven impacts of the impact scenario discussed so far in this section are shown below in Fig. 5.5.

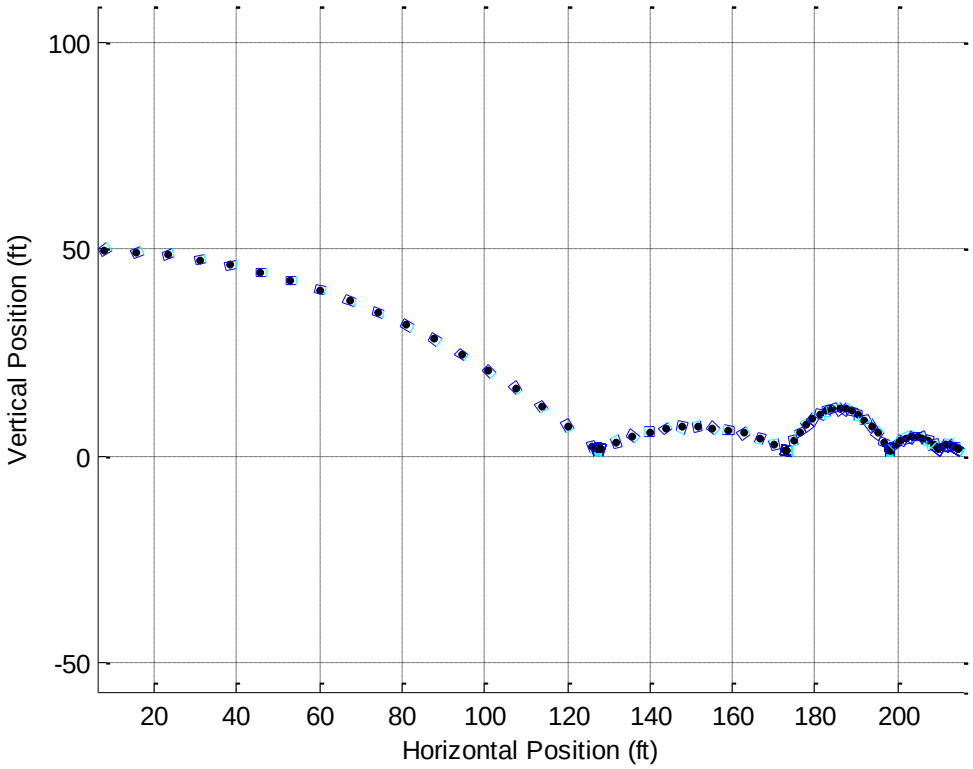

Figure 5.5*: Trajectory for the first seven impacts.*

At a first glance, it does not seem that the container has undergone seven impacts, but it has. Some of the impacts are double impacts, meaning that after the container impacts the

ground, it then impacts it again prior to completing a full rotation. These impacts are shown in the following Fig. 5.6.

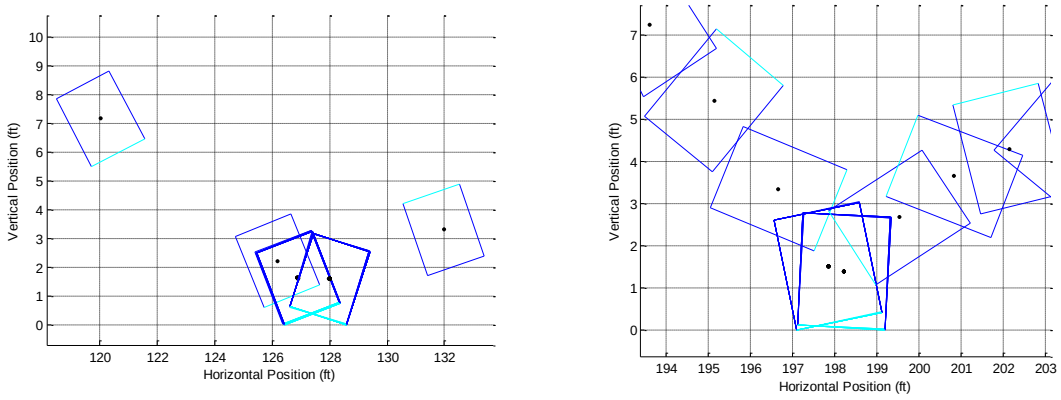

***Figure 5.6**: Double impacts.*

Fig. 5.7 shows the kinetic energy of the container throughout its motion, normalized with respect to the initial kinetic energy. The double impacts shown in Fig. 5.6 could also have been spotted in the energy plot as secondary discontinuities at 1.8 and 5.6 seconds.

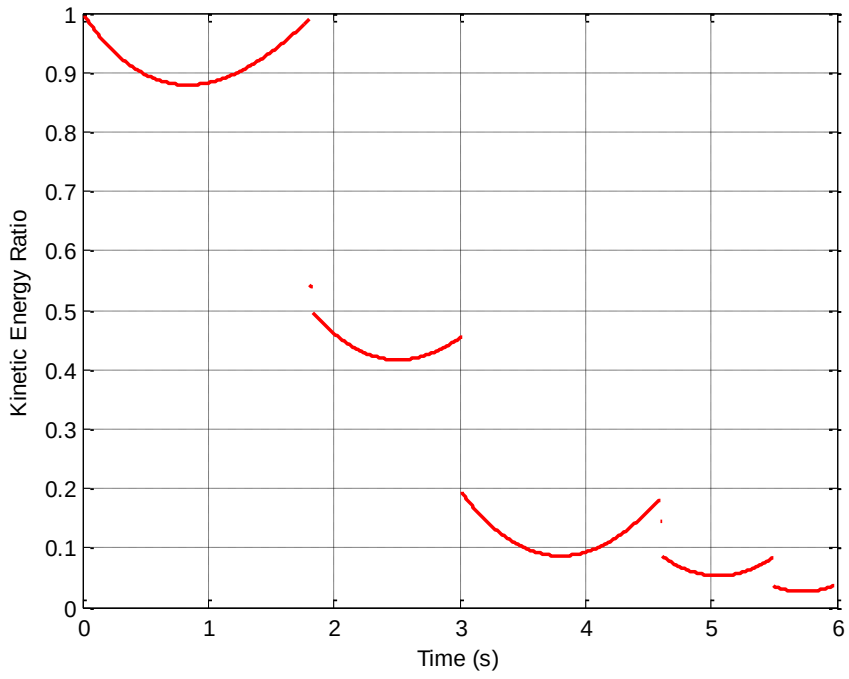

***Figure 5.7**: Kinetic energy ratio for the first seven impacts.*

The parabolic-like variation of the kinetic energy with time is due to the flight of the container between impacts while being acted upon by aerodynamic drag and gravity. It is sometimes observed that the kinetic energy at the end of flight is larger than at the beginning. This is due to the position of the container's center of mass which can be closer to the impacting surface at the end of the flight than at the beginning. The discontinuities in the kinetic energy ratio plot are due to the impacts themselves.

We know that eventually the container will come to rest and the question that remains to be answered is what criteria should be used to define the last impact. When the number of impacts to be calculated is increased and one looks at the later ones, we observe that the container undergoes a number of micro impacts.

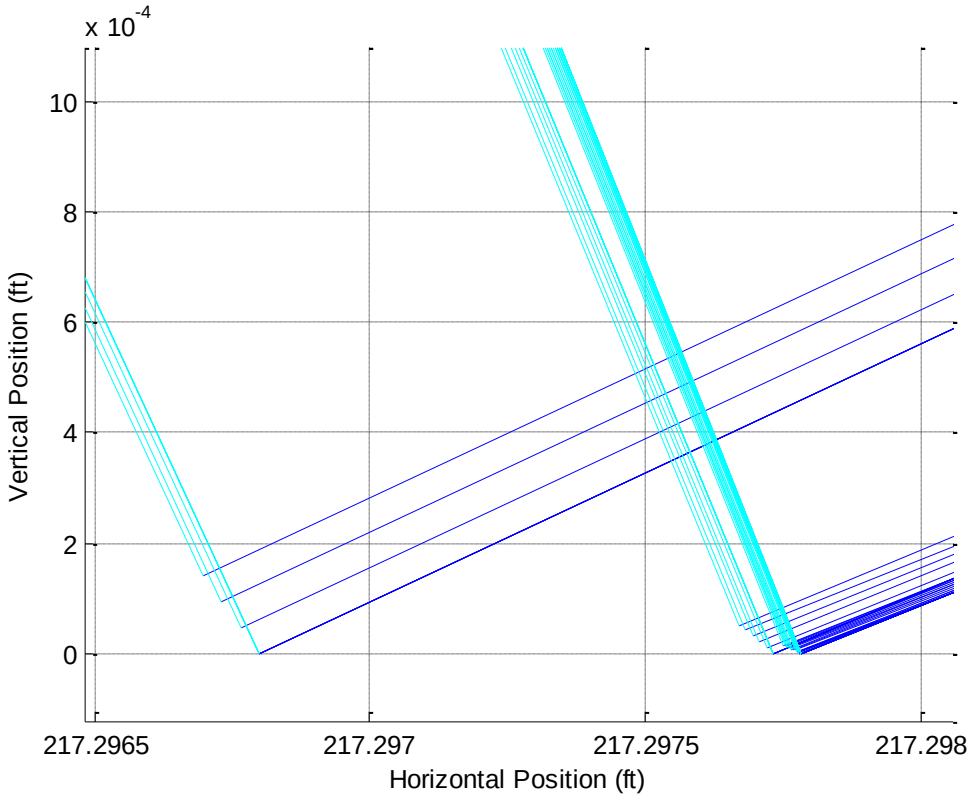

Figure 5.8*: Container's corner experiencing micro impacts.*

The container's corner experiencing micro impacts is shown in Fig. 5.8 above. These are impacts with a very small change in position, which occur because the rigid body model used to describe the impact phenomenon states that the post-impact vertical contact point velocity decreases by the value of the coefficient of restitution, indefinitely. This is the point where we need to select a cutoff value for the contact point velocity to be taken as zero, which should be based on the accuracy of the calculations made for the position of the container's impacting corner, previously demonstrated in Fig. 5.5. Once the final impact has been calculated, we know that the container will either pivot or slide and rotate until one of the sides comes into contact with the impacting surface. Which scenario takes place is governed by the force ratio which has already been evaluated in the calculation of the final quantities.

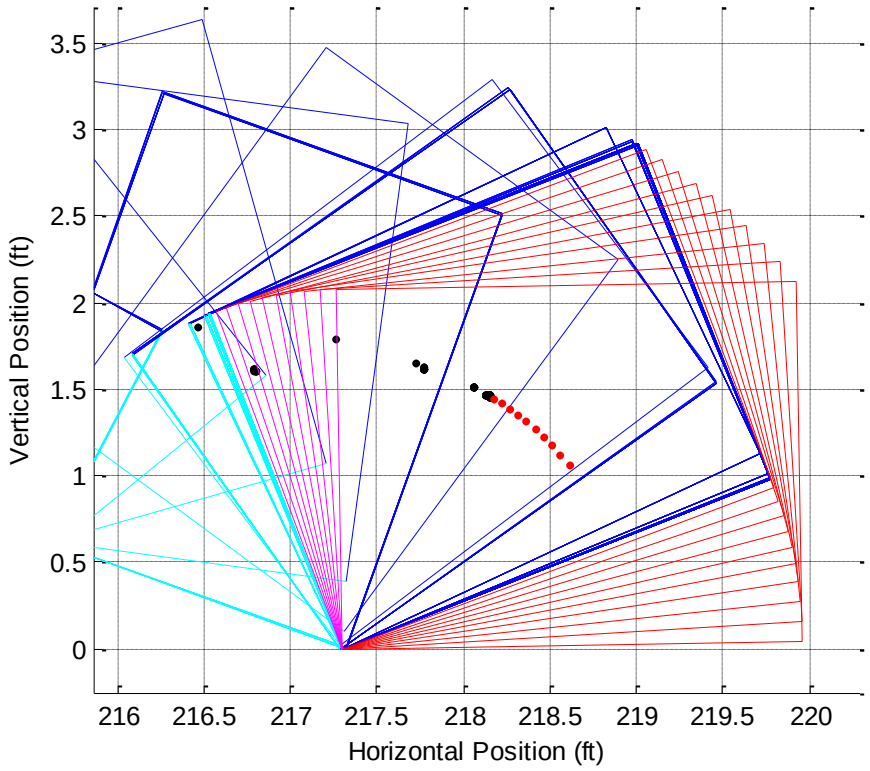

***Figure 5.9**: Initial pivot.*

The initial pivot for the impact of the container analyzed so far in this section is shown in Fig. 5.9. At this point the container can still oscillate from corner to corner with decreasing amplitude. This decrease is attributed to energy loss every time a side of the container impacts the ground while it is pivoting. Note that this is a different type of impact than the one analyzed in this section and therefore might require a different approach in modeling the energy absorption. The motion ceases when all of the energy is absorbed. Regardless of how many times the container oscillates after the last impact, which even for rigid materials would not be many, its center of mass will essentially remain in one place. Therefore, if one is simply concerned with the distance that the container travels while tumbling, the subsequent impact analysis is complete after the initial pivot.

One should note that, prior to beginning this analysis, a large number of parameters must be specified. For the aerodynamics we must specify the density of air, the mass of the container, its planform area, coefficient of drag, as well as the gravitational acceleration. Then for the impact mechanics we need to indicate the dimensions of the container, its moment of inertia, the coefficient of friction, and the coefficient of restitution. For the problem presented in this section, the dimensions of the container were taken as 32 inches by 25 inches, therefore $R = 20.3$ inches and $\psi = 38^o$. The density of air was taken as $\rho_{air} = 0.002362 \ \ slugs/ft^3$, the planform area as $A = 5.13 ft^2$, and the coefficient of drag as $C_D = 1$. The weight of the container is 100 *lb* with a gravitational acceleration of $32.2 ft/s^2$. The coefficient of friction is $\mu = 0.7$ and the coefficient of restitution is $e_n = 0.25$.

5.3 Comparison With Experiment

In this section we validate the use of the subsequent impact model introduced in this chapter by comparing it to experimental results. The model is applied in a manner that requires the input of the coefficient of restitution, which is accurately determined through comparison. The quantity analyzed is the tumbling distance which is defined as the distance from the initial impact until the container ceases to move. This distance is highly erratic as a function of the orientation of the container, but an interesting, repeatable behavior has been observed.

The test data used in the calculation was obtained from experiments designed to test the impact characteristics of certain cushioning materials. The container was constructed such that the cushioning material shrouded the cargo, which was much heavier. The two cushioning materials used were the chevron and the honeycomb patterned cardboard cushions. An open chevron cushion container which has undergone a corner impact is shown in Fig. 5.10.

Figure 5.10*: Container with cargo after corner impact.*

The dimensions of the container were the same as those used in the previous section, with $R = 20.3$ and $\psi = 38^o$. Once again the density of air, planform area and the coefficient of drag were taken as $\rho_{air} = 0.002362 \ \ slugs/\ ft^3$, $A = 5.13\, ft^2$, and $C_D = 1$. The coefficient

of friction was taken as $\mu = 0.7$. Also, the initial angular velocity was taken as zero. The reason for this will be explained in detail later in this section.

These containers were dropped via helicopter from heights of 50 and 65 feet above the ground. At the time of release the helicopter was traveling with a constant horizontal speed of either 50 or 65 knots (85.39 or 109.71 ft/s). The event, form the time the container impacted the ground to the time it came to rest, was recorded by a video camera from a safe distance. This video was then analyzed to determine the tumbling distance, accurate up to the nearest meter. The actual experimental data is shown in Appendix B. Due to the unpredictable variation in the tumbling distance we only analyze the averages for each or the four impact scenarios using each of the cushioning materials.

The computational model of subsequent impacts was presented in the previous section. The impacts were all taken to be planar, that is, we assumed that impact occurred at an edge rather than at a corner. This assumption is valid because, even in the case when impact occurs at a corner, the trajectory will still follow the direction of motion defined by the initial velocity. Since the container free falls to the ground, one has no control over the orientation angle. This is the reason why, for all impact scenarios, the tumbling distances are plotted as functions of all possible impact orientations. These results are then averaged to facilitate the comparison with the experimental results discussed earlier. The drop height, initial horizontal velocity, and the mass of the container were the three parameters which were given for each impact scenario. Once these parameters were entered and the computation completed, the average tumbling distances were determined and compared to the experimental values. If the value of the tumbling distance was too small, the coefficient of restitution had to be increased until

the accurate value was determined or vice versa. As a secondary check, this was done for all impact scenarios for each given material. As shown in Fig. 5.1, the orientation angle, χ, can take on 180 degrees of possible values. The next question that arose was how small of an increment in this angle is required to achieve accurate results. For this reason we carried out the calculation, first using a one degree interval, and then using a one tenth of a degree interval. The experimental data, as well as the computational results of these calculations for the chevron cushioned container, are presented in Table 5.1 below.

***Table 5.1**: Tumbling distances for the chevron cushion container.*

Drop Altitude (ft)	Horizontal Velocity (ft/s)	Mass (lb)	Tumbling Distance (ft)	STD of Tumbling (ft)
Experimental results				
50	85.4	103.8	**77.4**	32.0
50	109.7	105.2	**96.5**	28.2
65	85.4	110.6	**68.6**	18.0
65	109.7	112.5	**93.5**	30.3
Computational results: $e_n = 0.32$, 1799 impacts.				
50	85.4	103.8	**69.4**	40.7
50	109.7	105.2	**96.2**	47.1
65	85.4	110.6	**69.9**	45.5
65	109.7	112.5	**95.1**	52.2
Computational results: $e_n = 0.32$, 179 impacts.				
50	85.4	103.8	**68.3**	38.3
50	109.7	105.2	**96.2**	48.8
65	85.4	110.6	**72.1**	47.0
65	109.7	112.5	**93.6**	51.0

The results show that average tumbling distances were predicted to within 15 percent of the actual value in the worst case (altitude 50 ft, velocity 50 knots), other cases being much better. We have also determined the value of the coefficient of restitution for this container and material, it is $e_n = 0.32$. The increase in the number of increments of the orientation angle from one per degree to ten per degree did not show a significant

change in the average tumbling distance, nor the standard deviations. This is an important result because the computational time required is also increased tenfold with the increased increment of the orientation angle, because for each increment the program calculates the position of the container during the entire event arriving at a value of the tumbling distance. This procedure was then repeated up to 1799 times, a calculation which took between 1.5 and 3.5 hours depending on the computational machine used. A good measure of the distribution of the data is the standard deviation. The standard deviation (STD) of both the experimental and computational data was calculated and is also presented in Table 5.1. We see that the STD of the computational results is quite larger than that of the experimental data. This discrepancy in the standard deviations can be explained by the container either having aerodynamically favorable orientations at impact or since the container is released from a helicopter in a similar manner every time, the range of possible values of the orientation angle at impact is diminished. Note that in some cases, there was a minor angular velocity at first impact due to the nature of the release, which was not accounted for in this simulation, because of the complexity of predicting its magnitude.

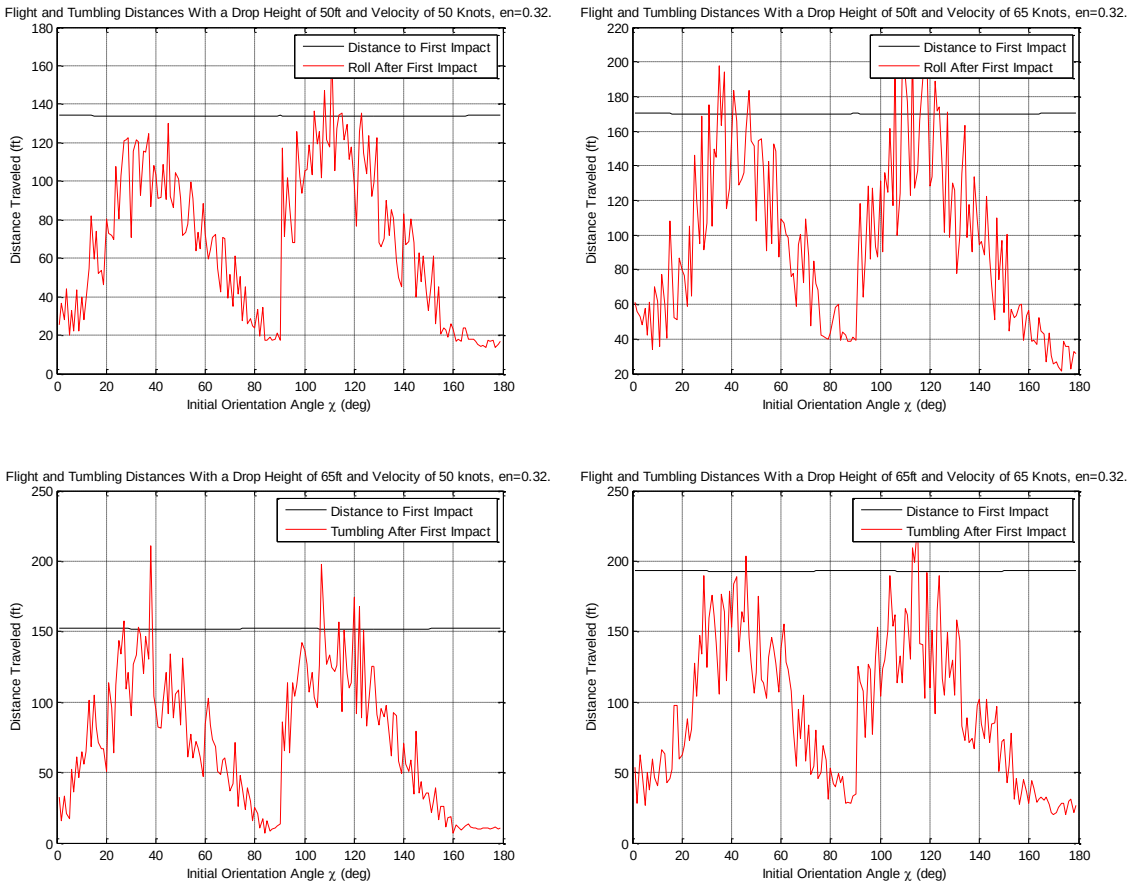

***Figure 5.11**: Flight and tumbling distances for the chevron cushion, 179 impacts.*

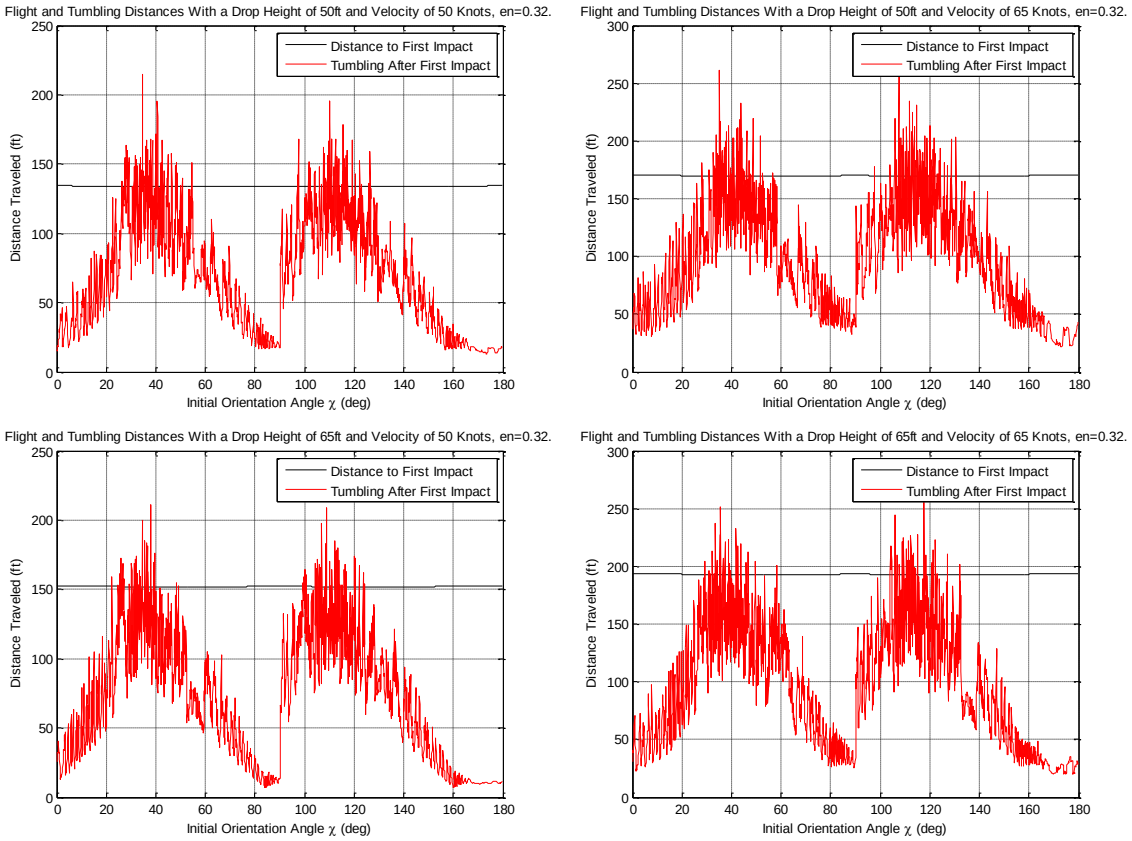

***Figure 5.12**: Flight and tumbling distances for the chevron cushion, 1799 impacts.*

The actual plots of the computational results for each of the four impact scenarios and for both increments of the orientation angle are shown in Fig. 5.11 and 5.12. As was discussed earlier, Fig. 5.11 and 5.12 show a lot of variation in the tumbling distance of the container for even a small range of values of the orientation angle. Despite this, we do observe an almost sinusoidal general behavior. The maximum tumbling distances occur at initial orientation angles of about 35 and 115 degrees. These values agree with Fig. 2.6 through Fig. 2.9 developed in Chapter 2 which indicate that the smallest energy loss occurs at the appropriate values of the angle γ, which is related to angle χ as is shown in Fig. 5.1. What this suggests is that, since very little energy is absorbed for these orientations during the first impact, a large amount of kinetic energy is left over to propel

the container further along the impacting surface. Note the discontinuity in the tumbling distance at 90 degrees, this is due to the fact that the computational model discussed in this chapter requires that only one corner impacts the surface, therefore it cannot handle the calculation when the impact occurs on a side. Along with the tumbling distance, the horizontal distance that the container flies until the first impact is also plotted in each figure. This value depends on the drop height, initial velocity, and the mass of the container.

One of the things that come to mind when one sees data such as that presented in Fig. 5.11 and Fig. 5.12 is to use the Fourier transform in order to obtain the frequency spectrum of the seemingly erratic variation. The fast Fourier transform of the first plot in Fig. 5.12 is shown below.

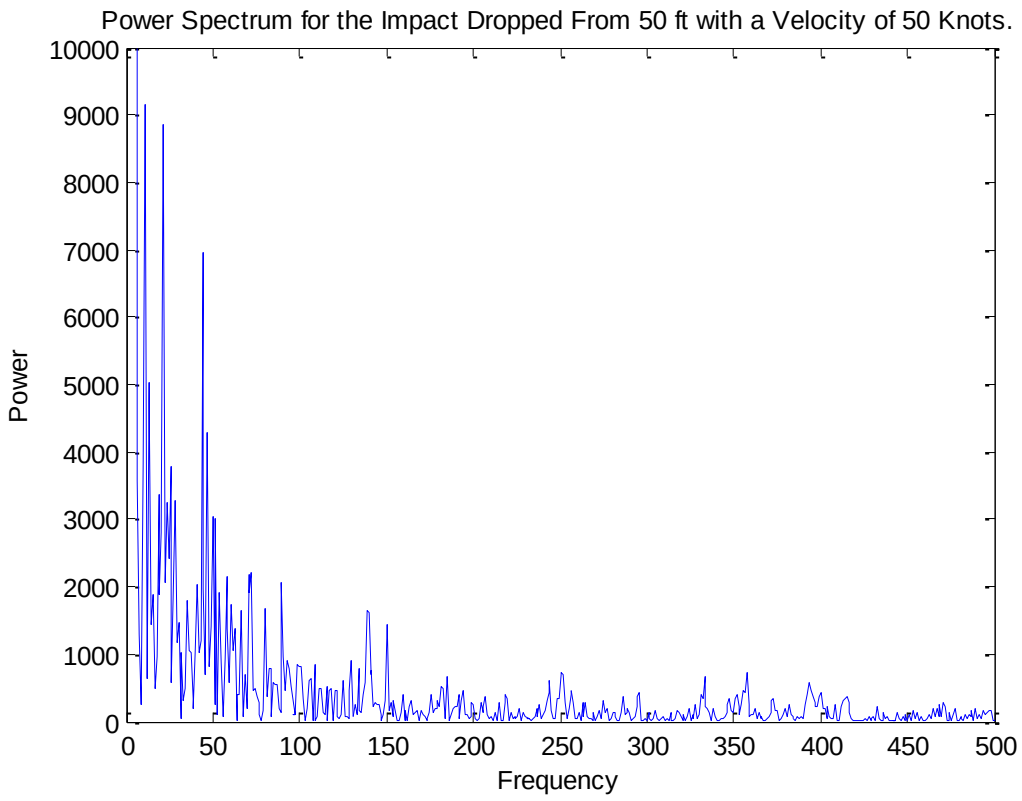

***Figure 5.13**: Power spectrum (50ft, 50 knots, and 1799 impacts).*

We see that there is no outstanding frequency that can be used to predict the behavior of the tumbling distances. This leads to the conclusion that, besides the general sinusoidal-like behavior of the tumbling distances, there is no simple model that can be devised by observing the frequency spectrum.

The same subsequent impact procedure was conducted for the honeycomb cushion material. The following table compares the computational data to the recorded experimental data.

Table 5.2*: Tumbling distances for the honeycomb cushion container.*

Drop Altitude (ft)	Horizontal Velocity (ft/s)	Mass (lb)	Tumbling Distance (ft)	STD of Tumbling (ft)
Experimental results				
50	85.4	78.9	**63.7**	23.0
50	109.7	77.2	**65.0**	19.4
65	85.4	92.3	**43.6**	15.2
65	109.7	85.5	**58.4**	19.4
Computational results: $e_n = 0.15$, 1799 impacts.				
50	85.4	78.9	**45.0**	27.8
50	109.7	77.2	**62.1**	33.6
65	85.4	92.3	**46.8**	30.8
65	109.7	85.5	**60.4**	36.1
Computational results: $e_n = 0.15$, 179 impacts.				
50	85.4	78.9	**45.5**	28.6
50	109.7	77.2	**61.4**	33.6
65	85.4	92.3	**46.6**	30.7
65	109.7	85.5	**60.1**	35.9

In Table 5.2, we see that once again the tumbling distance is accurately predicted by the computational model except for the impact dropped from 50 feet with a velocity of 50 knots, or $85.4\,ft/s$. This tells us the accurate value of the coefficient of restitution has been established and it is $e_n = 0.15$. It should be noted that this value is less than half of that for the chevron cushion. Once again we see that there is very little change between

the average tumbling distance obtained by calculating 179 impacts and those obtained by calculating 1799 impacts. Also, the standard deviations of the computational results are much higher than those of the experimental data.

The actual plots of the tumbling distances as functions of the orientation angle for all of the impact scenarios using the honeycomb cushioned container are given by Fig. 5.14 and Fig. 5.15.

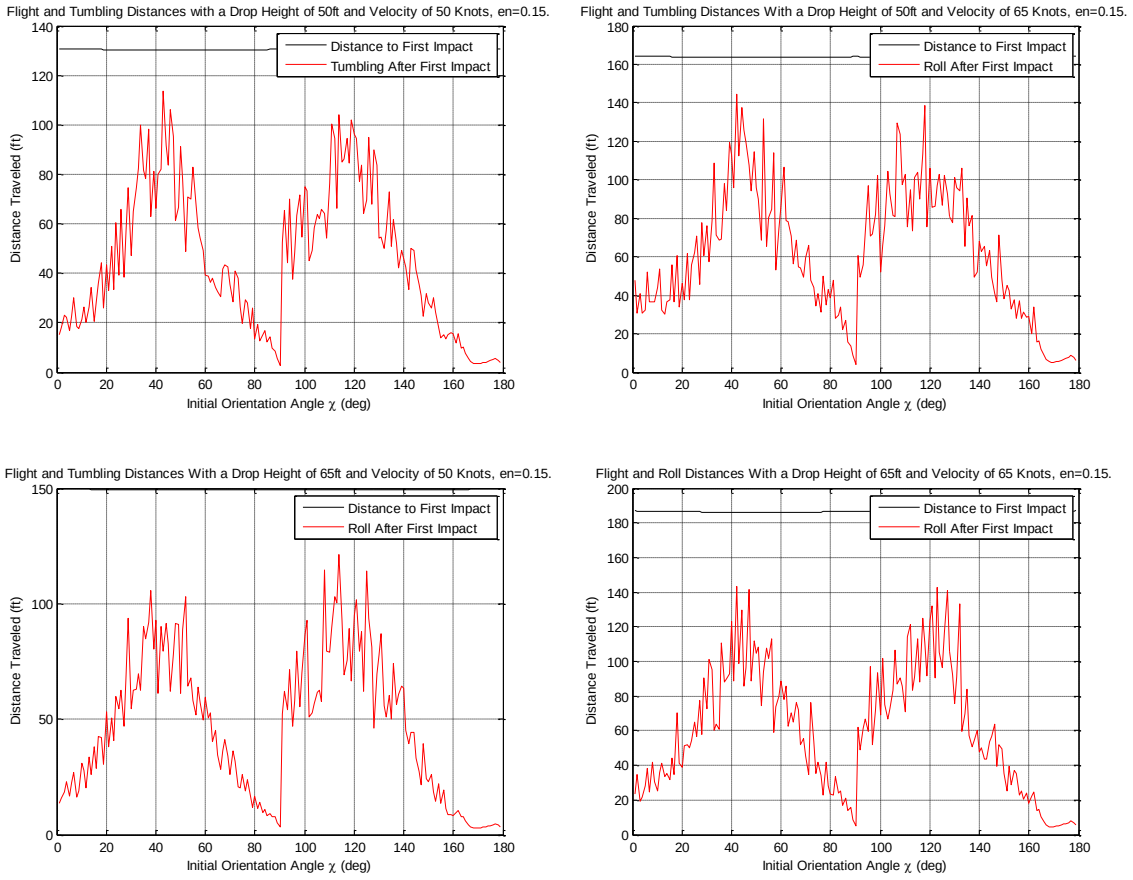

***Figure 5.14**: Flight and tumbling distances for the honeycomb cushion, 179 impacts.*

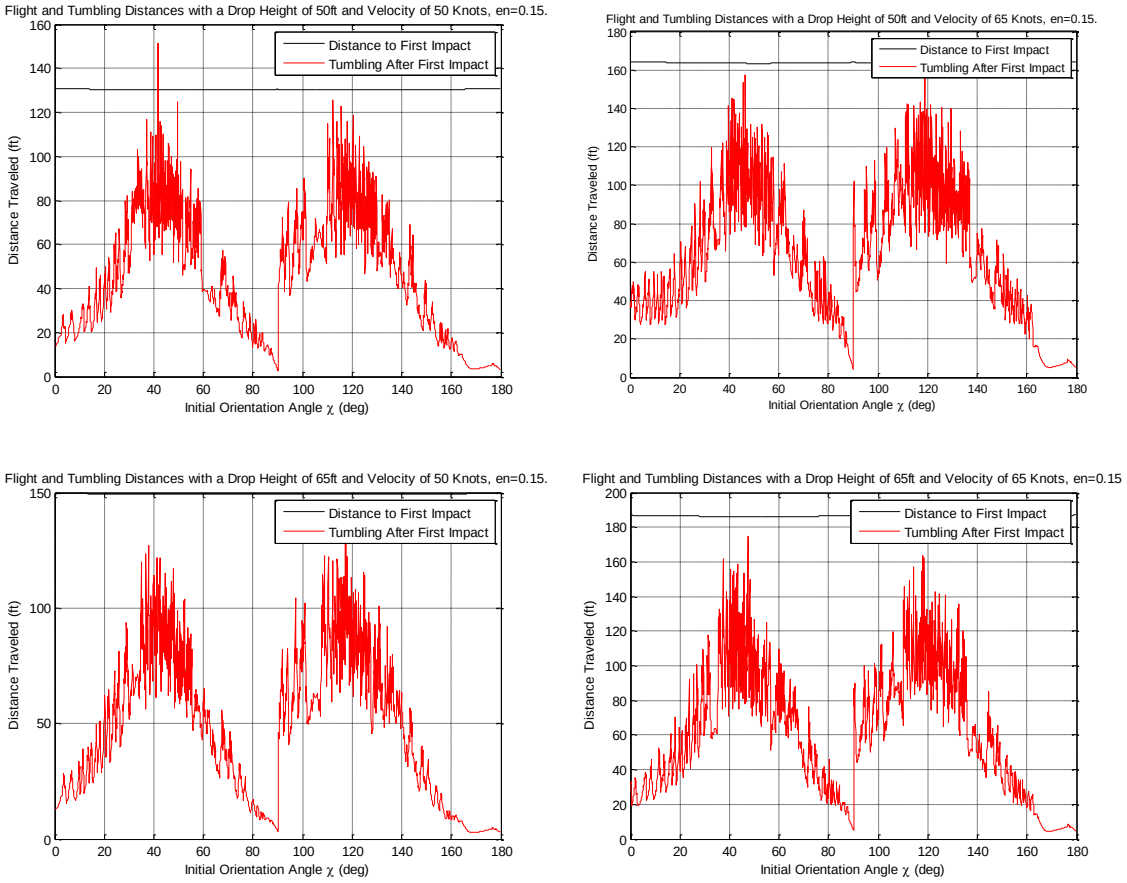

***Figure 5.15**: Flight and tumbling distances for the honeycomb cushion, 1799 impacts.*

The above figures show that the tumbling distance exhibits the same behavior that was observed for the chevron cushioned container. Namely, we observe that once again the tumbling distance looks sinusoidal-like, with the maximum occurring at 40 and 115 degrees. Besides this pattern, the local behavior is erratic and cannot produce an accurate model to be used in predicting the tumbling distance. This is the reason why the comparison presented in this chapter is based on statistical quantities such as the average and standard deviation of the tumbling distance.

In conclusion, we see that a number of interesting behaviors can be determined by analyzing subsequent impacts. If one has the ability to somehow control the orientation of the container at first impact, then they can somewhat control the tumbling distance or

"place" the container at a given position. The reason for saying somewhat in regards to the control is because of the unpredictable variation of the tumbling distance, even for a small range of values of the orientation angle. Initially, this might seem incorrect, but think about it this way, a small difference in the orientation angle for the first impact will have little effect on that impact, but the difference for the subsequent impacts will grow and change unpredictably thereby changing the total tumbling distance. From all the figures showing the computational results of the tumbling distance presented in this section, we see a region between 160 and 180 degrees of the orientation angle which is relatively smooth and can be predictable. This region also happens to be the place where the tumbling distance is at a minimum, a fact which is indeed advantageous if one desires that the container does not tumble far from the point of initial impact.

Many improvements can be made to this model. As we have stated earlier, we are considering the impact to be planar. This assumption can be removed by allowing the container to move in three dimensions. This would require a more complex algorithm to determine the position of the corner which impacts the ground. Another assumption made was that the initial orientation of the container was equal to zero. As far as the aerodynamic analysis is concerned, the assumption made was that the coefficient of drag and planform area remain constant. This is a valid assumption for a blunt body such as that presented here. An interesting addition that can be made to this model is making the impact surface non-flat and model the rotation of the container during flight. However, the non-flat surface can be too much for the rigid body model to handle because in real life the impact takes place on a non-flat surface and over a contact area as opposed to a contact point. Besides the numerous validated assumptions, we have shown that

modeling something as complex as subsequent impacts of objects can be done quite accurately using this methodology.

Chapter 6

Conclusions and Future Work

The main goal of this work was to be analyze the impact of a container with the ground. The complicated structure of the given container suggested that the rigid body impact model should be used, because it provides a better understanding of this type of impact than do other more complicated approximations. Nevertheless, we explored vibrational impact models as well. A substantial effort was also put into developing an accurate aerodynamic model, capable of describing the effects of the drag force during descent to impact. The aforementioned models were then combined to simulate the subsequent impacts of the actual container.

6.1 Summary of Key Results

We began this thesis by formulating the rigid body impact model and deriving the post-impact quantities for a planar oblique impact. These were then used to obtain the dimensionless kinetic energy loss expressions for both the sliding and no sliding impact regimes. By analyzing the behavior of the kinetic energy loss for axisymmetric as well as initially irrotational bodies, we obtained its dependence on the impact orientation and the initial angular velocity. This allowed us to specify the initial orientation and angular velocity which would yield the lowest energy loss. We then analyzed three dimensional rigid body impact by formulating the governing equations. The rigid body impact

analysis was concluded with an example which validated the use of the two dimensional model for analyzing certain three dimensional impacts.

Our discussion of the vibrational impact provided a transient description of the impact force, something that the rigid body impact model is not capable of. The linear two degree of freedom oscillator was used to model the interaction between the cushion and the cargo. This relationship allowed us to determine the stiffness ratio of the cushion and the cargo, which produced the best impact outcomes. We showed that a lower stiffness of the cargo causes it to oscillate faster than the cushion and to absorb more energy than the cushion. Therefore in order to have the best energy absorption, the stiffness of the cushion must be less than that of the cargo. This result was confirmed by experiment. We also investigated a nonlinear vibrational impact model which used the Hertzian contact stiffness. The model parameters were varied and the resulting behavior was analyzed. The energy lost during impact, which is the area enclosed by the hysteresis curve, behaved in a non-trivial fashion. However, this ease of manipulating the model proves its utility for fitting experimental data.

We then turned our attention to the aerodynamics of free fall prior to impact. After formulating and solving the nonlinear governing equations we were able to ascertain the pre-impact quantities for an object which was released with an initial velocity from some height above the impact surface. Several analytical solutions were presented for the nonlinear equations, but the general solution was obtained by numerical methods. When analyzing the behavior of the resultant velocity of the object during free fall we discovered that this velocity has a favorable minimum. This minimum resultant velocity is in most cases much less than the terminal velocity and occurs shortly after

release. This is an important result for someone designing a powered drop since the object's kinetic energy is also minimized at this time. An approximate solution to the aerodynamic equations was also presented and validated. The discussion of the aerodynamics was concluded with the three dimensional simulation of the object's trajectory under the influence of wind. This analysis showed that the amount of sideways drift was relatively small as long as the velocity of the wind was small compared to the terminal velocity.

The models developed were compiled in a simulation code capable of analyzing the subsequent impacts of the container which has been developed for the U.S. Army Logistics Innovation Agency for aerial resupply. We discussed and validated the subsequent impact model and the assumptions made during its formulation. This code was used to simulate the multiple collisions occurring after the object initially makes contact with the ground. The results showed that the tumbling distance, the total distance that the container traveled from the initial impact until its motion ceased, depends strongly on the orientation angle at the initial impact. Besides the small scale erratic behavior of the tumbling distance as a function of the initial orientation, the general shape of the function was almost sinusoidal. Using statistical methods to compare these simulations to actual drop test data, we were able to determine the coefficient of restitution for the given container. This value of the coefficient of restitution was then applied to different impact scenarios which accurately predicted the tumbling distances, thereby validating our analysis.

6.2 Future Work

Despite the long history of the study of impact mechanics there are still many questions that need to be answered. There are no impact models which can accurately describe the impact process for complex objects such as the container discussed in this thesis. This field of impact mechanics needs an analytical model stemming from physical principles capable of describing the impact of a container with the ground. These principles should include elasto-dynamics, buckling of cushion layers, contact of the cushion with the ground, as well as the tribology of impact. Such a model would close the gap between the theoretical models and experimental evidence. It will allow us to design a container capable of maximizing its energy absorbing capabilities while at the same time decreasing the required amount of cushioning material, thereby reducing cost. Furthermore, a closer study of friction during impact would be an essential part of this model. Early experiments suggest that one type of frictional regime, sliding as opposed to not sliding at time of impact, is more advantageous than the other, resulting in less damage. Therefore, instigating the onset, of one regime during impact has the potential of reducing the impact damage. A complete analysis of the appropriate range of the stiffness ratio between the cargo and the cushioning material would be essential, because it has been observed that this ratio plays a crucial role in the cargo's survivability. It would also be imperative to investigate the aerodynamics of free fall more rigorously. A closer look at the effect of the container's size, shape, and orientation at release could allow us to control its pre-impact velocities and orientation. Even with small flight duration of this container, the rotational motion during flight needs to be modeled. Note that the

aerodynamics, during the 2-2.5 seconds of impact are transient, while we are using a steady state model.

A mathematically rigorous model which anyone can apply will be the main goal of future work. The model's user-friendliness will speed up the progress in cushion design and further research in economic packaging. It will not only improve our understanding of impact mechanics, but also positively affect many aspects of the world around us.

References

[1] Baruh, H., *Analytical Dynamics*, McGraw-Hill, 1999

[2] Benaroya, H., Nagurka, M. L., *Mechanical Vibration: Analysis, Uncertainties, and Control*, 3rd ed., Taylor and Francis Group, Boca Raton, FL, 2010

[3] Berges, P., Bowling, A., "Rebound, Slip, and Compliance in the Modeling and Analysis of Discrete Impacts in Legged Locomotion", *J. Vib. Control*, Vol. 12, No. 12, 2006, pp. 1407-1430

[4] Bertin, J.J., Cummings, R.M., *Aerodynamics for Engineers*, 5th ed., Pearson Prentice-Hall, Upper Saddle River, NJ, 2009

[5] Bottega, W.J., *Engineering Vibrations*, Taylor and Francis Group, Boca Raton, FL, 2006

[6] Brach, R.M., *Mechanical Impact Mechanics: Rigid Body Collisions*, John Wiley & Sons, New York, 1991

[7] Brach, R.M., "Rigid Body Collisions", *ASME J. Appl. Mech*., Vol. 56, 1989, pp. 133-138

[8] Brogliato, B., *Nonsmooth Mechanics*, 2nd ed., Springer-Verlag, London, 1999

[9] Cross, R., "Increase in Friction Force with Sliding Speed", *Am. J. Phys.*, Vol. 73, No. 9, 2005, pp. 812-816

[10] Cross, R., "Measurements of the Horizontal Coefficient of Restitution for a Superball and a Tennis Ball", *Am. J. Phys.*, Vol. 70, No. 5, 2002, pp. 482-489

[11] Domenech, A., "A Classical Experiment Revisited: The Bounce of Balls and Superballs in Three Dimensions", *Am. J. Phys.*, Vol. 73, No. 1, 2005, pp. 28-36

[12] Elkaranshawy, H.A., "Rough Collisions in Three-Dimensional Rigid Multi-body System", *Proc. IMeschE. J. Multi-body Dynamics*, Vol. 221, Part K, 2007, pp. 541-550

[13] Goldsmith, W., *Impact: The Theory and Physical Behaviour of Colliding Solids*, Edward Arnold Publishers, London, 1960

[14] Greenburg, M.D., *Advanced Engineering Mathematics*, 2nd ed., Prentice-Hall, Upper Saddle River, NJ, 1998

[15] Hunt, K.H., Crossley, F.R.E., "Coefficient of Restitution Interpreted as Damping in Vibroimpact", *ASME J. Appl. Mech*., Volume 42, Issue 2, 1975, pp. 440-445

[16] Hussainova, I., Schade, K., Tisler, S., "Dynamic Coefficients in Impact Mechanics", *Proc. Estonian Acad. Sci. Eng.*, Vol. 12, No. 1, 2006, pp. 26-39

[17] Incropera, F.P., Dewitt, D.P., Bergman, T.L., Lavine, A.S., *Introduction to Heat Transfer*, 5th ed., John Wiley & Sons, 2007

[18] Ivanov, A.P.," A Constructive Model of Impact with Friction", *PMM U.S.S.R*, Vol. 52, No. 6, 1988, pp. 700-704

[19] Johnson, K.L., *Contact Mechanics*, Cambridge University Press, Cambridge, 1985

[20] Keller J.B., "Impact With Friction", *ASME J. Appl. Mech*., Vol. 53, 1986, pp. 1-4

[21] Kozlov, V.V., *Billiards: A Genetic Introduction to the Dynamics of Systems with Impacts*, American Mathematical Society, 1991

[22] Kundu, P.K., Cohen, I.M., *Fluid Mechanics*, 4th ed., Elsevier, 2008.

[23] Lankarani, H.M., Pereira, M.F.O.S., "Treatment of Impact with Friction in Planar Multibody Mechanical Systems", *Multibody Syst. Dyn.*, Vol. 6, 2001, pp. 203-227

[24] Mahmoud, S., Chen, X., Jankowski, R., "Structural Pounding Models with Hertz Spring And Nonlinear Damper", *J. Applied Sci.*, Vol. 8, No. 10, 2008, pp. 1850-1858

[25] Marghitu, D.B., Stoenescu, E.D.," Rigid Body Impact With Moment of Rolling Friction", *Nonlinear Dyn.*, Vol. 50, No.3, 2007, pp. 597-608

[26] Mathews, J.H., Fink, K.D., *Numerical Methods Using MATLAB*, 4th ed., Pearson Prentice-Hall, Upper Saddle River, NJ, 2004

[27] Mayo, J.M., "Application of the Generalized Impulse-Momentum Balance Equations to Impacts with Friction in Planar Flexible Multibody Dynamics", *Mech. Based Des. of Struct.*, Vol.34, 2006, pp. 431-448

[28] Osakue, E.E., "An Experimental Study of Friction During Planar Elastic Impact", *ASME J. Pressure Vessel Technology*, Vol. 123, 2001, pp. 493-500

[29] Persson, B.N.J., *Sliding Friction: Physical Principles and Applications*, Springer-Verlag, Berlin, 1998

[30] Pfeiffer, F., "Energy Considerations for Frictional Impacts", *Arch. Appl. Mech.*, Vol. 80, 2010, pp. 47-56

[31] Pfeiffer, F., "On Impacts with Friction", *Appl. Math. Comput.*, Vol. 217, 2010, pp. 1184-1192

[32] Polushko, S., Viba, J., Kononova, O., Sokolova, S., "Rigid Body Impact Models Partially Considering Deformation", *Proc. Estonian Acad. Sci. Eng.*, Vol. 13, No. 2, pp. 140-155

[33] Radil, K.C., Palazzolo, A.B., ”Influence of Temperature and Impact Velocity on The Coefficient of Restitution”, NASA-TM-106485, 1994

[34] Rangel, R.V., Thornhill, R.J., Smith, C.C., “Prediction of Impact Forces Using Hertzian Contact Theory and Measured Modal Structural Data”, *Mechanical Systems and Signal Processing*, Vol. 4, No. 4, 1990, pp. 287-294

[35] Routh, E.J., *Dynamics of a System of Rigid Bodies*, 5th ed., MacMillan, London, 1891

[36] Smith, P.A., Spencer, C.D., Jones, D.E., “Microcomputer Listens to the Coefficient of Restitution”, *Am. J. Phys.*, Vol. 49, No. 2, 1981, pp. 136-140

[37] Stronge, W.J., “Generalized Impulse and Momentum Applied to Multibody Impact with Friction”, *Mech. Struct. & Mach.*, Vol. 29, No. 2, 2001, pp. 239-260

[38] Stronge, W.J., *Impact Mechanics*, Cambridge University Press, Cambridge, 2000

[39] Stronge, W.J., James, R., Ravani, B., “Oblique Impact with Friction and Tangential Compliance”, *Phil. Trans. R. Soc. Lond.* A, Vol. 359, 2001, pp. 2447-2465

[40] Stronge, W.J., “Rigid Body Collisions with Friction”, *Proc. R. Soc. Lond.* A, Vol. 431, No. 1881, 1990, pp. 169-181

[41] Wang, Y., Kumar, R.V., “Simulation of Mechanical Systems with Multiple Frictional Contacts”, University of Pennsylvania Department of Computer Science Technical Report No. MS-CIS-92-16, 1992

[42] Wang, Y., Low, K.H., “Damped Response Analysis of Nonlinear Cushion Systems by a Linearization Method”, *Comput. Struct.*, Vol. 83, 2005, pp. 1584-1594

[43] Witters, J., Duymelinck, D., “Rolling and Sliding Resistive Forces on Balls Moving on a Flat Surface”, *Am. J. Phys.*, Vol. 54, No. 1, 1986, pp. 80-83

[44] Zhang, Y., Sharf, I., “Rigid Body Impact Modeling Using Integral Formulation, *ASME J. Comput. Nonlinear Dynam.*, Vol. 2, 2007, pp. 98-102

[45] Zukas, J.A., Nicholas, T., Swift, Hallock, F.S., Greszczuk, L.B., Curran, D.R., *Impact Dynamics*, John Wiley & Sons, New York, 1982

Appendix A

MATLAB Code, Simulation of the Subsequent Impacts

This appendix presents the MATLAB code used to simulate subsequent impacts of a container. Figure A.1 shows the diagram of the code and how the functions are interrelated. The six functions are shown below.

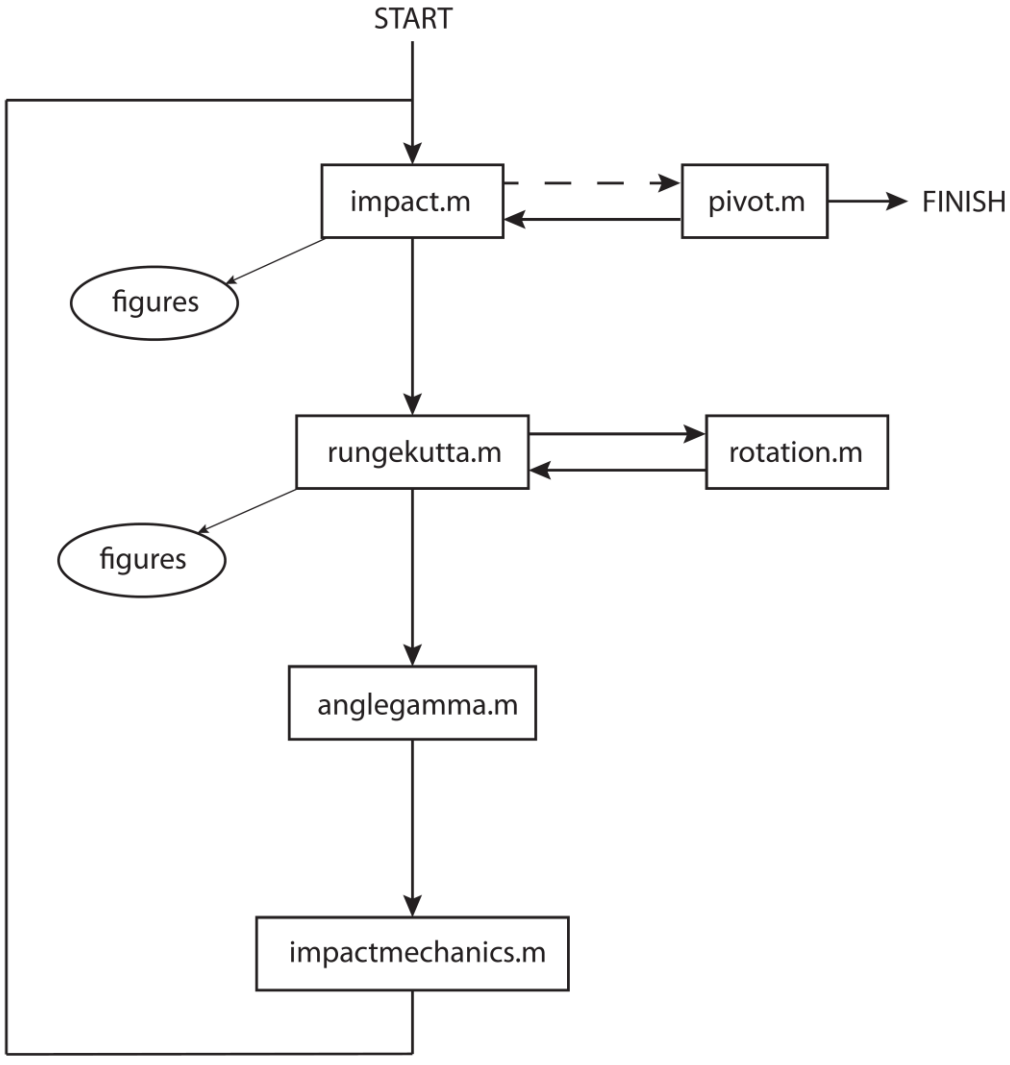

***Figure A.1**: Schematic of the simulation code.*

impact.m

```
%%% function impact

clear;
runtime1 = cputime;


%%% Number of impacts to be calculated
N = 5;
%%% Number of impact scenarios to be analyzed
M = 1;  % 179 for one degree increments


for ii = 1:M;

    %%% Initial horizontal position
    xi = 0;
    %%% Initial vertical position
    yi = 65;
    %%% Initial horizontal velocity
    Vxi = 84.39;    % 50 Knots=84.39 ft/s, 65 Knots=109.71ft/s
    %%% Initial vertical velocity
    Vyi = 0;
    %%% Initial rotation
    omi = 0;
    %%% Initial rotation angle, evenly incremented
    thetai = ((ii*10)/180)*pi;
    %%% Time begins at ti seconds
    ti = 0;


    global R phi a Ki;
    %%% Distance from the corner to the center of gravity
    R = 20.3/12;
    %%% Angle representative of the container's dimensions
    phi = (38/180)*pi;
    %%% Coefficient of the radius of gyration
    a = 2/3;
    %%% Initial Kinetic Energy
    Ki = (Vxi.^2)+(Vyi.^2)+(a.*(R.^2).*(omi.^2));


    figure(1);
    clf;
    figure(2);
    clf;
    figure(3);
    clf;
    figure(4);
    clf;
    figure(5);
```

```
    clf;
    figure(6);
    clf;
    figure(6);
    clf;

    %%% Specifying the initial pivoting decision variable
    pivoting = 0;


    %%% Analysis of the subsequent impacts
    for k = 1:N

        [xt, yt, x1t, y1t, x2t, y2t, x3t, y3t, x4t, y4t, Vxt, Vyt,...
            thetat, tt, xf, yf, x1f, y1f, x2f, y2f, x3f, y3f, x4f,
y4f,...
            Vxf, Vyf, thetaf, omf, tf] = rungekutta(xi, yi, Vxi, Vyi,...
            ti, omi, thetai);

        [gam, gamdeg, p] = anglegamma(xf, yf, x1f, y1f, x2f, y2f,
x3f,...
            y3f, x4f, y4f);

        [xi, yi, Vxi, Vyi, thetai, omi, ti, pivoting, ompivoti] =...
            impactmechanics(xf, yf, Vxf, Vyf, thetaf, omf, tf, gam, k);


        %%% Post impact position and velocity
        pos(k) = xf;
        VelocityX(k) = Vxf;
        VelocityY(k) = Vyf;
        VelocityR(k) = Vxf/Vyf;


        %%% Pivoting
        if pivoting == 1
            break;
        else
            clear xf yf Vxf Vyf thetaf omf tf gam
        end
    end


    %%% Number of pivots to be calculated
    H = 1;

    for q = 1:H

        [xf, yf, x1f, y1f, x2f, y2f, x3f, y3f, x4f, y4f, gam, thetaf,...
            tf, omf, Vxf, Vyf, p] = pivot(xf, yf, x1f, y1f, x2f, y2f,...
            x3f, y3f, x4f, y4f, tf, gam, ompivoti, p);

        pospiv(q) = xf;
```

```
    end


    %%% Initial orientation angle for each impact scenario
    THETA(ii) = (ii*10);

    %%% Flight and tumbling distances for each impact scenario
    Flight(ii) = pos(1);
    Roll(ii) = pos(k) - pos(1);
    Rollwpiv(ii) = pospiv(H) - pos(1);

end


%%% Plotting the tumbling distances
if M>1
    figure(6);
    plot(THETA,Flight,'k');
    hold on
    plot(THETA,Roll,'r');
    grid on
    title('Flight and Tumbling Distances With a Drop Height of 65ft and
Velocity of 50 Knots, en=0.32.')
    xlabel('Initial Orientaion Angle \chi (deg)');
    ylabel('Distance Traveled (ft)');
    legend('Distance to First Impact', 'Tumbling After First Impact');


    %%% Power spectrum of the tumbling distance
    Y = fft(Roll,1024);
    Pyy = Y.* conj(Y) / 1024;
    f = 1000*(0:512)/1024;
    figure(7);
    plot(f,Pyy(1:513));

else
end

runtime2 = cputime;
runtime = runtime2 - runtime1
```

rungekutta.m

```
function [xt, yt, x1t, y1t, x2t, y2t, x3t, y3t, x4t, y4t, Vxt, Vyt,...
    thetat, tt, xf, yf, x1f, y1f, x2f, y2f, x3f, y3f, x4f, y4f, Vxf,...
```

```
    Vyf, thetaf, omf, tf] = rungekutta(xi, yi, Vxi, Vyi, ti, omi,
thetai);


format long;

%%% Initial Kinetic Energy and other parameters
global R a Ki;

%%% Density of air
rho = 0.002362;
%%% Object's mass
m = 110.6/32.2;
%%% Object's planform area
A = 5.13;
%%% Gravitational acceleration
g = 32.2;
%%% Coefficient of drag
Cd = 1;


C = (.5).*(1./m).*(rho).*Cd.*A;
D = g;

%%% Terminal velocity
Vterm = ((m.*g)./(0.5.*rho.*Cd.*A)).^(1/2);


%%% Time increment
h = 0.001;
%%% Maximum number of iterations
N = (15)/h;

%%% Initial Conditions
x(1) = xi;
y(1) = yi;
VX(1) = Vxi;
VY(1) = Vyi;
t(1) = ti;
theta(1) = thetai;

%%% Determining the initial position of the container's corners
[x1(1), y1(1), x2(1), y2(1), x3(1), y3(1), x4(1), y4(1)] =...
    rotation(x(1), y(1), theta(1));


%%% The first loop will determine the general path of the object
for i = 1:N;

    %%% Runge-Kutta solution for a system of equations
    k1(i) = h*(-C.*VX(i).*sqrt((VX(i).^2) + (VY(i).^2)));
    l1(i) = h*(-D - C.*VY(i).*sqrt((VX(i).^2) + (VY(i).^2)));

    k2(i) = h*(-C.*(VX(i)+(k1(i)/2)).*sqrt(((VX(i)+(k1(i)/2)).^2) +...
```

```
        ((VY(i)+(l1(i)/2)).^2)));
    l2(i) = h*(-D - C.*(VY(i)+(l1(i)/2)).*sqrt(((VX(i)+(k1(i)/2)).^2)
+...
        ((VY(i)+(l1(i)/2)).^2)));

    k3(i) = h*(-C.*(VX(i)+(k2(i)/2)).*sqrt(((VX(i)+(k2(i)/2)).^2) +...
        ((VY(i)+(l2(i)/2)).^2)));
    l3(i) = h*(-D - C.*(VY(i)+(l2(i)/2)).*sqrt(((VX(i)+(k2(i)/2)).^2)
+...
        ((VY(i)+(l2(i)/2)).^2)));

    k4(i) = h*(-C.*(VX(i)+(k3(i))).*sqrt(((VX(i)+(k3(i))).^2) +...
        ((VY(i)+(l3(i))).^2)));
    l4(i) = h*(-D - C.*(VY(i)+(l3(i))).*sqrt(((VX(i)+(k3(i))).^2) +...
        ((VY(i)+(l3(i))).^2)));

    k(i) = (1/6)*(k1(i)+(2*k2(i))+(2*k3(i))+k4(i));
    l(i) = (1/6)*(l1(i)+(2*l2(i))+(2*l3(i))+l4(i));

    t(i+1) = t(i) + h;
    VX(i+1) = VX(i) + k(i);
    VY(i+1) = VY(i) + l(i);

    m1(i) = h*(VX(i));
    n1(i) = h*(VY(i));

    m2(i) = h*(VX(i)+k2(i));
    n2(i) = h*(VY(i)+l2(i));

    m3(i) = h*(VX(i)+k3(i));
    n3(i) = h*(VY(i)+l3(i));

    m4(i) = h*(VX(i)+k4(i));
    n4(i) = h*(VY(i)+k4(i));

    m(i) = (1/6)*(m1(i)+(2*m2(i))+(2*m3(i))+m4(i));
    n(i) = (1/6)*(n1(i)+(2*n2(i))+(2*n3(i))+n4(i));

    x(i+1) = x(i) + m(i);
    y(i+1) = y(i) + n(i);

    theta(i+1) = theta(i) + (omi*h);


    %%% Position of the corner's after a time increment h
    [x1(i+1), y1(i+1), x2(i+1), y2(i+1), x3(i+1), y3(i+1), x4(i+1)...
        , y4(i+1)] = rotation(x(i+1), y(i+1), theta(i+1));


    %%% The following statement will break the loop when
    %%% one of the corners hits the impact surface
    if (y1(i+1)<0 | y2(i+1)<0 | y3(i+1)<0 | y4(i+1)<0);
        break;
    else
```

```
    end

end



%%% The next loop will take the last term in the position arrays prior
to
%%% hitting the ground and continue to calculate more points using a
%%% smaller time interval.

j = i;
h = h/1000;

while (y1(j)>0 & y2(j)>0 & y3(j)>0 & y4(j)>0);

    i = j;

    %%% Runge-Kutta solution for a system of equations
    k1(i) = h*(-C.*VX(i).*sqrt((VX(i).^2) + (VY(i).^2)));
    l1(i) = h*(-D - C.*VY(i).*sqrt((VX(i).^2) + (VY(i).^2)));

    k2(i) = h*(-C.*(VX(i)+(k1(i)/2)).*sqrt(((VX(i)+(k1(i)/2)).^2) +...
        ((VY(i)+(l1(i)/2)).^2)));
    l2(i) = h*(-D - C.*(VY(i)+(l1(i)/2)).*sqrt(((VX(i)+(k1(i)/2)).^2)
+...
        ((VY(i)+(l1(i)/2)).^2)));

    k3(i) = h*(-C.*(VX(i)+(k2(i)/2)).*sqrt(((VX(i)+(k2(i)/2)).^2) +...
        ((VY(i)+(l2(i)/2)).^2)));
    l3(i) = h*(-D - C.*(VY(i)+(l2(i)/2)).*sqrt(((VX(i)+(k2(i)/2)).^2)
+...
        ((VY(i)+(l2(i)/2)).^2)));

    k4(i) = h*(-C.*(VX(i)+(k3(i))).*sqrt(((VX(i)+(k3(i))).^2) +
((VY(i)+...
        (l3(i))).^2)));
    l4(i) = h*(-D - C.*(VY(i)+(l3(i))).*sqrt(((VX(i)+(k3(i))).^2) +...
        ((VY(i)+(l3(i))).^2)));

    k(i) = (1/6)*(k1(i)+(2*k2(i))+(2*k3(i))+k4(i));
    l(i) = (1/6)*(l1(i)+(2*l2(i))+(2*l3(i))+l4(i));

    t(i+1) = t(i) + h;
    VX(i+1) = VX(i) + k(i);
    VY(i+1) = VY(i) + l(i);

    m1(i) = h*(VX(i));
    n1(i) = h*(VY(i));

    m2(i) = h*(VX(i)+k2(i));
    n2(i) = h*(VY(i)+l2(i));
```

```
    m3(i) = h*(VX(i)+k3(i));
    n3(i) = h*(VY(i)+l3(i));

    m4(i) = h*(VX(i)+k4(i));
    n4(i) = h*(VY(i)+k4(i));

    m(i) = (1/6)*(m1(i)+(2*m2(i))+(2*m3(i))+m4(i));
    n(i) = (1/6)*(n1(i)+(2*n2(i))+(2*n3(i))+n4(i));

    x(i+1) = x(i) + m(i);
    y(i+1) = y(i) + n(i);

    theta(i+1) = theta(i) + (omi*h);


    [x1(i+1), y1(i+1), x2(i+1), y2(i+1), x3(i+1), y3(i+1), x4(i+1),...
        y4(i+1)] = rotation(x(i+1), y(i+1), theta(i+1));


    j = i + 1;
end




%%% This following loop will take the last term prior to hitting the
ground
%%% in the position array of the previous loop and recalculate the
%%% position with an EVEN SMALLER time interval.

j = i;
h = h/1000;

while (y1(j)>0 & y2(j)>0 & y3(j)>0 & y4(j)>0);

    i = j;

    k1(i) = h*(-C.*VX(i).*sqrt((VX(i).^2) + (VY(i).^2)));
    l1(i) = h*(-D - C.*VY(i).*sqrt((VX(i).^2) + (VY(i).^2)));

    k2(i) = h*(-C.*(VX(i)+(k1(i)/2)).*sqrt(((VX(i)+(k1(i)/2)).^2) +...
        ((VY(i)+(l1(i)/2)).^2)));
    l2(i) = h*(-D - C.*(VY(i)+(l1(i)/2)).*sqrt(((VX(i)+(k1(i)/2)).^2)
+...
        ((VY(i)+(l1(i)/2)).^2)));

    k3(i) = h*(-C.*(VX(i)+(k2(i)/2)).*sqrt(((VX(i)+(k2(i)/2)).^2) +...
        ((VY(i)+(l2(i)/2)).^2)));
    l3(i) = h*(-D - C.*(VY(i)+(l2(i)/2)).*sqrt(((VX(i)+(k2(i)/2)).^2)
+...
        ((VY(i)+(l2(i)/2)).^2)));
```

```
    k4(i) = h*(-C.*(VX(i)+(k3(i))).*sqrt(((VX(i)+(k3(i))).^2) +...
        ((VY(i)+(l3(i))).^2)));
    l4(i) = h*(-D - C.*(VY(i)+(l3(i))).*sqrt(((VX(i)+(k3(i))).^2) +...
        ((VY(i)+(l3(i))).^2)));

    k(i) = (1/6)*(k1(i)+(2*k2(i))+(2*k3(i))+k4(i));
    l(i) = (1/6)*(l1(i)+(2*l2(i))+(2*l3(i))+l4(i));

    t(i+1) = t(i) + h;
    VX(i+1) = VX(i) + k(i);
    VY(i+1) = VY(i) + l(i);

    m1(i) = h*(VX(i));
    n1(i) = h*(VY(i));

    m2(i) = h*(VX(i)+k2(i));
    n2(i) = h*(VY(i)+l2(i));

    m3(i) = h*(VX(i)+k3(i));
    n3(i) = h*(VY(i)+l3(i));

    m4(i) = h*(VX(i)+k4(i));
    n4(i) = h*(VY(i)+k4(i));

    m(i) = (1/6)*(m1(i)+(2*m2(i))+(2*m3(i))+m4(i));
    n(i) = (1/6)*(n1(i)+(2*n2(i))+(2*n3(i))+n4(i));

    x(i+1) = x(i) + m(i);
    y(i+1) = y(i) + n(i);

    theta(i+1) = theta(i) + (omi*h);


    %%% Position of the corner's after a time interval
    [x1(i+1), y1(i+1), x2(i+1), y2(i+1), x3(i+1), y3(i+1), x4(i+1),...
        y4(i+1)] = rotation(x(i+1), y(i+1), theta(i+1));


    j = i + 1;
end



%%% The following loop will remove the last term from all of the arrays,
%%% because this y-position, of the lowest corner, is negative.

rr = (length(x)-1);

for jj = 1:rr
    xt(jj) = x(jj);
    yt(jj) = y(jj);
    x1t(jj) = x1(jj);
    y1t(jj) = y1(jj);
```

```
    x2t(jj) = x2(jj);
    y2t(jj) = y2(jj);
    x3t(jj) = x3(jj);
    y3t(jj) = y3(jj);
    x4t(jj) = x4(jj);
    y4t(jj) = y4(jj);

    Vxt(jj) = VX(jj);
    Vyt(jj) = VY(jj);

    thetat(jj) = theta(jj);

    tt(jj) = t(jj);
end

xf = xt(rr);
yf = yt(rr);
x1f = x1t(rr);
y1f = y1t(rr);
x2f = x2t(rr);
y2f = y2t(rr);
x3f = x3t(rr);
y3f = y3t(rr);
x4f = x4t(rr);
y4f = y4t(rr);
Vxf = Vxt(rr);
Vyf = Vyt(rr);

tf = tt(rr);

omf = omi;

%%% KInetic energy during flight
Kf = (Vxt.^2)+(Vyt.^2)+(a.*(R.^2).*(omf.^2));
KR = Kf./Ki;

Kft = Kf(rr);
KRt = Kft./Ki;

thetaf = thetat(rr);


%%% Transient velocity
figure(1);
hold on
plot(tt,Vxt,'r');
hold on
grid on
plot(tt,Vyt,'b');
xlabel('Time (s)');
ylabel('Velocity (ft/s)');

%%% Transient resultant velocity
VR = sqrt((Vxt.^2)+(Vyt.^2));
```

```
plot(tt,VR,'k--');
legend('Horizontal Velocity', 'Vertical Velocity','Resultant Velocity')

%%% Transient position of the center of gravity
figure(2);
hold on
plot(tt,xt,'r');
hold on
grid on
plot(tt,yt,'b');
xlabel('Time (s)');
ylabel('Position (ft)');
legend('Horizontal Position','Vertical Position');

%%% Transient angular velocity
figure(3);
hold on
plot(tt,omi,'k.');
xlabel('Time (s)');
ylabel('Angular Velocity (rad/s)');
grid on


%%% Transient position of the container's corners
figure(4);
skip = 100;
skipint = length(xt)/skip;

for oo = 1:skipint;

    o = skip*oo;
    hold on
    plot(xt(o),yt(o),'k.',[x1t(o) x2t(o)],[y1t(o) y2t(o)],'b',...
        [x2t(o) x3t(o)],[y2t(o) y3t(o)],'b',[x3t(o) x4t(o)],...
        [y3t(o) y4t(o)],'b',[x4t(o) x1t(o)],[y4t(o) y1t(o)],'cyan');

end

xlabel('Horizontal Position (ft)');
ylabel('Vertical Position (ft)');
grid on
axis equal

%%% Transient kinetic energy plot
figure(5);
plot(tt,KR,'r','LineWidth',2);
hold on
grid on
xlabel('Time (s)');
ylabel('Kinetic Energy Ratio');


end
```

anglegamma.m

```
function [gam, gamdeg, p] = anglegamma(xf, yf, x1f, y1f, x2f, y2f,
x3f,...
    y3f, x4f, y4f)


%%% finla vertical position of the corners
Ycorners = [y1f y2f y3f y4f];
%%% Determination of the lowest corner
Ymin = min(Ycorners);
p = find(Ycorners == Ymin);


%%% Calculation of the orientation angle gamma
if p == 1;
    gam = atan((x1f - xf)/(yf - y1f));
    gamdeg = (gam*180)/pi;
elseif p == 2;
    gam = atan((x2f - xf)/(yf - y2f));
    gamdeg = (gam*180)/pi;
elseif p == 3;
    gam = atan((x3f - xf)/(yf - y3f));
    gamdeg = (gam*180)/pi;
else
    gam = atan((x4f - xf)/(yf - y4f));
    gamdeg = (gam*180)/pi;
end

end
```

impactmechanics.m

```
function [xi, yi, Vxi, Vyi, thetai, omi, ti, pivoting, ompivoti, Ki]
=...
    impactmechanics(xf, yf, Vxf, Vyf, thetaf, omf, tf, gam, k);


global a en mu;
%%% Coefficient of the radius of gyration
a = 2/3;
%%% Coefficient of restitution
en = 0.32;
%%% Coefficient of friction
mu = 0.7;
%%% Distance from corner to center of gravity
global R;
```

```
%%% Angle representative of box dimensions
global phi;


%%% Definitions and abbreviations
Vx = Vxf;
Vy = Vyf;
om = omf;

rho = Vx/Vy;
lam = (omf*R)/Vy;

cg = cos(gam);
sg = sin(gam);
cg2 = cos(gam)^2;
sg2 = sin(gam)^2;


%%% Calculation of the force ratio
ForceRatio = abs(((rho*(a+sg2))-((1+en)*cg*sg)+(lam*(a-(en*sg2))*cg))...
    /((rho*cg*sg)-((1+en)*(a+cg2))-(lam*((a*(en+1))+(en*cg2))*sg)));


if ForceRatio>mu
    %%% Sliding occurs
    fprintf('The object exibited SLIDING during impact number %2d
!\n',k);

    %%% Calculation of the final velocities and rotations
    %%% Ls*Qs = Ms
    Ls = [1 0 0 1 0; 0 1 0 0 -1 ; 0 0 a cg -sg ; 0 1 sg 0 0 ; 0 0 0 1 -
mu];
    Ms = [rho ; 1 ; a*lam ; -en*(1 + (lam*sg)) ; 0];
    Qs = (Ls^-1)*Ms;
    Vxx2 = Qs(1);
    Vyy2 = Qs(2);
    omm2 = Qs(3);



else
    %%% No Sliding occurs
    fprintf('The object exibited NO SLIDING during impact number %2d
!\n',k);

    %%% Calculation of the final velocities and rotations
    %%% Lns*Qns = Mns
    Lns = [1 0 0 1 0; 0 1 0 0 -1 ; 0 0 a cg -sg ; 0 1 sg 0 0 ; 1 0 cg 0
0];
    Mns = [rho ; 1 ; a*lam ; -en*(1 + (lam*sg)) ; 0];
    Qns = (Lns^-1)*Mns;
    Vxx2 = Qns(1);
    Vyy2 = Qns(2);
    omm2 = Qns(3);
```

```
end


%%% Final dimensional velocities and angular velocities
Vxi = Vxx2*Vy;
Vyi = Vyy2*Vy;
omi = omm2*(Vy/R);


%%% Check of the FINAL contact point velocities
Vcx = Vxi + (omi*R*cos(gam));
Vcy = Vyi + (omi*R*sin(gam));

%%% Angular velocity for the first pivot
ompivoti = omi;


if Vcy<0.001;      %%% Minimum velocity, user specified
    pivoting = 1;
    fprintf('The object will now pivot !\n');
    beep; pause(0.35); beep; pause(0.35); beep;
else
    pivoting = 0;
end


%%% Post-impact position and orientation of the container
xi = xf;
yi = yf;
thetai = thetaf;
ti = tf;


end
```

rotation.m

```
function [x1, y1, x2, y2, x3, y3, x4, y4] = rotation(x, y, theta);

global R phi

 %%% Position of the container's corners as it moves through the air
for ii = 1:length(theta);
```

```
    x1pre(ii) = + (R*cos(phi));
    y1pre(ii) = + (R*sin(phi));

    x2pre(ii) = - (R*cos(phi));
    y2pre(ii) = + (R*sin(phi));

    x3pre(ii) = - (R*cos(phi));
    y3pre(ii) = - (R*sin(phi));

    x4pre(ii) = + (R*cos(phi));
    y4pre(ii) = - (R*sin(phi));


    x1(ii) = x(ii)+(x1pre(ii)*cos(theta(ii)))-
(y1pre(ii)*sin(theta(ii)));
    y1(ii) =
y(ii)+(x1pre(ii)*sin(theta(ii)))+(y1pre(ii)*cos(theta(ii)));

    x2(ii) = x(ii)+(x2pre(ii)*cos(theta(ii)))-
(y2pre(ii)*sin(theta(ii)));
    y2(ii) =
y(ii)+(x2pre(ii)*sin(theta(ii)))+(y2pre(ii)*cos(theta(ii)));

    x3(ii) = x(ii)+(x3pre(ii)*cos(theta(ii)))-
(y3pre(ii)*sin(theta(ii)));
    y3(ii) =
y(ii)+(x3pre(ii)*sin(theta(ii)))+(y3pre(ii)*cos(theta(ii)));

    x4(ii) = x(ii)+(x4pre(ii)*cos(theta(ii)))-
(y4pre(ii)*sin(theta(ii)));
    y4(ii) =
y(ii)+(x4pre(ii)*sin(theta(ii)))+(y4pre(ii)*cos(theta(ii)));

end

end
```

pivot.m

```
function [xf, yf, x1f, y1f, x2f, y2f, x3f, y3f, x4f, y4f, gam,
thetaf,...
    tf, omf, Vxf, Vyf, p] = pivot(xf, yf, x1f, y1f, x2f, y2f, x3f,
y3f,...
    x4f, y4f, tf, gam, ompivoti, p);
```

```
clear  x y x1 y1 x2 y2 x3 y3 xy y4 tt o;


global R a phi Ki;
g = 32.2;

%%% The container's position during pivot will be calculated this many
times
parts = 200;
%%% The corresponding angular increment
delt = (pi/abs(ompivoti))/(parts);
%%% Angle range for the calculation
N = 1e4;
t = [0:delt:N*delt];


%%% Pre-pivot orientation and angular velocity
gampivot(1) = gam;
ompivot(1) = ompivoti;

for pp = 2:N

    gampivot(pp) = gampivot(pp-1) + (ompivot(pp-1).*delt);
    ompivot(pp) = ompivot(pp-1) + ((g.*sin(gampivot(pp-
1)).*delt)./(a*R));

end



%%% Pivot calculation if impact occurs at CORNER 1
if p == 1
    for qq = 2:N;

        x(qq) = x1f - (R*sin(gampivot(qq)));
        y(qq) = y1f + (R*cos(gampivot(qq)));

        x2(qq) = x1f + (2*R*cos(phi)*sin(phi - gampivot(qq)));
        y2(qq) = y1f + (2*R*cos(phi)*cos(phi - gampivot(qq)));

        x3(qq) = x1f - (2*R*sin(gampivot(qq)));
        y3(qq) = y1f + (2*R*cos(gampivot(qq)));

        x4(qq) = x1f - (2*R*sin(phi)*cos(phi - gampivot(qq)));
        y4(qq) = y1f + (2*R*sin(phi)*sin(phi - gampivot(qq)));


        if (y2(qq)<0 | y3(qq)<0 | y4(qq)<0);
            break;
        else
        end
```

```
        figure(4);
        hold on
        plot(x(qq),y(qq),'cyan.',[x1f x2(qq)],[y1f y2(qq)],'r',...
            [x2(qq) x3(qq)],[y2(qq) y3(qq)],'g',[x3(qq) x4(qq)],...
            [y3(qq) y4(qq)],'b',[x4(qq) x1f],[y4(qq) y1f],'yellow');

    end

tt = (length(x)-1);

for ww = 1:tt;

    xpiv(ww) = x(ww);
    ypiv(ww) = y(ww);
    x1piv(ww) = x1f;
    y1piv(ww) = y1f;
    x2piv(ww) = x2(ww);
    y2piv(ww) = y2(ww);
    x3piv(ww) = x3(ww);
    y3piv(ww) = y3(ww);
    x4piv(ww) = x4(ww);
    y4piv(ww) = y4(ww);
    tpiv(ww) = tf + t(ww);
    ompiv(ww) = ompivot(ww);
    Kf(ww) = (a.*(R.^2).*(ompiv(ww).^2));

end
xf = xpiv(tt);
yf = ypiv(tt);
x1f = x1piv(tt);
y1f = y1piv(tt);
x2f = x2piv(tt);
y2f = y2piv(tt);
x3f = x3piv(tt);
y3f = y3piv(tt);
x4f = x4piv(tt);
y4f = y4piv(tt);
tf = tpiv(tt);

Gampivot = gampivot(tt);

thetaf = 0;

omf = ompiv(tt);

Vxf = omf*R*cos(phi);
Vyf = -omf*R*sin(phi);

%%% Next corner to pivot about
if (x2f - x1f) > (x1f - x4f)
    p = 2;
    gam = (pi/2) - phi;
else
    p = 4;
    gam = -phi;
```

```
end



%%% Pivot calculation if impact occurs at CORNER 2
elseif p == 2
    for qq=1:N;

        x(qq) = x2f - (R*sin(gampivot(qq)));
        y(qq) = y2f + (R*cos(gampivot(qq)));

        x1(qq) = x2f - (2*R*cos(phi)*sin(phi + gampivot(qq)));
        y1(qq) = y2f + (2*R*cos(phi)*cos(phi + gampivot(qq)));

        x3(qq) = x2f + (2*R*sin(phi)*cos(phi + gampivot(qq)));
        y3(qq) = y2f + (2*R*sin(phi)*sin(phi + gampivot(qq)));

        x4(qq) = x2f - (2*R*sin(gampivot(qq)));
        y4(qq) = y2f + (2*R*cos(gampivot(qq)));


        if (y1(qq)<0 | y3(qq)<0 | y4(qq)<0);
            break;
        else
        end

        figure(4);
        hold on
        plot(x(qq),y(qq),'cyan.',[x1(qq) x2f],[y1(qq) y2f],'r',...
            [x2f x3(qq)],[y2f y3(qq)],'g',[x3(qq) x4(qq)],...
            [y3(qq) y4(qq)],'b',[x4(qq) x1(qq)],[y4(qq)
y1(qq)],'yellow');

    end


tt = (length(x)-1);

for ww = 1:tt;

    xpiv(ww) = x(ww);
    ypiv(ww) = y(ww);
    x1piv(ww) = x1(ww);
    y1piv(ww) = y1(ww);
    x2piv(ww) = x2f;
    y2piv(ww) = y2f;
    x3piv(ww) = x3(ww);
    y3piv(ww) = y3(ww);
    x4piv(ww) = x4(ww);
    y4piv(ww) = y4(ww);
    tpiv(ww) = tf + t(ww);
    ompiv(ww) = ompivot(ww);
```

```
    Kf(ww) = (a.*(R.^2).*(ompiv(ww).^2));

end
xf = xpiv(tt);
yf = ypiv(tt);
x1f = x1piv(tt);
y1f = y1piv(tt);
x2f = x2piv(tt);
y2f = y2piv(tt);
x3f = x3piv(tt);
y3f = y3piv(tt);
x4f = x4piv(tt);
y4f = y4piv(tt);
tf = tpiv(tt);

Gampivot = gampivot(tt);

thetaf = 0;

omf = ompiv(tt);

Vxf = omf*R*cos(phi);
Vyf = -omf*R*sin(phi);


%%% Next corner to pivot about
if (x2f - x1f) > (x3f - x2f)
    p = 1;
    gam = -((pi/2) - phi);
else
    p = 3;
    gam = phi;
end




%%% Pivot calculation if impact occurs at CORNER 3
elseif p == 3
    for qq = 1:N;

        x(qq) = x3f - (R*sin(gampivot(qq)));
        y(qq) = y3f + (R*cos(gampivot(qq)));

        x1(qq) = x3f - (2*R*sin(gampivot(qq)));
        y1(qq) = y3f + (2*R*cos(gampivot(qq)));

        x2(qq) = x3f - (2*R*sin(phi)*cos(phi - gampivot(qq)));
        y2(qq) = y3f + (2*R*sin(phi)*sin(phi - gampivot(qq)));

        x4(qq) = x3f + (2*R*cos(phi)*sin(phi - gampivot(qq)));
        y4(qq) = y3f + (2*R*cos(phi)*cos(phi - gampivot(qq)));
```

```
        if (y1(qq)<0 | y2(qq)<0 | y4(qq)<0);
            break;
        else
        end

        figure(4);
        hold on
        plot(x(qq),y(qq),'cyan.',[x1(qq) x2(qq)],[y1(qq) y2(qq)],'r',...
            [x2(qq) x3f],[y2(qq) y3f],'g',[x3f x4(qq)],[y3f
y4(qq)],'b',...
            [x4(qq) x1(qq)],[y4(qq) y1(qq)],'yellow');

    end

tt = (length(x)-1);

for ww = 1:tt;

    xpiv(ww) = x(ww);
    ypiv(ww) = y(ww);
    x1piv(ww) = x1(ww);
    y1piv(ww) = y1(ww);
    x2piv(ww) = x2(ww);
    y2piv(ww) = y2(ww);
    x3piv(ww) = x3f;
    y3piv(ww) = y3f;
    x4piv(ww) = x4(ww);
    y4piv(ww) = y4(ww);
    tpiv(ww) = tf + t(ww);
    ompiv(ww) = ompivot(ww);
    Kf(ww) = (a.*(R.^2).*(ompiv(ww).^2));

end
xf = xpiv(tt);
yf = ypiv(tt);
x1f = x1piv(tt);
y1f = y1piv(tt);
x2f = x2piv(tt);
y2f = y2piv(tt);
x3f = x3piv(tt);
y3f = y3piv(tt);
x4f = x4piv(tt);
y4f = y4piv(tt);
tf = tpiv(tt);

Gampivot = gampivot(tt);

thetaf = 0;

omf = ompiv(tt);

Vxf = omf*R*cos(phi);
Vyf = -omf*R*sin(phi);
```

```
%%% Next corner to pivot about
if (x4f - x3f) > (x3f - x2f)
    p = 4;
    gam = (pi/2) - phi;
else
    p = 2;
    gam = -phi;
end




%%% Pivot calculation if impact occurs at CORNER 4
else
    for qq = 1:N;

        x(qq) = x4f - (R*sin(gampivot(qq)));
        y(qq) = y4f + (R*cos(gampivot(qq)));

        x1(qq) = x4f + (2*R*sin(phi)*cos(phi + gampivot(qq)));
        y1(qq) = y4f + (2*R*sin(phi)*sin(phi + gampivot(qq)));

        x2(qq) = x4f - (2*R*sin(gampivot(qq)));
        y2(qq) = y4f + (2*R*cos(gampivot(qq)));

        x3(qq) = x4f - (2*R*cos(phi)*sin(phi + gampivot(qq)));
        y3(qq) = y4f + (2*R*cos(phi)*cos(phi + gampivot(qq)));


        if (y1(qq)<0 | y2(qq)<0 | y3(qq)<0);
            break;
        else
        end

        figure(4);
        hold on
        plot(x(qq),y(qq),'cyan.',[x1(qq) x2(qq)],[y1(qq) y2(qq)],'r'
,...
            [x2(qq) x3(qq)],[y2(qq) y3(qq)],'g',[x3(qq) x4f],...
            [y3(qq) y4f],'b',[x4f x1(qq)],[y4f y1(qq)],'yellow');

    end

tt = (length(x)-1);

for ww = 1:tt;

    xpiv(ww) = x(ww);
    ypiv(ww) = y(ww);
    x1piv(ww) = x1(ww);
    y1piv(ww) = y1(ww);
    x2piv(ww) = x2(ww);
```

```
    y2piv(ww) = y2(ww);
    x3piv(ww) = x3(ww);
    y3piv(ww) = y3(ww);
    x4piv(ww) = x4f;
    y4piv(ww) = y4f;
    tpiv(ww) = tf + t(ww);
    ompiv(ww) = ompivot(ww);
    Kf(ww) = (a.*(R.^2).*(ompiv(ww).^2));

end
xf = xpiv(tt);
yf = ypiv(tt);
x1f = x1piv(tt);
y1f = y1piv(tt);
x2f = x2piv(tt);
y2f = y2piv(tt);
x3f = x3piv(tt);
y3f = y3piv(tt);
x4f = x4piv(tt);
y4f = y4piv(tt);
tf = tpiv(tt);

Gampivot = gampivot(tt);

thetaf = 0;

omf = ompiv(tt);

Vxf = omf*R*cos(phi);
Vyf = -omf*R*sin(phi);

%%% Next corner to pivot about
if (x4f - x3f) > (x1f - x4f)
    p = 3;
    gam = -((pi/2) - phi);
else
    p = 1;
    gam = phi;
end

end
```

Appendix B

Experimental Data of the Tumbling Distances

The data below presents the tumbling (roll) distances from drop tests conducted at various drop heights and release velocities. The weight of each container is also shown.

Table B.1*: Raw tumbling distances for the chevron cushion container.*

CHEVRON CUSHION				
EVENT	**ALTITUDE (FT. AGL)**	**AIRSPEED (KIAS)**	**WEIGHT (LBS)**	**ROLL (METERS)**
11	50	50	87.6	**32**
9	50	50	78.0	**15**
9	50	50	78.0	**9**
10	50	50	82.8	**17**
10	50	50	81.5	**19**
9	50	50	95.3	**25**
10	50	50	93.4	**13**
10	50	50	93.3	**15**
9	50	50	98.3	**31**
9	50	50	110.0	**31**
9	50	50	105.0	**10**
9	50	50	122.9	**35**
9	50	50	127.7	**33**
10	50	50	130.7	**17**
10	50	50	124.5	**40**
10	50	50	130.4	**29**
10	50	50	125.3	**31**
11	50	65	87.8	**19**
11	50	65	85.1	**23**
11	50	65	92.4	**21**
11	50	65	89.2	**23**
11	50	65	93.4	**27**
11	50	65	85.3	**17**
11	50	65	86.3	**12**
11	50	65	118.2	**37**

11	50	65	116.4	**33**
11	50	65	124.1	**20**
9	50	65	79.0	**31**
10	50	65	82.0	**27**
10	50	65	82.8	**41**
10	50	65	81.3	**48**
9	50	65	95.4	**25**
9	50	65	86.0	**38**
10	50	65	95.1	**16**
10	50	65	95.2	**19**
10	50	65	94.0	**19**
10	50	65	95.4	**34**
9	50	65	98.8	**28**
9	50	65	110.6	**31**
10	50	65	108.1	**37**
10	50	65	109.2	**29**
10	50	65	111.7	**24**
9	50	65	122.7	**36**
9	50	65	127.9	**34**
9	50	65	124.0	**41**
10	50	65	129.8	**29**
10	50	65	123.4	**33**
10	50	65	129.5	**33**
10	50	65	130.9	**38**
10	50	65	125.9	**40**
10	50	65	125.5	**37**
9	65	50	92.0	**19**
9	65	50	91.0	**20**
10	65	50	96.0	**28**
9	65	50	98.2	**15**
9	65	50	110.1	**23**
9	65	50	105.0	**15**
10	65	50	101.8	**19**
10	65	50	109.1	**16**
9	65	50	122.1	**22**
10	65	50	130.0	**16**
10	65	50	124.4	**19**
10	65	50	129.7	**29**
10	65	50	124.3	**33**
10	65	50	115.0	**19**
11	65	65	97.3	**16**

11	65	65	114.1	**21**
11	65	65	115.8	**18**
11	65	65	116.7	**12**
11	65	65	128.2	**32**
9	65	65	93.8	**27**
9	65	65	91.0	**18**
9	65	65	91.0	**27**
10	65	65	94.6	**20**
9	65	65	99.4	**37**
9	65	65	110.5	**33**
9	65	65	106.0	**26**
10	65	65	109.3	**31**
10	65	65	108.8	**26**
9	65	65	122.6	**45**
9	65	65	127.3	**35**
10	65	65	131.1	**42**
10	65	65	123.9	**22**
10	65	65	129.8	**32**
10	65	65	125.4	**38**
10	65	65	125.2	**41**

Table B.2*: Raw tumbling distances for the honeycomb cushion container.*

HONEYCOMB CUSHION				
EVENT	**ALTITUDE (FT. AGL)**	**AIRSPEED (KIAS)**	**WEIGHT (LBS)**	**ROLL (METERS)**
11	50	50	58.5	**10**
11	50	50	68.4	**22**
11	50	50	61.3	**18**
11	50	50	58.8	**14**
11	50	50	100.4	**18**
11	50	50	104.4	**32**
11	50	50	100.3	**22**
11	50	65	68.6	**18**
11	50	65	69.5	**27**
11	50	65	57.8	**22**
11	50	65	65.2	**17**
11	50	65	58.9	**17**

11	50	65	65.3	**17**
11	50	65	68.3	**18**
11	50	65	62.3	**15**
11	50	65	70.3	**18**
11	50	65	67.7	**16**
11	50	65	64.8	**23**
11	50	65	69.2	**15**
11	50	65	57.2	**3**
11	50	65	83.9	**13**
11	50	65	58.4	**18**
11	50	65	68.0	**18**
11	50	65	58.3	**16**
11	50	65	84.9	**32**
11	50	65	89.2	**21**
11	50	65	90.7	**31**
11	50	65	86.5	**16**
11	50	65	104.6	**18**
11	50	65	103.7	**26**
11	50	65	105.9	**22**
11	50	65	104.4	**23**
11	50	65	99.9	**27**
11	50	65	99.7	**19**
11	65	50	75.6	**8**
11	65	50	84.9	**7**
11	65	50	87.6	**18**
11	65	50	104.3	**15**
11	65	50	100.4	**16**
11	65	50	100.8	**16**
11	65	65	73.5	**11**
11	65	65	68.6	**13**
11	65	65	69.6	**18**
11	65	65	70.3	**17**
11	65	65	85.4	**18**
11	65	65	89.1	**13**
11	65	65	90.5	**14**
11	65	65	85.2	**17**
11	65	65	104.5	**26**
11	65	65	99.6	**18**
11	65	65	103.8	**31**

Vita

Alexey Titovich

2001 - 2005	Jackson Memorial High School, Jackson, New Jersey
2005 - 2009	Attended Rutgers University, School of Engineering, New Brunswick, New Jersey
2009	B.S., Mechanical and Aerospace Engineering, Rutgers University, New Brunswick, New Jersey
2009 – 2011	Attended Graduate School, Rutgers University, New Brunswick, New Jersey
2009 - 2011	Teaching Assistant, Department of Mechanical and Aerospace Engineering, Rutgers University
2010	Summer Lecturer, Department of Mechanical and Aerospace Engineering, Rutgers University
2011	M.S., Mechanical and Aerospace Engineering, Rutgers University, New Brunswick, New Jersey